

Coupled crane vessel dynamics

M.J. van Veenendaal



Coupled crane vessel dynamics

MSc. Thesis

by

M.J. van Veenendaal

Student number: 4011961
Project duration: November 2nd, 2015 – June 23rd, 2016
Thesis committee: Prof. dr. A. V. Metrikine, TU Delft, committee chairman
Ir. S. Sanchez Gómez, TU Delft, 1st supervisor
Ir. A. Jarquin Laguna, TU Delft, 2nd supervisor
Ir. A. A. G. Velthoen, EMAS AMC, company supervisor

This thesis is confidential and cannot be made public until further notice.

Summary

Most, if not all, vessel new builds within the offshore heavy lifting industry are designed with specific characteristics (stability, dynamic response, transition speed etc.) in mind. Subsequently a crane is designed and supplemented to the vessel complying with the characteristics of the vessel. However, what happens if this design process is turned around? That is, for specific crane design and maximum lifting load, what is the optimum vessel geometry? If one would exactly know what the soul operational purpose of a new build vessel would be, designing a vessel in this manner could be more cost effective. This method of analysis would provide a different approach and possibly a different outcome to the design process.

A first and important step in this new design process is to define how/whether the geometric properties of a vessel are of influence on the response characteristics during lifting operations. This report provides a method of analysis to combine vessel response terms, obtained from hydrodynamic diffraction software, with the terms related to the crane load motion, defined through the Lagrangian method. An example vessel, namely the Lewek Connector, is chosen to analyze the model.

This coupled model of analysis has been compared with the current method of analysis, where the crane load is modeled as a lump loaded mass at the crane tip. The two separate model set-ups are evaluated within the frequency domain, focusing on the resonance frequency, maximum excitation at the resonance frequency and the effective motion of the system. The coupled system provides a better representation of reality compared to the current lump loaded system.

Using the coupled set-up, a model has been created enabling the user to alter the geometric properties of a vessel. Either the length, width, and/or depth of the vessel can be changed. All parameters (Center of gravity/buoyancy, radii of gyration, mass, draft) linked to the geometry of the vessel are calculated within the model. Altering the vessel geometry of the example vessel will in fact make the model imaginary and non-existent in real life, hence there is no existing vessel with the altered Lewek Connector's geometry.

It has been shown that the swaying of the crane motion only affects the vessel motion within roll. The crane load will not affect the pitch motion, even for increasingly small vessel sizes dynamic coupled motion within pitch does not occur. The inertia forces generated by the swaying crane load are not large enough to force the pitch motion to exert any coupled behavior. Due to the model set-up, with a single large crane at the aft of the vessel, the static pitch excitation increases for increasingly smaller vessels.

It has been shown that swaying of the crane load will have a greater influence on the roll motion for increasingly smaller vessels. However, the damping of the crane load highly dictates the maximum occurring motion. Further research must include any form of CFD analysis and/or structural damping analysis in order to determine the occurring crane load damping.

Both resonance frequency related to the vessel motion as well as the resonance frequency related to the swaying crane load motion are dependent on the vessel geometry. Therefore it cannot be assumed the crane load will resonate at the natural frequency of a freely swaying pendulum that's only dependent on the crane cable length.

Preface

The report laying in front of you is the accumulation of 7 months worth of work and research. I am grateful and thankful for the opportunity to work at a company I truly enjoyed working for. Therefore I would like to thank Gerard Velthoen, my daily supervisor, for giving me the chance and freedom to perform my research.

During the spring of 2015 I approached EMAS AMC with a research proposal regarding coupled vessel dynamics. We have met some challenges starting up the research, but in November 2015 I was able to start at the newly opened Rotterdam office. Therefore I would like to thank all employees at the Rotterdam office, especially Susanne den Hoed, whom helped me set up my working environment.

During my research I had the opportunity to work a month alongside the engineering department in Oslo Norway. Therefore I want to thank everyone involved, especially Jon Refsnes who arranged part of my stay. I would like to thank Sean van Steel and Christian Juell Gudbrandsen who helped greatly in understanding the necessary software programs and being open for discussion on the subject. I would also like to thank Marit Gamre who was kindhearted to give advice on what to do and what to see in my spare time in Oslo.

I would also like thank my university supervisors Antonio Jarquin Laguna and Sergio Sanchez. They both helped me tremendously in understanding the theory and guiding me in the correct direction.

Last but not least I would like to thank my girlfriend Stephanie van Sprang whom helped make all the illustrations. Without her help the report would definitely be less presentable and far less understandable. Stephanie's ability to clearly illustrate and summarize the essence of the subject far surpasses my own capabilities and qualifications.

Mark van Veenendaal.

Contents

Summary	iii
Preface	v
1 Introduction	1
1.1 Problem statement	2
1.1.1 Research question	2
2 Reference study	3
2.1 Coupled crane vessel motion	3
2.2 Analytic coupled vessel motion	4
2.3 Numerical coupled vessel motion.	5
3 Diffraction software calculation	7
3.1 Vessel properties	8
3.2 Environmental properties.	8
3.3 Analyses set-up	8
3.3.1 Base case analysis	9
3.3.2 Proportional sensitivity analysis	9
3.3.3 Dis-proportional sensitivity analysis	9
3.4 Numerical parameter calculation	10
3.4.1 Assumptions.	11
3.4.2 Base vessel parameter calculation	11
3.4.3 Geometrically altered vessel parameter calculation	12
3.5 Validation.	13
3.6 Output values	14
4 Model set-up	17
4.1 Degrees of freedom analyzed	17
4.1.1 Crane dynamics	17
4.2 Linearity assumption	20
4.2.1 Time domain response 2DOF	22
4.2.2 Natural frequencies 2DOF	22
4.3 Coupling of crane terms	24
4.3.1 Lump loaded system.	25
4.3.2 Coupled system	26
4.4 Frequency domain vessel response	28
4.4.1 Phase shift	28
4.4.2 Damping ratio	29
4.4.3 Example frequency response and phase shift	30
4.4.4 Sensitivity relations	31
4.4.5 Effective excitation, root mean square (RMS)	32
5 Base case analysis	33
5.1 Roll governed motion	34
5.2 Pitch governed motion	36
5.3 Polar representation	38
5.4 Conclusion base case analysis	39

6	Proportional sensitivity analysis	41
6.1	Roll governed motion	42
6.1.1	Frequency shift roll governed motion	44
6.1.2	Peak shift roll governed motion	44
6.1.3	Roll damping ratio shift	45
6.1.4	Effective excitation (RMS) roll governed motion	46
6.2	Pitch governed motion	47
6.2.1	Frequency shift pitch governed motion	49
6.2.2	Static pitch excitation	49
6.3	Conclusion proportional sensitivity analysis	50
6.4	Data errors	51
7	Disproportional sensitivity analyses	53
7.1	Length sensitivity	53
7.1.1	Frequency shift	56
7.1.2	Peak shift	56
7.1.3	Roll damping ratio shift	57
7.1.4	Effective excitation (RMS) roll governed motion	57
7.1.5	Conclusion length sensitivity analysis	58
7.2	Width sensitivity	59
7.2.1	Frequency shift	59
7.2.2	Peak shift	61
7.2.3	Roll damping ratio shift	62
7.2.4	Effective excitation (RMS) roll governed motion	62
7.2.5	Conclusion width sensitivity analysis	63
7.3	Depth sensitivity	64
7.3.1	Frequency shift	66
7.3.2	Peak shift	66
7.3.3	Roll damping ratio shift	67
7.3.4	Effective excitation (RMS) roll governed motion	68
7.3.5	Conclusion depth sensitivity analysis	69
7.4	Comparative peak shift	69
7.5	Comparative effective motion (RMS)	71
8	Conclusions	73
8.1	Summary	73
8.2	Research questions	73
9	Recommendations	77
9.1	Implementation	77
9.2	Recommendations for implementation	78
9.3	Recommendation for future research	79
A	Euler Lagrangian calculations	81
A.1	Euler Lagrangian calculations 2DOF	81
A.1.1	Non linear system	83
A.1.2	Linearization.	83
A.2	Euler Lagrangian calculations 6DOF	84
A.3	Euler Lagrangian calculations 8DOF	87
B	Damping sensitivity, pitch governed motion	91
C	Proportional sensitivity analysis 6DOF	93
C.0.1	Frequency shift	93
C.0.2	Peak shift	95
C.0.3	Damping ratio shift	95
C.0.4	Effective excitation (RMS)	96
C.0.5	Conclusion 6DOF proportional sensitivity analysis	97

Introduction

In the past 10 years the offshore oil & gas industry has seen an increasing demand in offshore installation work. With larger oilfields discovered and deeper waters accessible, the offshore construction market reacted to this demand by building more and larger construction assets and crane ships. Most, if not all, of these construction assets have been monohull vessels, as like the in 2007 built EMAS vessel Lewek Champion seen in figure 1.1. Despite the fact currently the offshore vessel new-build market is slow, future investments for large heavy lift crane vessels is expected. To keep investment and operational costs competitive, owners tend to build relatively small vessels with large heavy lift cranes. This may come in conflict with the operational capabilities like stability and wave motion response. For the owner it is interesting to have a tool at hand at the conceptual phase of a new-build vessel, helping to determine better dimensional properties with respect to operability characteristics.



Figure 1.1: Lewek Champion

1.1. Problem statement

A primary field of difficulty with respect to optimizing crane vessel dimensions is the dynamic interaction between vessel and the crane suspended load, also known as dynamic coupling. The approach currently used by EMAS to analyze the dynamic response of the crane vessel system, is to model the crane load lumped at the crane tip as seen in figure 1.2a. This implies that the excitation of the load is simply a prescribed motion of the crane tip. Lump loading the crane load at the crane tip is a fully legitimate and validated method of analysis for static stability analysis. Regarding the dynamic interaction between the crane load and vessel motion, as illustrated in figure 1.2b, the lump loaded analysis method neglects the influence of the suspended crane load motion on the motion of the vessel. The general consensus is that the crane load is relatively small compared to the actual mass of the vessel. However, reducing the vessel size will inadvertently have consequences on the coupled motion behavior of the vessel/crane system. This thesis therefore challenges the assertion made.

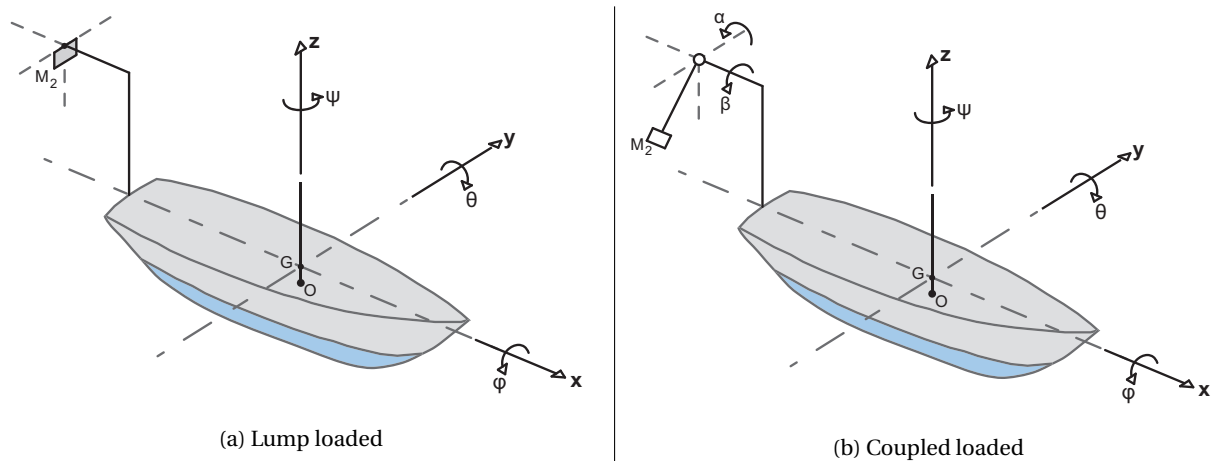


Figure 1.2: Lump loaded vs. coupled loaded

1.1.1. Research question

EMAS AMC has clearly stated a vision for future investments, new built crane vessel designs must be optimized to reduce construction costs and maximize operational up-time of the vessel. As explained in section 1.1, reducing vessel dimensions may have an effect on dynamic coupling. Therefore the research question for this research thesis has been defined as:

"What is the effect of vessel geometry on dynamic crane load coupling?"

To accurately answer the main research question a subdivision into several sub questions must be made. These sub questions will cover all aspects of the main question and will assist in structuring the research thesis. The sub questions for this research are defined as:

1. *What is dynamic coupled motion?*
2. *What induces crane load coupled motion on a crane vessel?*
3. *In which degrees of freedom does dynamic crane load coupled motion occur?*
4. *Does dynamic crane load coupled motion occur during current operations and is this significant with respect to current method of analysis?*
5. *Which geometrical vessel parameters have the most influence on dynamic crane load coupled motion?*

2

Reference study

As preparation, several research papers have been examined used as reference throughout the research. To be able to understand the general challenges regarding dynamic coupling of crane vessels, the problems these reference papers faced must be set out.

2.1. Coupled crane vessel motion

First of all, one must know what is defined as a dynamically coupled system. A dynamic coupled system is one composed of subsystems, that is, the states of certain subsystems affect the time-evolution of the other [11]. The coupled system researched will be the vessel coupled with the crane system. Dynamic coupling with respect to this system would therefore be, the influence of the vessel motion on the crane load motion and vice versa.

In general, the roll and pitch motion of a crane vessel are seen as the most governing motion with respect to the operability during lifting operations. EMAS has done an initial research performed by Vu et. al. [10] into roll and pitch characteristics of a generalized barge like crane vessel. The research examines the relationship between swinging of the lifted crane load on the natural frequency for either roll or pitch. By using the hydrostatic stability equations, a highly simplified dynamic system was created. In essence the system researched is represented as a 2 degrees of freedom system. The aim of the research was to have a simple rudimentary model at hand to predict natural periods of vessel and crane load. If correct, a system like this could quickly give an educated guesstimate into the natural frequency of the vessel and crane load without the need for extensive computing power and programming efforts.

The main conclusion from the research is a large difference between the natural crane period calculated by the analytic formulation and the actual natural periods calculated by numerical dynamic software (MOSES). The error between the analytic and numerical natural load frequencies are anywhere between 0.0% and 27.9%. Although not included in the conclusion of the research, the natural period for roll also shows a great discrepancy. The error for roll is anywhere between 0.2% and 9.0%.

This discrepancy is credited to the modeled stiffness of the crane system. This assertion however is not entirely correct. The unknown stiffness of the crane system will most likely contribute to the discrepancy examined, however this is not the only contributor in the dynamic system. Results from the research are rather monolithic in nature, it does not account for higher order natural frequencies, it does not incorporate higher degrees of freedom, and both environmental loading conditions and damping terms are not present. To better understand the actual system, it must be expanded to a higher degree of freedom, removing the incited simplification in order to better understand the problem. This implies the system can no longer be described by the hydrostatic characteristics of a generalized barge like vessel in 2 degrees of freedom. There is a vast array of possible contributors to the discrepancy examined, the assumed simplifications to describe the system therefore just does not represent the actual system.

The research performed by Coric et. al.[3] implements a more complex dynamic model incorporating both the vessel motion as well as the crane load motion. Compared to the more simplistic model research by Vu et. al. [10], this model incorporates three additional degrees of freedom due to the swinging of the crane load and elongation of the crane cable. This implies the set-up system has 9 degrees of freedom, three vessel translation motions (surge, sway and heave), three rotational vessel motions (roll, pitch and yaw), two

additional angular motions of the crane cable and finally the crane cable elongation motion. This model is only viable for small oscillatory motions, for greater oscillatory motions nonlinear effects come into play. The crane load is modeled as a singularity load, which implies the load only has mass properties and no further dimensional properties such as rotational moment of inertia.

The model has been verified with towing tank testing and shows very good comparison in data trend, maximum error is equal to 2.2%. Greater errors occur when the mass is lifted significantly from the deck towards the tip of the crane, a maximum error of 18.4% has been observed. This however is not a real world scenario, hence there is no real reason to hoist a mass towards the tip of the crane. The main conclusion of the research is that the data show acceptable accuracy for practical applications.

Not included in the model is the initial displacement of the vessel, the model only looks at dynamic displacements due to incoming waves. It must however be notified this assertion most likely is correct evaluating rolling motion, hence the crane is symmetrically placed at the aft of the vessel and therefore does not give any initial rolling displacement. For pitch however, this assertion is not entirely correct. Although the effect most likely is not even noticeable, it must not be discarded without proof.

2.2. Analytic coupled vessel motion

A more in depth mathematical research by Ibrahim and Grace [7] into vessel motion has been performed. This research examines two different approaches to analytically describe vessel motions in 6 degrees of freedom (surge, sway, heave, roll, pitch & yaw). The first approach utilizes a mathematical development based on a Taylor expansion of the force function. I.e. the system is described as a system at a certain equilibrium. This method accounts for the vessel inertia forces, inertia moments and restoring forces. This method would give a rather accurate display of the nonlinear equations of motion in 6 degrees of freedom. The second method employs the integration of hydrodynamic pressure acting on the ship's wetted surface to derive the external forces and moments.

However modeling the roll damping is much more complicated. Existing information on the structural damping of ships is far from satisfactory [2]. Symmetric responses to wave excitation can be estimated on the basis of existing hydrodynamic theories, with use of rough estimates of hull damping. Limited knowledge of structural damping is likely to be a handicap. Much less is known about antisymmetric responses to waves and the effect of hull damping [2].

For small roll angles, the damping moment is directly proportional to the angular roll velocity. But with increasing roll angle, nonlinear damping will become significant. Due to the occurrence of strong viscous effect, roll damping moments cannot be computed by means of potential theory [7].

A research performed by Y. Himeno [6] lists all linear and nonlinear contributors to the roll damping coefficients. The total roll damping with all individual contributors is seen in equation 2.1.

$$b_{44}(\omega) = B_E + B_F + B_L + B_W + B_{BKH} + B_{BKN} + B_{BKW} \quad (2.1)$$

Eddy damping B_E , nonlinear damping caused by the pressure variation on the naked hull, excluding the effect of waves and bilge keels. The nonlinearity is proportional to the quadratic angular roll velocity term of the vessel motion.

Friction damping B_F is caused by the skin-friction stress on the hull in roll motion. Therefore it may be influenced by the presence of waves and bilge keels.

Lift effect B_L , at forward speed a vessel exerts an upward lift force. This effect in turn will increase the roll damping of a vessel linearly.

Wave damping B_W , denotes the increment of the hull-pressure damping due to presence of free surface waves, so it includes the interaction between waves and eddies and between waves and lift. Free surface waves being waves without the presence of any shear stress.

Hull-pressure damping due to bilge keels B_{BKH} , corresponds to the pressure change on the hull when bilge keels are installed. This term stands for an interaction between hull and bilge keels.

Normal force damping of bilge keels B_{BKN} , is due to the normal force on the bilge keels themselves.

Wave damping of bilge keels B_{BKW} , the damping induced by the interaction of free surface waves.

Although the mathematical approach gives the coupled vessel motion in 6 degrees of freedom it does not suit the needs for this research. Damping terms are highly nonlinear and difficult to accurately calculate through analytic calculations. Therefore an analytic approach to the research is deemed to be fruitless. If possible, a software program that calculates the dynamic properties of a vessel accurately and predicatively should be incorporated.

2.3. Numerical coupled vessel motion

The research must incorporate numerical modeling of vessel dynamics to accurately compute the dynamic properties of the vessel. Several software programs exist to calculate these dynamic properties of the vessel. These software packages use geometry dependent diffraction theory. Different sea states are implementable, damping terms related to the vessel damping as well as to the bilge keels are implemented and subsequently give a better approximation compared to the analytic estimates described in section 2.2.

The crane system implementing the degrees of freedom related to the crane load movement must be added to the system increasing the number of degrees of freedom as seen in the research performed by Coric. et. al. [3]. Simplifications made to the system may only be implemented whenever there is proof it will not compromise the results. The dynamic system will be evaluated within the frequency domain, this will ensure all dynamic properties are easily obtainable.

The set-up of the modeled system therefore may be subdivided into two separate parts. First the hydrodynamic model describing the vessel motion will be set up and secondly the additional crane terms will be added. This adaptation of the crane terms to the vessel is only possible whenever all terms involved are within the linear domain. Therefore it has to be proven the subsequent crane terms are modeled correctly within the linear domain.

The performed analyses are subdivided into three parts. First the current method of analysis will be compared to the coupled system within the base case. Implying, a known vessel will be used to compare the different methods of analysis. Secondly, the geometric vessel properties will be reshaped proportionally, implying the vessel is made smaller or bigger. Thirdly a disproportional sensitivity analyses is performed evaluating the dependency of either the length, width or depth of the vessel on the motion characteristics.

Finalizing the research, conclusions are made and the research questions are answered followed by recommendations on how to incorporate the researched model and what to research next. The set-up of the research may be seen in figure 2.1.

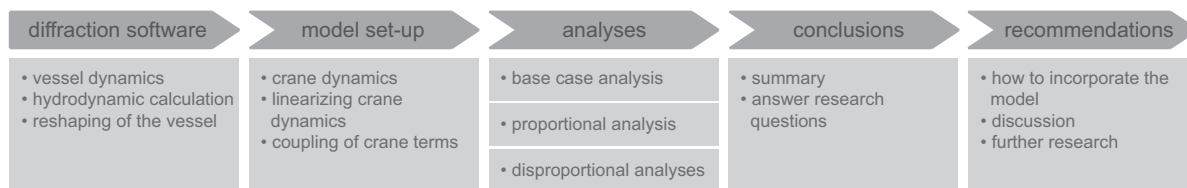


Figure 2.1: Research set-up

Subquestions

1. What is dynamic coupled motion?

A coupled dynamical system is one composed of subsystems, that is, the states of certain subsystems affect the time-evolution of others [11]. The system researched is respectively the vessel system and secondly the crane system, i.e., the effect of the vessel motion on the crane load motion and vice versa.

3

Diffraction software calculation



Figure 3.1: Research set-up

In able create the matrices related to the vessel motion, diffraction software is used. To be able to answer the premise of the research the set-up of the diffraction software calculations must be done correctly for all cases examined. I.e., all properties related to the geometric parametric commutation must be calculated correctly. This chapter, figure 3.1, will discuss how the diffraction software was implemented before moving on to coupling of the crane terms.

This research will evaluate the dimensional parametric modification based on an existing vessel. The Lewek Connector is chosen as a suitable candidate vessel, the Connector is a SURF vessel with a record of high dynamic stability during installation. The vessel has two medium sized subsea knuckle boom cranes located respectively at the aft and amidship [1]. These cranes however will not be used throughout the research. The model will be set up as a traditional heavy lift vessel with a single large crane dead center at the aft of the ship. This configuration is usually used for heavy lifting operations, the maximum lift capacity is greater compared to lifting from the side of the vessel, this will be discussed in chapter 4.

The diffraction software package used is the WADAM HydroD package by DNV GL™ provided by EMAS AMC. This software is able to calculate the mass-inertia-, damping- and stiffness- matrices as well as the force vectors representing the wave response of the vessel. The diffraction software is able to include bilge keels that give the vessel better roll damping characteristics.

The calculations performed by the diffraction software are all in stationary position, no forward speed is added. Second order wave drift terms are not included into the calculations hence the natural period of these terms is very large and not noticeable for the crane load. This has been done to reduce the computing time needed.

The wave forces calculated by the diffraction software must be evaluated for different wave encounter angles, hence the forcing of the system is both dependent on wave frequency as well as encounter angle. The encounter angle μ will be set at small increments for head and following waves (see figure 3.2), hence these angles will give the most desirable dynamic output and therefore will most likely be the wave encounter angles used during operation. For bow, beam and quartering waves the increments are set further apart due to the fact that these encounter angles will not be used during operations hence the dynamic characteristics of the vessel with these encounter angles is highly unfavorable. The encounter angles evaluated are listed in equation 3.1 with respect to the vessel as seen in figure 3.2.

$$\mu = [0^\circ, 5^\circ, 10^\circ, 15^\circ, 20^\circ, 25^\circ, 45^\circ, 90^\circ, 135^\circ, 155^\circ, 160^\circ, 165^\circ, 170^\circ, 175^\circ, 180^\circ] \quad (3.1)$$

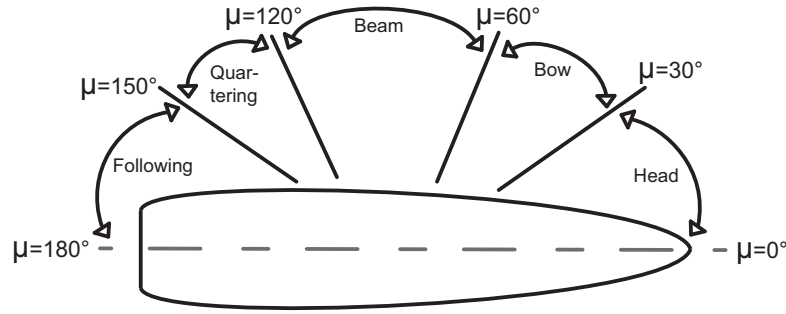


Figure 3.2: Encounter angles

3.1. Vessel properties

The Lewek Connector's geometrical properties are listed in table 3.1. The vessel draft T_{pp} is dependent on the loading condition of the vessel. During vessel transition the draft is equal to the unloaded draft $T_{pp} = 6.5\text{m}$, during lifting operation the ballast tanks are filled to get the draft down to $T_{pp} = 8.5\text{m}$. This draft increase, increases the static- and dynamic- stability of the vessel.

The dimensional parameters listed in table 3.1 are the main parameters that will be evaluated in the model, the model will be set up in such a way that it is possible to increase or decrease each dimensional parameter independently. Implying that the vessel can either be elongated-shortened, widened-contracted or elevated-lowered.

Table 3.1: Vessel properties

	Parameter	Value	Unit
Length	L_{pp}	153.0	m
Width	B_{pp}	32.0	m
Depth	H_{pp}	12.1	m
Draft	T_{pp}	8.5	m

3.2. Environmental properties

Analysis for heavy lifting operations usually considers a certain sea state for which motion analysis is performed. I.e., given sea state A, what is the vessel response? To ensure the research questions are answerable, the environmental conditions are taken constant throughout the research. This research will compare the vessel response for different vessel sizes within a certain sea state. In further research studies the effect of the encountered sea state may be evaluated.

The environmental conditions are set as input values for the diffraction software WADAM. The water depth is set at 300m, this is the minimum water depth for which the shape of the waves are not scanted due to frictional terms of the sea floor and at which the computational 'cost' is lowest [15].

A typical analysis wave spectrum used for dynamic analysis is a low energy Jonswap spectrum. The Jonswap (Joint North Sea Wave Project) spectrum is specifically designed to represent limited fetch North Sea sea states. A typical Jonswap spectrum used for dynamic analysis is a wave height of 2m and a significant wave period of 10s.

3.3. Analyses set-up

To determine whether the vessel shows coupled motion with the crane load and what the effects of the independent geometrical parameters are, three different analyses are set up. First the unaltered vessel will be evaluated (Base case analysis), secondly the vessel will be proportionally geometrically altered (Proportional sensitivity analysis) and thirdly the independent dimensional parameters will be altered (Dis-proportional sensitivity analysis).

3.3.1. Base case analysis

The base case analysis will use the Lewek Connector vessel to compare the current method of analysis with the coupled method of analysis. The base case analysis will determine whether the crane load has an effect on the vessel motion within current operations. I.e., is the coupled vessel - crane load motion relevant for the current operations.

3.3.2. Proportional sensitivity analysis

The proportional sensitivity analysis will give insight into whether the dynamic coupled motion is dependent on the size of the vessel. That is, how does the dynamic coupled motion change for smaller and larger vessels? If the base case is not dynamically coupled, the proportional sensitivity analysis will determine if different vessel sizes will induce dynamic coupled motion. Again the Lewek Connector vessel is used to perform the analysis.

The sensitivity vector $\underline{\lambda}$ is defined as seen in equation 3.2. Where the independent scalars account for the sensitivity multiplier in either X-, Y- or Z- direction. Consider the dimensional properties of the base vessel as seen in equation 3.3.

$$\underline{\lambda} = \begin{bmatrix} \lambda_x \\ \lambda_y \\ \lambda_z \end{bmatrix} \quad (3.2)$$

$$\underline{\lambda}_{\text{base}} = \begin{bmatrix} 1.00 \\ 1.00 \\ 1.00 \end{bmatrix} \quad (3.3)$$

The geometrically altered length (L_{pp}), width (B_{pp}) and height (H_{pp}) are determined by the product of the base geometry with the sensitivity vector $\underline{\lambda}$.

$$\begin{bmatrix} L_{pp} \\ B_{pp} \\ H_{pp} \end{bmatrix} = \begin{bmatrix} L_{pp,\text{base}} \\ B_{pp,\text{base}} \\ H_{pp,\text{base}} \end{bmatrix} \circ \begin{bmatrix} \lambda_x \\ \lambda_y \\ \lambda_z \end{bmatrix} \quad (3.4)$$

Within the proportional sensitivity analysis the sensitivity multipliers in either X-, Y- or Z- direction are equal, equation 3.5. A total of 21 different cases are analyzed for the proportional sensitivity study, seen in equation 3.6. Although the vessel will be geometrically altered, the proportions of the vessel will not change. Sensitivity multipliers smaller than $\lambda < 1.00$ imply a vessel that is smaller than the base case vessel and sensitivity multipliers $\lambda > 1.00$ imply a vessel that is larger than the base case vessel.

$$\lambda_X = \lambda_Y = \lambda_Z = \lambda \quad (3.5)$$

$$\underline{\lambda} = \begin{bmatrix} 0.50 \\ 0.50 \\ 0.50 \end{bmatrix}; \begin{bmatrix} 0.55 \\ 0.55 \\ 0.55 \end{bmatrix}; \begin{bmatrix} 0.60 \\ 0.60 \\ 0.60 \end{bmatrix}; \dots; \begin{bmatrix} 1.50 \\ 1.50 \\ 1.50 \end{bmatrix} \quad (3.6)$$

3.3.3. Dis-proportional sensitivity analysis

Secondly, the vessel will be geometrically altered dis-proportionally in both length- (X), width- (Y) and depth- (Z) direction. The vessel will be shortened and elongated in a single direction by equations 3.7 - 3.9. Note that by reshaping the vessel in a single direction, whether in X-, Y- or Z- direction, the relative geometric proportions are altered.

$$\underline{\lambda}_X = \begin{bmatrix} 0.50 \\ 1.00 \\ 1.00 \end{bmatrix}; \begin{bmatrix} 0.55 \\ 1.00 \\ 1.00 \end{bmatrix}; \begin{bmatrix} 0.60 \\ 1.00 \\ 1.00 \end{bmatrix}; \dots; \begin{bmatrix} 1.50 \\ 1.00 \\ 1.00 \end{bmatrix} \quad (3.7)$$

$$\underline{\lambda}_Y = \begin{bmatrix} 1.00 \\ 0.50 \\ 1.00 \end{bmatrix}; \begin{bmatrix} 1.00 \\ 0.55 \\ 1.00 \end{bmatrix}; \begin{bmatrix} 1.00 \\ 0.60 \\ 1.00 \end{bmatrix}; \dots; \begin{bmatrix} 1.00 \\ 1.50 \\ 1.00 \end{bmatrix} \quad (3.8)$$

$$\underline{\lambda}_Z = \begin{bmatrix} 1.00 \\ 1.00 \\ 0.50 \end{bmatrix}; \begin{bmatrix} 1.00 \\ 1.00 \\ 0.55 \end{bmatrix}; \begin{bmatrix} 1.00 \\ 1.00 \\ 0.60 \end{bmatrix}; \dots; \begin{bmatrix} 1.00 \\ 1.00 \\ 1.50 \end{bmatrix} \quad (3.9)$$

The four different sensitivity studies will give insight into the dimensional dependency of the system. Knowing the relation between the dimensional properties and the dynamic output of the system will be the first step into optimizing the vessel dimensions with respect to the dynamic characteristics of the vessel.

3.4. Numerical parameter calculation

To understand the diffraction software package used, the distinction between both WADAM and HydroD will be explained. The HydroD software package uses a graphical user interface to set-up the analyses, the analyses afterwards will be executed by WADAM.

Another method to set-up an analyses is through scripted commands and run it directly to WADAM. This method is preferred over graphically computing the analyses, hence multiple cases will be run, if computed correctly it does not need any manual effort to compute all the independent analyses and subsequently human error is eliminated.

As discussed in section 3.3, the vessel geometric properties will be altered either proportionally or disproportionally throughout the sensitivity analysis. The only thing necessary to compute an analyses is a geometry file of the vessel that represents the vessel as a set of independent panels. A program has been developed that enables the user to alter the geometric properties of a vessel based on the sensitivity vector $\underline{\lambda}$. Besides altering the geometric properties of the vessel according to the sensitivity vector, the properties of the bilge keels are altered as well. The properties that are dependent of the geometry of the vessel are:

- Draft
- Mass
- Center of gravity (COG)
- Center of buoyancy (COB)
- Radii of gyration (k_x , k_y and k_z)

To define the mass of the vessel, HydroD can calculate the the uniformly distributed mass of the vessel based on the displaced volume of water of the vessel. The displaced volume of water in turn is calculated using the draft of the vessel. Although HydroD is able to calculate the mass based on the draft through the graphical user interface, it is not possible to calculate the mass of the vessel through the scripted WADAM commands. Whenever one would use the scripted command feature, the mass of the vessel must be known. For normal analysis computed by EMAS this has never been an issue, hence the mass and all the specifications are known for a specific vessel.

Usually all these properties of a preexisting vessel are known and do not have to be calculated. Altering the dimensional properties of the vessel will in turn also alter these properties. A numerical model has been created to calculate the dimensional dependent properties. The numerical model must be validated to ensure the properties are calculated correctly. Comparing the calculated properties with the known properties of the base vessel will validate the numerical model.

3.4.1. Assumptions

Although an actual vessel does not have an uniform mass distribution, mass is distributed rather unevenly throughout the vessel, there is no accurate method to determine the distribution of mass. Therefore the distribution is assumed to be uniform throughout the entire vessel. Assuming an uniform mass distribution will influence the COG, COB and all three radii of gyration.

Another assumption related to the mass is 'constant average density'. The average vessel density is calculated using the base vessel specifications, see equation 3.10. The vessel density is constant throughout the sensitivity analysis and is used to compute the draft of the geometrically altered vessels.

$$\rho_{\text{vessel}} = \frac{\nabla \rho_w}{V_{\text{vessel}}} \quad (3.10)$$

Where: ∇ = Displacement

ρ_w = water density

V_{vessel} = Volume vessel

To accurately determine the location of the COG and COB it is assumed that there's no heel nor trim. Assuming that the vessel has no initial heel nor trim, both the x-coordinate and the y-coordinate of the center of gravity (COG) and center of buoyancy (COB) align. Hence, whenever the COG does not align with the COB in either x- or y- coordinate, a torque moment will be present and will subsequently result in a new stationary equilibrium position.

3.4.2. Base vessel parameter calculation

To validate the methods used to calculate the parameters, the numerical model is compared with the known values for the base vessel. The draft for the base vessel, as mentioned earlier, is set at $T_{pp} = 8.5\text{m}$. The displacement of a vessel is defined as seen in equation 3.11. In order to approximate this integral numerically, the geometry file used in WADAM HydroD is loaded into Matlab and used to compute the displacement ∇ .

$$\nabla = \int_0^{T_{pp}} \iint_A f(x, y, z) dx dy dz \quad (3.11)$$

Where: $f(x, y, z)$ = vessel geometry

It is known from hydrostatics that the mass of the vessel is equal to the mass of the displaced volume of water.

$$M_1 = \nabla \rho_w \quad (3.12)$$

As seen in equation 3.10, the average density can now be computed, hence the total volumetric measurement of the vessel is equal to:

$$V_{\text{vessel}} = \iiint_V f(x, y, z) dx dy dz \quad (3.13)$$

Previously it has been established the x- and y- coordinate of the COB and COG are aligned through the assumption of no heel and no trim. The center of gravity is defined as the average location of the weight of an object [12]. The center of buoyancy is defined as the center of gravity of the volume of water which a hull displaces [14]. The numerical definition of COG and COB is given in equation 3.14, where \vec{R} is defined as the spatial vector including the x-, y- and z- coordinate. Implying that for a spatial distributed number of elements N with corresponding mass m_i and coordinate \vec{r}_i the center of gravity can be calculated using equation 3.14.

$$\vec{R} = \frac{\sum_{i=1}^N m_i \vec{r}_i}{\sum_{i=1}^N m_i} \quad (3.14)$$

Where: \vec{R} = Center of mass

N = Number of elements

m_i = Mass element i

\vec{r}_i = Coordinate within reference frame element i

As mentioned, a uniform mass distribution is assumed. In order to calculate the COB and COG the vessel geometry file is 'filled' with an equally spaced mesh of coordinate points, see figure 3.3. The COB and COG formulation as seen in equation 3.14 can now be simplified, hence the mass is irrelevant to the equation.

$$m_i = m_j \quad \text{for: } i \neq j \text{ \& } i = j \quad (3.15)$$

$$\text{Therefore: } \vec{R} = \frac{\sum_{i=1}^N \vec{r}_i}{N} \quad (3.16)$$

Similarly the radii of gyration can be computed. The radius of gyration is defined as the equivalent distance of the mass from the axis of rotation [9]. This is mathematically similar to the root mean square distance of the vessel with respect to the center of gravity. Numerically the radii of gyration can be defined as seen in equation 3.17. Where \vec{K}^2 is equal to the radii of gyration for either k_x , k_y or k_z representing the radii of gyration for roll, pitch and yaw.

$$\vec{K}^2 = \frac{1}{N} \sum_{i=1}^N (\vec{r}_i - \vec{R})^2 \quad (3.17)$$

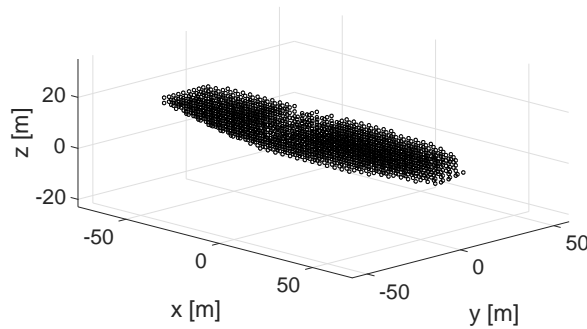


Figure 3.3: Equally spaced coordinate points

3.4.3. Geometrically altered vessel parameter calculation

Unlike the base vessel parameter calculation, the geometrically altered vessel does not have a predetermined draft T_{pp} . Hence, altering the vessel geometry either proportionally or dis-proportionally influences the draft of the vessel. Although the draft is not able to be computed using the sensitivity factor $\underline{\lambda}$, hence the shape of the vessel is not linear, using the assumption of constant average density the draft of the altered vessel can be calculated, equation 3.20.

$$V_{\text{vessel}}\rho_{\text{vessel}} = \nabla\rho_w \quad (3.18)$$

$$\nabla = \frac{V_{\text{vessel}}\rho_{\text{vessel}}}{\rho_w} \quad (3.19)$$

$$\int_0^{T_{\text{pp}}} \iint_A f(x, y, z) dx dy dz = \frac{V_{\text{vessel}}\rho_{\text{vessel}}}{\rho_w} \quad (3.20)$$

Numerically this implies a search function will find the draft T_{pp} for which the displaced water is equal to the mass of the vessel under the assumption that the vessel has constant average density throughout the sensitivity cases. The center of gravity, center of buoyancy and radii of gyration are calculated similarly to the base vessel parameter calculation seen in equation 3.16 and 3.17.

3.5. Validation

Observing the discrepancy between the numerical model and HydroD, as seen in table 3.2, the error for all numerically calculated properties is relatively low and within the same ball park range as the calculated HydroD calculated values.

Table 3.2: Numerical model vs. HydroD

Parameter	Numerical model	HydroD	Unit	Error
Draft (T_{pp})	8.50	8.50	[m]	0.0%
Mass (M_1)	$27.35 \cdot 10^6$	$25.54 \cdot 10^6$	[kg]	7.1%
COG ([x, y, z])	[-4.90, 0.00, 6.59]	[-4.65, 0.00, 6.59]	[m]	[5.4, 0.0, 0.0]%
COB ([x, y, z])	[-4.90, 0.00, 4.68]	[-4.65, 0.00, 4.77]	[m]	[5.4, 0.0, -1.9]%
Radii of gyr. ($[k_x, k_y, k_z]$)	[11.01, 39.17, 39.30]	[10.53, 39.08, 39.62]	[m]	[4.6, 0.2, -0.8]%

The highest error is observed for the mass of the vessel. HydroD uses the same approach to calculate the mass as the numerical model. Like the numerical model, HydroD is able to compute a homogeneous mass model based on the draft of the vessel. The discrepancy however may be due to Matlab's ability to describe the volume of complex shapes. Computing the volume of a complex shape, like a vessel, Matlab creates a convex hull to approximate the shape. Convex hull shapes use Delaunay triangulation theory to estimate the volume of the vessel based on the geometry points. Think of the convex hull approximation as a rubber band rapped around an arbitrary shape as seen in figure 3.4. The area included within the perimeter of the rubber band will always be greater than the area of the actual arbitrary shape. Therefore for smooth sections of the vessel this convex hull shape of the vessel is a rather good approximation, however sharp cavities are difficult to approximate using a convex hull [13]. Using the convex hull to approximate the vessel therefore will always give a greater volume and subsequently greater mass than the HydroD approximation.

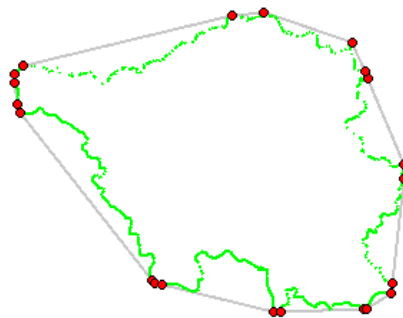


Figure 3.4: Convex hull, (http://doc.cgal.org/latest/Convex_hull_2/)

The exact volumetric approximation algorithm HydroD implements is unclear. The discrepancy is the only observable difference between HydroD and the numerical model.

Similarly to the volumetric approximation of the vessel, the equally spaced mesh dots seen in figure 3.3, used to compute the COG, COB, and radii of gyration, are also created using a convex hull approximation. The discrepancy however is slightly lower.

Seen in figure 3.5 the bow of both the convex hull and the bow of the HydroD model are on display. Based on the visual assessment, it can be seen that the convex hull approximation is less precise than the HydroD model.

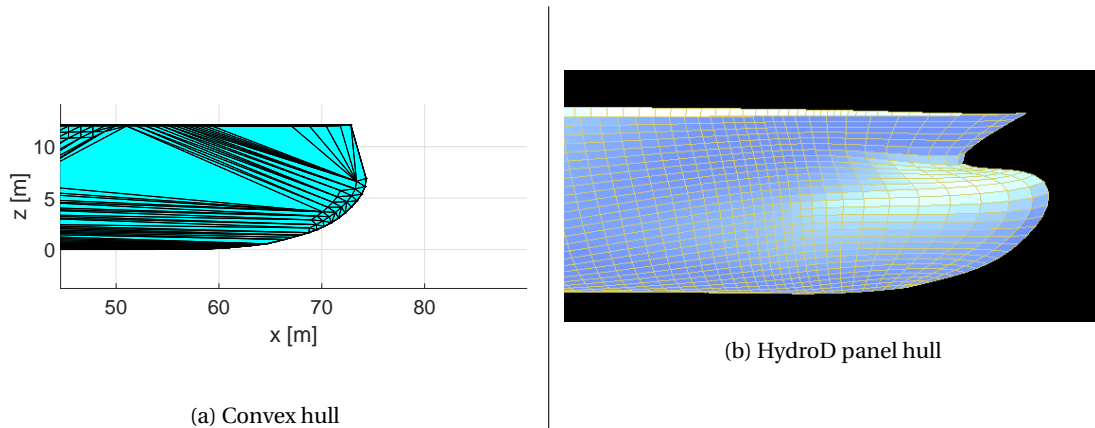


Figure 3.5: Convex hull vs. panel hull

As explained, HydroD is the graphical user interface representation of the hydrodynamic software WADAM. The input parameters will be checked by WADAM and must be within certain error bounds for WADAM to 'approve' the system. WADAM will not allow a mass discrepancy greater than 10%. The x- and y- coordinate of the COG and COB must comparatively not have a discrepancy greater than 1%, hence otherwise an initial heeling- or rolling- arm would be present and the assumed equilibrium position of the vessel is no longer valid.

If WADAM completes a run without giving an error one may conclude the numerical calculated input parameters are accurately enough, this is a rather rudimentary check to validate the numerical calculations. Throughout the entire research there have not been any errors due to input parameter miscalculation.

The only parameters that are not subject to a WADAM check are the radii of gyration. The radii of gyration represent how far away mass is allocated relative to the COG. For example the COG may be exactly the same for different radius of gyration.

3.6. Output values

Diffraction software will calculate all matrices incorporating all dynamic properties of the vessel. The mass and inertia properties are determined in form of a mass-inertia matrix (\mathbf{M}) and the frequency dependent added mass ($\mathbf{a}(\omega)$) due to the memory effect. Secondly the frequency dependent damping is calculated ($\mathbf{C}(\omega)$). Thirdly the restoring force matrix is created (\mathbf{K}). Note that the restoring force matrix is independent of the frequency ω .

Besides the matrices, the frequency and encounter angle dependent wave force vector $\underline{F}(\omega, \mu)$ is calculated using the diffraction software. This force vector is determined by the environmental properties defined in section 3.2. The force vector incorporates both a real and imaginary part, corresponding to a magnitude ($|\Re + \Im|$) and phase shift ($\arg(\Re + \Im)$) of the force. The system response is dependent on the environmental properties attributed to the diffraction software calculation. Throughout this research the environmental properties are equal and unaltered.

Within the displayed reference system, see figure 3.6, it is known that a vessel has 3 displacement motions (surge [x], sway [y] and heave [z]) and 3 angular motions (roll [ϕ], pitch [θ] and yaw [ψ]) [9].

Surge and sway motions provide no restoring forces within this reference frame [4]. Imagine pushing a floating rubber duck and giving it a certain forward (surge), sideward (sway) or angular yaw velocity, does the rubber duck return to its initial position from before you pushed the duck? No, there are no restoring forces present to push the duck back in its initial position. Now try to imagine that same duck and either pushing it downwards (heave) or tilting it sideways (roll) or frontward (pitch), does the duck return floating upright?

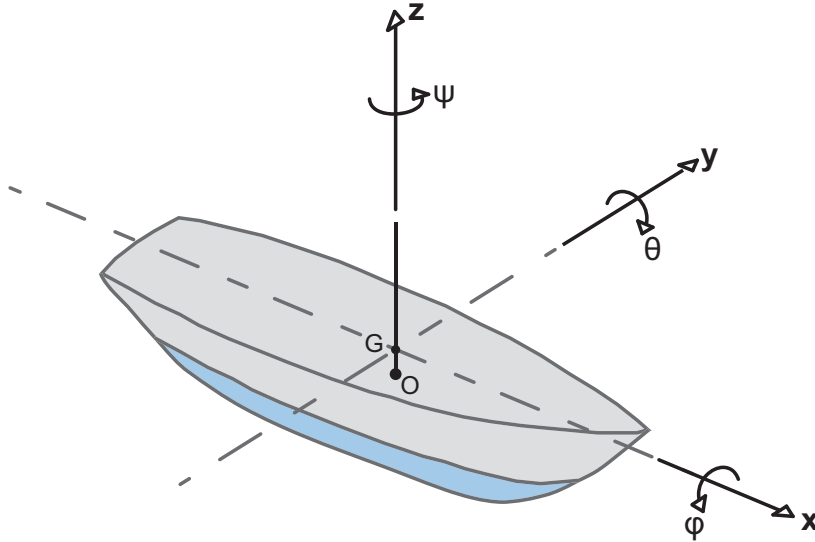


Figure 3.6: 6 degrees of freedom vessel

Yes, the duck will restore its natural equilibrium, this is due to the hydrodynamic restoring forces acting upon the rubber duck.

In general it may be assumed that a offshore lifting vessel has transverse symmetric properties, i.e. port and starboard are symmetrical. The vessel however is asymmetrical within the sagittal plane, hence the bow of the vessel has got a different shape than the stern of the vessel.

Whenever the vessel is transversely symmetric combined with the absence of restoring forces for both surge and sway it gives the reduced form for the matrices [4] as seen in equation 3.21-3.23.

$$\mathbf{M} = \begin{bmatrix} m_{11} & 0 & m_{13} & 0 & m_{15} & 0 \\ 0 & m_{22} & 0 & m_{24} & 0 & m_{26} \\ m_{31} & 0 & m_{33} & 0 & m_{35} & 0 \\ 0 & m_{42} & 0 & m_{44} & 0 & m_{46} \\ m_{51} & 0 & m_{53} & 0 & m_{55} & 0 \\ 0 & m_{62} & 0 & m_{64} & 0 & m_{66} \end{bmatrix} \quad (3.21)$$

$$\mathbf{C} = \begin{bmatrix} c_{11} & 0 & c_{13} & 0 & c_{15} & 0 \\ 0 & c_{22} & 0 & c_{24} & 0 & c_{26} \\ c_{31} & 0 & c_{33} & 0 & c_{35} & 0 \\ 0 & c_{42} & 0 & c_{44} & 0 & c_{46} \\ c_{51} & 0 & c_{53} & 0 & c_{55} & 0 \\ 0 & c_{62} & 0 & c_{64} & 0 & c_{66} \end{bmatrix} \quad (3.22)$$

$$\mathbf{K} = \begin{bmatrix} 0 & 0 & 0 & 0 & 0 & 0 \\ 0 & 0 & 0 & 0 & 0 & 0 \\ k_{31} & 0 & k_{33} & 0 & k_{34} & 0 \\ 0 & k_{42} & 0 & k_{44} & 0 & k_{46} \\ k_{51} & 0 & k_{53} & 0 & k_{55} & 0 \\ 0 & 0 & 0 & 0 & 0 & 0 \end{bmatrix} \quad (3.23)$$

The frequency dependent added mass and damping are of the same size as the static mass and damping matrices (\mathbf{M} and \mathbf{C}). Hydrodynamic diffraction software calculates the frequency dependent matrices and force vector, calculations are performed around a static equilibrium position of the vessel [15]. The obtained matrices and force vectors will be used to describe the dynamics of the vessel, within chapter 4 it will be explained how to use these matrices and how to obtain results.

4

Model set-up



Figure 4.1: Research set-up

As discussed in chapter 2 the most viable model will be numerical, implementing the additional degrees of freedom due to the crane system to couple both the vessel motion and the crane motion. It is known from Coric et. al. [3] the coupled crane vessel system is a 9 degrees of freedom system, three translation motions (surge, sway, heave), three angular vessel motion (roll, pitch, yaw), two degrees of freedom related to the swaying pendulum motion and the last related to the crane cable elongation. However, questions may be asked whether all additional degrees of freedom related to the crane load motion are of influence on the vessel motion. I.e., do the additional degrees of freedom influence the dynamic response or may they be discarded as negligible? This chapter, figure 4.1, will couple the crane terms with the vessel terms as discussed in chapter 3.

Furthermore, it is known that a swaying mass pendulum system is nonlinear. A coupled vessel crane system therefore must in place be a nonlinear system [5]. Therefore the linearity assumption must be validated, this will be done in section 4.2.

As stated in chapter 1, EMAS currently uses a simplified lump loaded system to analyze the vessel motion. The difference in dynamic set-up must be discussed between a lump loaded system and a coupled loaded system seen in section 4.3.

4.1. Degrees of freedom analyzed

Previously it has been established that a vessel has 3 displacement motions (surge [x], sway [y] and heave [z]) and 3 angular motions (roll [ϕ], pitch [θ] and yaw [ψ])[9]. The mass (\mathbf{M}), frequency dependent added mass($\mathbf{a}(\omega)$), frequency dependent damping ($\mathbf{C}(\omega)$), stiffness matrices (\mathbf{K}) and frequency and encounter angle dependent wave force vector ($\underline{F}(\omega, \mu)$) are calculated by means of the diffraction software as discussed in chapter 3.

4.1.1. Crane dynamics

According to Coric et.al. [3] the crane system can be modeled as a simplified 3 degree of freedom pendulum as seen in figure 4.2. The three degrees of freedom are comprised of two angular motions (α and β) and the crane cable elongation (Δl). Defining the equation of motion for this independent dynamic system could easily be computed using the Euler Lagrangian method.

To define whether the designated degrees of freedom (either α , β or Δl) of the crane system will interact with the vessel, the natural frequencies of the independent degrees of freedom must be within reasonable

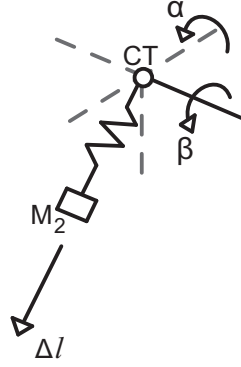


Figure 4.2: 3 degrees of freedom crane

margin of the natural frequency of the vessel. I.e., if an independent natural frequency is much greater than the natural frequency of the vessel it will not cause any exciting motion to the vessel. Hence, a vessel does not respond to higher frequency forces [9]. In general large offshore vessels have a natural frequency for both roll and pitch anywhere between 0.5 and 1.5 rad/s [9], respectively natural frequency periods between 4.2 and 12.6 seconds.

The natural frequency equations for either pendulum swaying motion (ω_p) and crane cable elongation ($\omega_{\Delta l}$) are seen in equation 4.1 - 4.2. Note that the natural frequency for either α or β are irrespective of the crane load M_2 but dependent on merely the crane cable length L_c . The natural frequency for crane cable elongation is both dependent on the mass M_2 , cable cross-sectional area A and crane load M_2 .

$$\omega_p = \sqrt{\frac{g}{L_c}} \quad \text{for: } \alpha(t) \& \beta(t) \quad (4.1)$$

$$\omega_{\Delta l} = \sqrt{\frac{EA}{M_2 L_c}} \quad \text{for: } \Delta l(t) \quad (4.2)$$

$$A = \frac{1}{4} \pi D^2 \quad (4.3)$$

Example crane properties are listed in table 4.1. The crane cable length is evaluated from 10 m to 50 m representative of approximate emerged lifting operations, whenever the crane load would be submerged frictional and viscous terms would inhibit swaying motion. To exemplify the effect of the mass on the independent natural frequencies, the mass is chosen between 100 MT and 400 MT. The Young's modulus E is that of steel and the crane cable diameter is set at 0.10 m. This cable diameter is rather small, especially considering the fact that usually the crane load is suspended from multiple cables. A 100 mm cable has a factored maximum capacity of 250 MT, implying that the 400 MT crane load must be suspended from two crane cables of 100 mm. However, looking at the natural frequency equation of the crane cable elongation, equation 4.2, is linearly proportional to the crane cable diameter ($\omega_{\Delta l} \propto D$). Increasing the cable diameter will inadvertently increase the natural frequency.

Table 4.1: Pendulum properties

	Parameter	Value	Unit
Cable length	L_c	[10 50]	m
Crane load mass	M_2	[$100 \cdot 10^3$ $400 \cdot 10^3$]	kg
Young's modulus	E	$210 \cdot 10^9$	Pa
Cable diameter	D	0.10	m
Cable area	$A = \frac{1}{4} \pi D^2$	$7.9 \cdot 10^{-3}$	m ²

Seen in figure 4.3a -4.3b one can clearly see the natural frequency of the pendulum (α and β) is within the same frequency domain as the natural frequency of vessel movement. The natural frequency for crane cable elongation (Δl) however is nowhere near the natural frequency of a vessel. The natural frequency for crane

cable elongation in this particular case would come into play at a cable length of approximately 1800 meters and beyond. At these cable lengths, a large array of other influences come into play (ex. vibrations of crane cable, hydrodynamic forces on crane cable). This research is limited to air lifts, i.e. lifts where no hydrodynamic effects on either the crane load or crane cable occur. The crane cable is set at an unrealistically small diameter, however increasing the crane cable diameter would only further increase the natural frequency of the crane cable elongation. Therefore it may be concluded that the elongation of the crane cable may be discarded as a noticeable influence on the coupled motion.

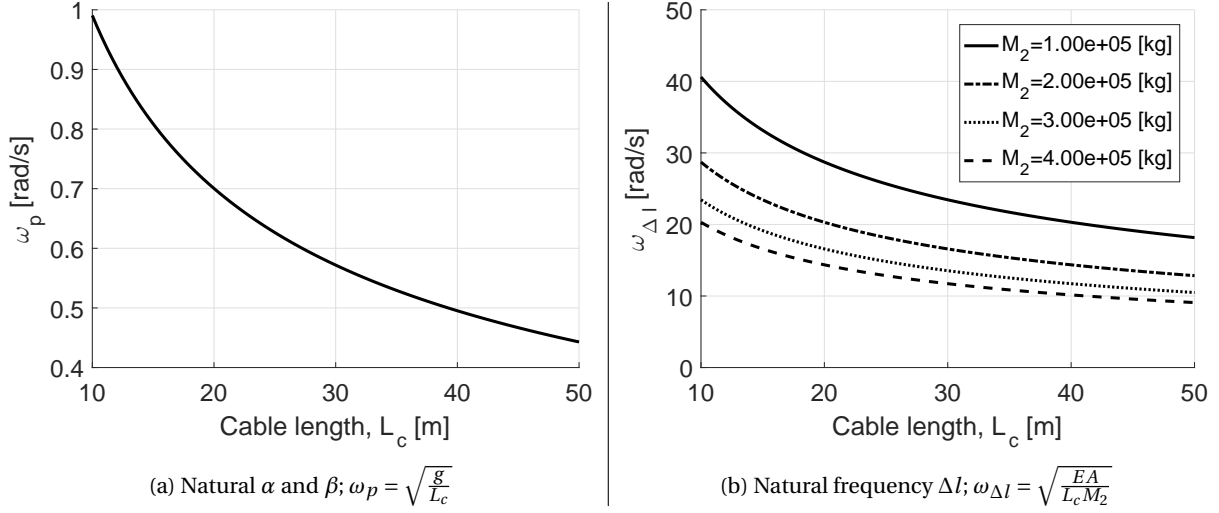


Figure 4.3: Natural frequencies

The equations of motion can now be expanded to include the two additional degrees of freedom $\alpha(t)$ and $\beta(t)$. Additional damping terms related to the swinging load are difficult to accurately measure/compute. K. Ellerman [5] concluded that damping on the swinging load has little to no effect on the dynamics of the system. The natural frequency due to the swaying of the pendulum is not altered due to the damping terms, however the maximum displacement or in this case maximum angular displacement is suppressed by the damping. The crane load damping may be implemented ($c \leq 0.1c_{crit}$). This additional damping will suppress extreme swinging excitation and therefore give more stable results at the natural frequencies.

$$\underline{\eta}(t) = \begin{bmatrix} x(t) \\ y(t) \\ z(t) \\ \phi(t) \\ \theta(t) \\ \psi(t) \\ \alpha(t) \\ \beta(t) \end{bmatrix} \quad (4.4)$$

K. Ellerman [5] has concluded that for a perfectly balanced vessel, heave motion is coupled with other degrees of freedom only through nonlinear terms. However, it can act under certain circumstances as a parametric excitation on the swinging load. What this implies is that the coupling between roll, pitch, load swing and heave motion is a 'one way street' of dynamic interaction. Roll, pitch and swing motion do not effect the dynamic behavior of the vessel in heave, but the heave motion may have effect on the roll, pitch and swing motion.

4.2. Linearity assumption

In order to accurately add the additional degrees of freedom to the coupled system, the terms related to the crane must be linear. It is generally known that the swaying of a pendulum is a nonlinear system [10] and therefore coupled dynamic systems with a swaying pendulum as an independent degree of freedom are nonlinear.

To prove linearity assumptions are valid, a dynamic model representing a generalized barge like vessel may be assumed. This barge like vessel has length, width, height and draft dimensions L_{pp} , B_{pp} , H_{pp} and T_{pp} related to the EMAS vessel Lewek Connector, see table 4.2. The actual design of the Lewek Connector is anything but barge like, but for this 2 degree of freedom example it may be assumed the vessel is a box shaped hull. In this case the hydrostatic properties are easily computed. It is known that the rolling motion of a vessel is the less stable degree of freedom, the model will therefore be set up with respect to the rolling motion of the vessel.

The metacentric height for roll (GM_4) will be used as the contributing restoring force in the system. This may be assumed if the rolling angles of the system are less than 10° [9]. In terms of offshore lifting operability, 10° roll is seen as extreme and non-occurring.

Table 4.2: Vessel properties Lewek Connector

	Parameter	Value	Unit
Length	L_{pp}	153	[m]
Width	B_{pp}	32	[m]
Depth	H_{pp}	12.1	[m]
Draft	T_{pp}	8.5	[m]
Water density	ρ_w	1025	[kg·m ⁻³]
Vessel mass	$M_1 = L_{pp}B_{pp}T_{pp}\rho_w$	$42.7 \cdot 10^6$	[kg]

The crane properties for this 2DOF example are listed in table 4.3 with crane height H_0 , crane cable length L_c and suspended crane load M_2 . The rear view of the 2DOF system can be seen in figure 4.4. Note that the crane load is emerged. The angles displayed are an exaggeration of actual vessel movement.

Table 4.3: Crane properties

	Parameter	Value	Unit
Crane height	H_0	30	[m]
Cable length	L_c	25	[m]
Crane load	M_2	$400 \cdot 10^3$	[kg]

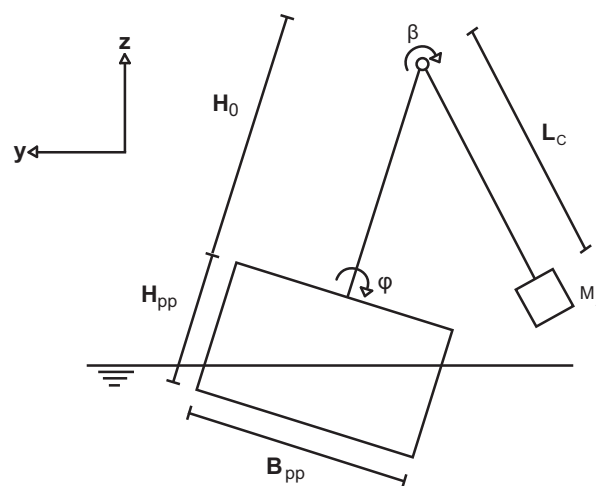


Figure 4.4: 2 degrees of freedom system

The roll restoring force (k_r) within this 2DOF system is defined by the roll metacentric height (GM_4), a measurement of the static stability of a vessel, and the vessel mass (M_1) of a square box shaped vessel as seen in equation 4.6.

$$GM_4 = \frac{1}{2} H_{pp} \left(\frac{T_{pp}}{H_{pp}} - 1 \right) + \frac{B_{pp}^2}{12T_{pp}} \quad (4.5)$$

$$k_r = M_1 GM_4 g \quad (4.6)$$

The vessel has got a certain rotational inertia, assuming that the mass is equally distributed throughout the vessel ¹, the rotational inertia of a vessel may be approximated by the rotational moment of inertia of a square box.

$$J_1 = \frac{M_1}{12} \left(H_{pp}^2 + B_{pp}^2 \right) \quad (4.7)$$

In Appendix A.1, by means of the Euler Lagrangian method, the nonlinear and linear equation of motion are determined for the equation of motion as seen in equation 4.8. Note that the force vector for the nonlinear case, equation 4.11, does not include any zeros. This is not due to any external forcing, the squared and cross terms are better represented within the forcing vector.

$$\mathbf{M}\ddot{\underline{\eta}} + \mathbf{C}\dot{\underline{\eta}} + \mathbf{K}\underline{\eta} = \underline{F} \quad (4.8)$$

$$\text{Where: } \underline{\eta} = \begin{bmatrix} \phi(t) \\ \beta(t) \end{bmatrix}$$

Nonlinear system

$$\mathbf{M} = \begin{bmatrix} H_0^2 M_2 + J_1 & H_0 L_c M_2 (\cos(\phi(t)) \cos(\beta(t)) - \sin(\phi(t)) \sin(\beta(t))) \\ H_0 L_c M_2 (\cos(\phi(t)) \cos(\beta(t)) - \sin(\phi(t)) \sin(\beta(t))) & M_2 L_c^2 \end{bmatrix} \quad (4.9)$$

$$\mathbf{K} = \begin{bmatrix} k_r & 0 \\ 0 & 0 \end{bmatrix} \quad (4.10)$$

$$\underline{F} = \begin{bmatrix} H_0 L_c M_2 (\cos(\phi(t)) \sin(\beta(t)) + \cos(\beta(t)) \sin(\phi(t))) \dot{\beta}(t)^2 + M_2 g H_0 \sin(\phi(t)) \\ H_0 L_c M_2 (\cos(\phi(t)) \sin(\beta(t)) + \cos(\beta(t)) \sin(\phi(t))) \dot{\phi}(t)^2 - M_2 g L_c \sin(\beta(t)) \end{bmatrix} \quad (4.11)$$

Linear system

$$\mathbf{M} = \begin{bmatrix} H_0^2 M_2 + J_1 & H_0 L_c M_2 \\ H_0 L_c M_2 & M_2 L_c^2 \end{bmatrix} \quad (4.12)$$

$$\mathbf{K} = \begin{bmatrix} -M_2 g H_0 + k_r & 0 \\ 0 & M_2 L_c g \end{bmatrix} \quad (4.13)$$

$$\underline{F} = \begin{bmatrix} 0 \\ 0 \end{bmatrix} \quad (4.14)$$

¹Although the mass throughout a vessel is anything but equally distributed, including ballast tanks would ensure the vessel would be at even keel position. Assuming equally distributed mass does not affect the dynamic properties too greatly[15].

Damping terms

No damping terms have been defined in this representation of the vessel, therefore it is assumed the damping is equal to 4% of the critical damping. This rather arbitrary damping amount is relatively small. Increasing the damping would only decrease the maximum error. The critical damping term is a function of the *linear* mass and stiffness matrix. This is also valid for the nonlinear case. This rather arbitrary number is within the maximum damping range ($\mathbf{C} \leq 0.1\mathbf{C}_{\text{crit}}$). This is done to model the energy dissipation caused by the system.

$$\begin{aligned}\mathbf{C} &= 0.04 \cdot \mathbf{C}_{\text{crit}} \\ &= 0.04 \cdot 2\sqrt{\mathbf{K} \cdot \mathbf{M}}\end{aligned}\quad (4.15)$$

$$C_{11} = 0.04 \cdot 2\sqrt{(H_0^2 M_2 + J_1)(-M_2 g H_0 + k_r)} \quad (4.16)$$

$$C_{22} = 0.04 \cdot 2M_2 L_c \sqrt{L_c g} \quad (4.17)$$

$$\mathbf{C} = 0.04 \cdot \begin{bmatrix} 2\sqrt{(H_0^2 M_2 + J_1)(-M_2 g H_0 + k_r)} & 0 \\ 0 & 2M_2 L_c \sqrt{L_c g} \end{bmatrix} \quad (4.18)$$

4.2.1. Time domain response 2DOF

A 60 second free vibration time trace for both the nonlinear and the linear case have been created and compared, seen in figure 4.5. It can clearly be seen that for relatively small initial rolling angles, $0^\circ < \phi(t) < 5^\circ$, the error is small and the system can be assumed to be linear. The maximum error between the linear and nonlinear system are listed in 4.4. For greater rolling angles, $\phi > 10^\circ$, the system will start moving differently, the nonlinear terms would increasingly come into play. Therefore it may be assumed the system is linear, hence rolling angles greater than 5 degrees should never be experienced during operations.

Table 4.4: Maximum error time trace

	Max error $\phi(t)$ [rad]	Max error $\beta(t)$ [rad]
Initial condition $\phi = 1^\circ$	$9.55 \cdot 10^{-6}$	$6.63 \cdot 10^{-5}$
Initial condition $\phi = 3^\circ$	$2.57 \cdot 10^{-4}$	$1.78 \cdot 10^{-3}$
Initial condition $\phi = 5^\circ$	$1.18 \cdot 10^{-3}$	$8.22 \cdot 10^{-3}$
Initial condition $\phi = 10^\circ$	$9.92 \cdot 10^{-3}$	$6.38 \cdot 10^{-2}$

4.2.2. Natural frequencies 2DOF

The (undamped) natural frequencies for the linearized 2DOF system can be calculated according to the research performed by Vu et. al. [10]. Representing the mass and restoring force matrices as factors of α , β^2 and γ , the natural frequencies are calculated according to equation 4.22.

$$\mathbf{M} = \begin{bmatrix} \alpha_1 & \beta_1 \\ \beta_1 & \alpha_2 \end{bmatrix} \quad (4.19)$$

$$\mathbf{K} = \begin{bmatrix} \gamma_1 & 0 \\ 0 & \gamma_2 \end{bmatrix} \quad (4.20)$$

$$|\mathbf{K} - \mathbf{M}\omega^2| = 0 \quad (4.21)$$

$$\omega_{1,2}^2 = \frac{(\alpha_1 \gamma_2 + \alpha_2 \gamma_1) \pm \sqrt{(\alpha_1 \gamma_2 + \alpha_2 \gamma_1)^2 - 4\gamma_1 \gamma_2 (\alpha_1 \alpha_2 - \beta_1^2)}}{2(\alpha_1 \alpha_2 - \beta_1^2)} \quad (4.22)$$

² β does not represent the degree of freedom as seen in figure 4.4. α, β and γ in this case are used to display the indices of the mass matrix \mathbf{M} and restoring force matrix \mathbf{K}

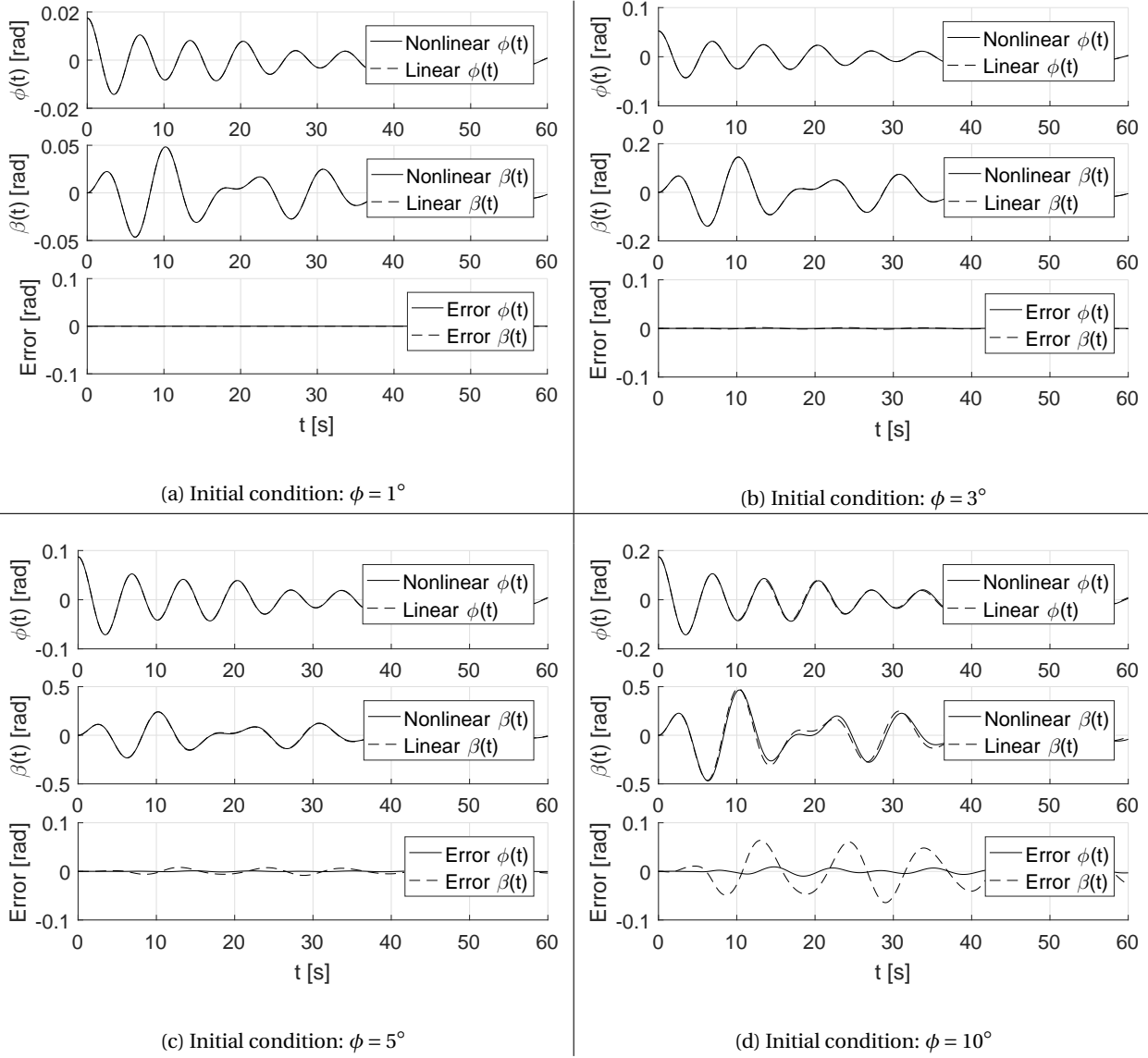


Figure 4.5: Time domain response 2DOF, free vibration

The natural frequencies of the highly simplified barge like vessel are listed in table 4.5. These values will later on be compared with the actual higher degree of freedom system, see chapter 5. It is known from section 4.1.1, that the natural frequency of an independent swaying pendulum is defined as $\omega_p = \sqrt{\frac{g}{L_c}} = 0.63$ [rad/s]. The natural frequency of an independently rolling vessel, vessel without added crane load, can be seen in equation 4.25. The coupled natural frequencies seen in table 4.5 therefore have a natural frequency dependent on the swaying of the pendulum ω_p and a natural frequency dependent on the vessel roll motion ω_v . When comparing the natural frequency of the coupled system, the two natural frequencies observed are slightly skewed compared to the natural frequency of both independent (1DOF) natural frequencies.

Table 4.5: Natural frequencies independent natural frequencies vs. 2DOF

1DOF		2DOF	
ω_p [rad/s]	ω_v [rad/s]	ω_p [rad/s]	ω_v [rad/s]
0.63	0.91	0.60	0.93

$$\omega_v = \sqrt{\frac{k_r}{J_1}} \quad (4.23)$$

$$= \sqrt{\frac{12 \cdot GM_4 g}{H_{pp}^2 + B_{pp}^2}} \quad (4.24)$$

$$= \sqrt{\frac{12 \cdot \left(\frac{1}{2} H_{pp} \left(\frac{T_{pp}}{H_{pp}} - 1 \right) + \frac{B_{pp}^2}{12 \cdot T_{pp}^2} \right) g}{H_{pp}^2 + B_{pp}^2}} \quad (4.25)$$

$$= 0.91 \text{ [rad/s]} \quad (4.26)$$

4.3. Coupling of crane terms

In order to research the effect of dynamic coupling of crane terms, the coupled system must be compared to the current crane load model implemented by EMAS. The current analysis of vessel motion is to load the crane load at the crane tip, seen in figure 4.6. This model does not give any additional degrees of freedom to the 6 degrees of freedom represented by the vessel motion. The additional mass at the crane tip however does give additional terms for the 6 degree of freedom equation of motion. It is established in section 4.1.1 that the coupled system has an additional 2 degrees of freedom represented by the swinging of the load. As established the crane cable elongation is not a viable degree of freedom that would exert coupled vessel motion. In section 4.2 it has been shown that swinging motion of the load may be assumed to be linear. Therefore, the linear terms due to the swinging load may be superpositioned to the 6 degree of freedom system.

The geometric properties as well as the suspended crane load mass will be set as constant throughout the research as seen in table 4.6. The crane characteristics are largely similar to the heavy lift vessel Lewek Champion except for the maximum crane load. The (current) maximum crane load of the Lewek Champion is equal to 800MT. The evaluated vessel however, the Lewek Connector, has a maximum lifting load of 400MT suspended from the largest of the two knuckle boom cranes. To comply with the current maximum lifting load, the maximum lifting load of the Lewek Connector is used as crane load. The crane characteristics therefore are a combination of the crane dimensions of the Lewek Champion combined with the maximum lift capacity of the Lewek Connector.

The cable length is set at 25m, corresponding to emerged lift at which the crane load would be suspended at deck level. At this crane cable length it is known the natural frequency related to the swaying of the crane load is within the same realm as the natural frequency of the vessel response as seen in equation 4.27.

$$\omega_p = \sqrt{\frac{g}{L_c}} = \sqrt{\frac{9.81}{25}} = 0.63 \text{ [rad/s]} \quad 0.5 \text{ [rad/s]} \leq \omega_p \leq 1.5 \text{ [rad/s]} \quad (4.27)$$

The dynamic characteristics of the crane vessel is dependent on the crane properties. If one would change the crane properties the system would be coupled system would be different. The crane properties are set as constant in able to answer the premise of the research, what is the effect of the vessel geometry on dynamic coupled behavior.

Table 4.6: Crane properties

	Value	Unit
Crane height	30	[m]
Overhang crane	15	[m]
Crane cable length	25	[m]
Mass crane load	$400 \cdot 10^3$	[kg]

4.3.1. Lump loaded system

Seen in figure 4.6, the lump loaded 6 degrees of freedom vessel is shown. In this representation the geometric and forcing parameters are defined as seen in table 4.7.

Table 4.7: Parameters vessel 6DOF

L_{pp}	Length vessel
B_{pp}	Width vessel
H_{pp}	Height vessel
T_{pp}	Draft vessel
H_0	Height crane
L_{OH}	Overhang crane
M_2	Mass crane load
CT	Crane tip

In Appendix A.2 the additional mass terms due to the lump loading are determined and listed in equation 4.28. These additional terms may be superpositioned to the 6 degrees of freedom matrices calculated by hydrodynamic diffraction software. It must be noted, the force terms in F_{stat} , equation 4.29, are static forces. These forces may not be superpositioned to the force vector calculated by the hydrodynamic software, in section 4.4 it will be discussed how to implement these static forces. The lump loaded system does not exert any additional degrees of freedom. Therefore the equation of motion remains a similar 6 degree of freedom system as like any other vessel.

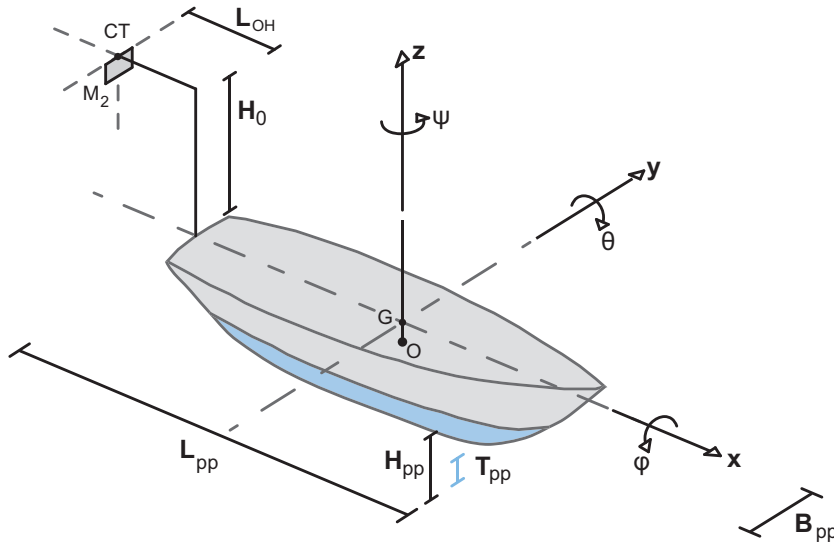


Figure 4.6: Lumped 6DOF system

Due to the reallocation of mass at the crane tip there are super-positioned mass terms. Using the geometry relations, as seen in figure 4.6, the mass terms due to the lump loading at the crane terms are computed by means of Euler Lagrangian formulation seen in Appendix A.2. Where x_{ct} , y_{ct} and z_{ct} are defined as the spatial coordinates of the crane tip with respect to the center of gravity.

$$\mathbf{M} = M_2 \begin{bmatrix} 1 & 0 & 0 & 0 & z_{ct} & -y_{ct} \\ 0 & 1 & 0 & -z_{ct} & 0 & x_{ct} \\ 0 & 0 & 1 & y_{ct} & -x_{ct} & 0 \\ 0 & -z_{ct} & y_{ct} & (y_{ct}^2 + z_{ct}^2) & -x_{ct}y_{ct} & -x_{ct}z_{ct} \\ z_{ct} & 0 & -x_{ct} & -x_{ct}y_{ct} & (x_{ct}^2 + z_{ct}^2) & -y_{ct}z_{ct} \\ -y_{ct} & x_{ct} & 0 & -x_{ct}z_{ct} & -y_{ct}z_{ct} & (x_{ct}^2 + y_{ct}^2) \end{bmatrix} \quad (4.28)$$

Since there are no additional degrees of freedom added to the system no additional damping or stiffness terms will be present. Due to gravitational forces there will be an additional static forcing vector present.

$$\underline{F}_{\text{stat}} = M_2 g \begin{bmatrix} 0 \\ 0 \\ -1 \\ -y_{ct} \\ x_{ct} \\ 0 \end{bmatrix} \quad (4.29)$$

4.3.2. Coupled system

Seen in figure 4.7, the 8DOF coupled system is shown. The two additional degrees of freedom (α and β) related to the swaying of the pendulum and the additional crane cable length (L_c) distinguish the 8DOF system from the 6DOF system. Note that all other dimensional properties are the same as that in the 6DOF system.

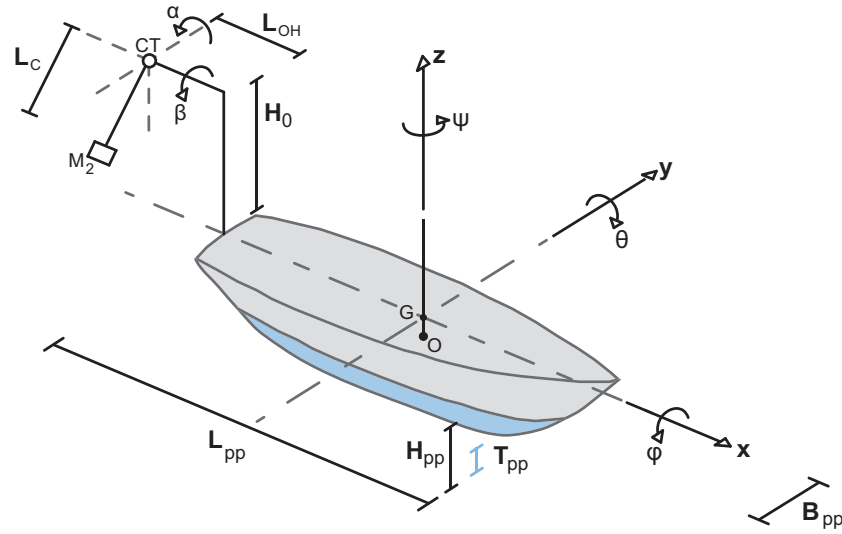


Figure 4.7: Coupled 8DOF system

The additional linearized coupled terms for the 8 degrees of freedom system have been computed in Appendix A.3. Similar to the 6DOF system, these matrices must be superpositioned to the hydrodynamic matrices calculated by the diffraction software. Note that the superpositioning matrices described by the coupled system give 8 by 8 dimensional matrices compared to the 6 by 6 matrices defined by the diffraction software. Therefore the matrices defined by the diffraction will be expanded to include the two additional independent degrees of freedom (α and β) due to the swinging of the crane load.

$$\underline{\mathbf{M}}\dot{\underline{\eta}} + \underline{\mathbf{C}}\dot{\underline{\eta}} + \underline{\mathbf{K}}\underline{\eta} = \underline{\mathbf{F}} \quad (4.30)$$

$$\text{Where: } \underline{\eta} = \begin{bmatrix} x(t) \\ y(t) \\ z(t) \\ \phi(t) \\ \theta(t) \\ \psi(t) \\ \alpha(t) \\ \beta(t) \end{bmatrix}$$

When comparing both the lump loaded superpositioned mass matrix, equation 4.28, with the coupled loaded mass matrix, equation 4.31, it must be noted that both matrices are largely similar except for the terms related to the two additional degrees of freedom related to the swinging of the crane load. Whenever the mass would be hoisted all the way up to the crane tip ($L_c = 0$), both the mass- and stiffness matrix for the coupled loaded case would be exactly the same as that of the lump loaded case.

$$\mathbf{M} = M_2 \begin{bmatrix} 1 & 0 & 0 & 0 & z_{ct} & -y_{ct} & L_c & 0 \\ 0 & 1 & 0 & -z_{ct} & 0 & x_{ct} & 0 & L_c \\ 0 & 0 & 1 & y_{ct} & -x_{ct} & 0 & 0 & 0 \\ 0 & -z_{ct} & y_{ct} & (y_{ct}^2 + z_{ct}^2) & -x_{ct}y_{ct} & -x_{ct}z_{ct} & 0 & -L_c z_{ct} \\ z_{ct} & 0 & -x_{ct} & -x_{ct}y_{ct} & (x_{ct}^2 + z_{ct}^2) & -y_{ct}z_{ct} & L_c z_{ct} & 0 \\ -y_{ct} & x_{ct} & 0 & -x_{ct}z_{ct} & -y_{ct}z_{ct} & (x_{ct}^2 + y_{ct}^2) & -L_c y_{ct} & L_c x_{ct} \\ L_c & 0 & 0 & 0 & L_c z_{ct} & -L_c y_{ct} & L_c^2 & 0 \\ 0 & L_c & 0 & -L_c z_{ct} & 0 & L_c x_{ct} & 0 & L_c^2 \end{bmatrix} \quad (4.31)$$

Since the coupled loaded system has got two additional degrees of freedom related to the swinging of the pendulum, there will be two additional restoring terms acting upon the crane load, equation 4.32. Note that the restoring terms due to the swinging of the pendulum are caused by the gravitational forces acting on the crane load. There are no additional restoring forces acting upon any degree of freedom of the vessel.

$$\{K_{77}, K_{88}\} = M_2 L_c g \quad (4.32)$$

The damping terms related to the swinging of the pendulum is set at 10% of critical damping. This has been done to restrict the maximum motion of the suspended crane load and thus the influence of the crane load on the system. This amount of damping is considered reasonably high, therefore if the 8DOF system would exert dynamic coupled motion, the effects of dynamic coupling would increase for less applied damping.

$$\{C_{77}, C_{88}\} = 0.1 \cdot 2 \sqrt{K_{77} M_{77}} \quad (4.33)$$

$$= 0.2 \cdot M_2 L_c \sqrt{L_c g} \quad (4.34)$$

Similarly to the lump loaded case, due to gravitational forces there will be an additional static forcing vector present. Note that there are no additional forces present related to the two additional degrees of freedom. No forces have been specified to account for forces (ex. wind) acting upon the crane load

$$\underline{F}_{\text{stat}} = M_2 g \begin{bmatrix} 0 \\ 0 \\ -1 \\ -y_{ct} \\ x_{ct} \\ 0 \\ 0 \\ 0 \end{bmatrix} \quad (4.35)$$

4.4. Frequency domain vessel response

The coupled matrices describing either the 6DOF as well as the 8DOF must be evaluated within the frequency domain. The frequency response ($\underline{\eta}_{\text{dyn}}$) is defined as the dynamic response of the vessel to the wave force ($\underline{F}_{\text{dyn}}$). The frequency response is complex valued due to the damping present.

$$\begin{aligned} (-\omega^2 (\mathbf{M} + \mathbf{a}(\omega)) + i\omega \mathbf{C}(\omega) + \mathbf{K}) \tilde{\eta}_{\text{dyn}}(\omega, \mu) &= \tilde{F}_{\text{dyn}}(\omega, \mu) \\ \Rightarrow \tilde{\eta}_{\text{dyn}}(\omega, \mu) &= (-\omega^2 (\mathbf{M} + \mathbf{a}(\omega)) + i\omega \mathbf{C}(\omega) + \mathbf{K})^{-1} \tilde{F}_{\text{dyn}}(\omega, \mu) \end{aligned} \quad (4.36)$$

The magnitude of the frequency response therefore gives the absolute motion at wave frequency ω and encounter angle μ . This frequency domain vessel response relation gives the absolute displacement for the three translatory motions ($x(\omega, \mu)$, $y(\omega, \mu)$ and $z(\omega, \mu)$), the three angular vessel motions ($\phi(\omega, \mu)$, $\theta(\omega, \mu)$ and $\psi(\omega, \mu)$) and, for the 8DOF system, the two additional angular degrees of freedom ($\alpha(\omega, \mu)$ and $\beta(\omega, \mu)$) as seen in equation 4.37. This response function will be used throughout the research as result function where the characteristics of the function gives certain properties regarding the resonance frequencies and maximum exerted motion.

$$\begin{aligned} \text{Magnitude: } & \left| \tilde{\eta}_{\text{dyn}}(\omega, \mu) \right| \\ \text{Where: } & \left| \tilde{\eta}_{\text{dyn}}(\omega, \mu) \right| = \left\| \begin{bmatrix} \tilde{x}(\omega, \mu) \\ \tilde{y}(\omega, \mu) \\ \tilde{z}(\omega, \mu) \\ \tilde{\phi}(\omega, \mu) \\ \tilde{\theta}(\omega, \mu) \\ \tilde{\psi}(\omega, \mu) \\ \sim \tilde{\alpha}(\omega, \mu) \sim \\ \sim \tilde{\beta}(\omega, \mu) \sim \end{bmatrix} \right\| \end{aligned} \quad (4.37)$$

As established in section 4.3.1 and 4.3.2, the allocation of the crane load will also in effect result in a static force ($\underline{F}_{\text{stat}}$) and therefore result in a static response ($\underline{\eta}_{\text{stat}}$). The static response is only defined by the static force and the stiffness matrix \mathbf{K} as seen in equation 4.38. Throughout this research the crane is located dead center at the aft of the ship as seen in figure 4.7. This implies due to the static excitation one would expect a certain initial pitch angle (θ) but no initial rolling angle (ϕ) hence the y-coordinate of the crane tip is equal to 0 ($y_{ct} = 0$). Therefore the static pitch excitation will be evaluated.

$$\underline{\eta}_{\text{stat}} = \mathbf{K}^{-1} \underline{F}_{\text{stat}} \quad (4.38)$$

The total frequency domain vessel response is defined as the static response supplemented to the dynamic frequency response function, equation 4.39. This function represents the maximum excitation from the horizontal unloaded equilibrium at wave frequency ω and wave encounter angle μ . However, throughout this research the dynamic response and static response will be evaluated separately.

$$\left| \underline{\tilde{\eta}}(\omega, \mu) \right| = \left| \tilde{\eta}_{\text{dyn}}(\omega, \mu) \right| + \left| \underline{\eta}_{\text{stat}} \right| \quad (4.39)$$

4.4.1. Phase shift

The phase shift is defined as the angular phase of the transfer function $\underline{H}(\omega)$, equation 4.41. The frequency at which the phase shift is equal to $\pm \frac{1}{2} \pi$ is equal to the natural frequency.

$$\underline{H}(\omega) = \frac{\underline{\eta}_{\text{dyn}}(\omega, \mu)}{\underline{F}_{\text{dyn}}(\omega, \mu)} \quad (4.40)$$

$$\underline{\phi}_p(\omega) = \arg(\underline{H}(\omega)) \in [-\pi, \pi] \quad (4.41)$$

4.4.2. Damping ratio

The damping acting upon the vessel is frequency dependent, a useful measure to define how much damping is present at any given frequency is through the damping ratio. As like the frequency response function the damping ratio is dependent on the frequency ω , hence both the damping and added mass are frequency dependent.

$$\underline{\zeta}(\omega) = \frac{\mathbf{C}(\omega)}{\mathbf{C}_{\text{crit}}(\omega)} = \frac{\mathbf{C}(\omega)}{2\sqrt{\mathbf{K}(\mathbf{M} + \mathbf{a}(\omega))}} \quad (4.42)$$

Seen in figure 4.8 an example damping ratio figure is shown. The damping ratio at low forcing frequencies ($0 < \omega < 0.3$ [rad/s]), the damping ratio is equal to zero.

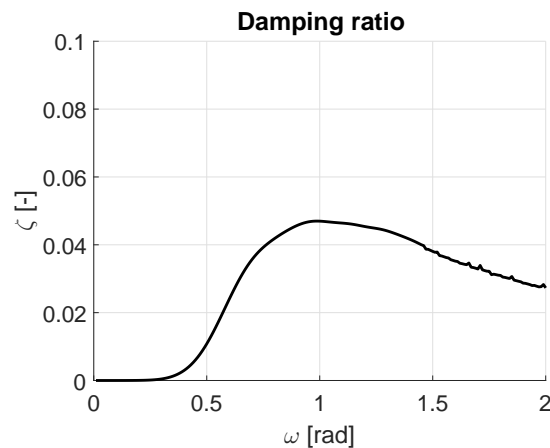


Figure 4.8: Example damping ratio

It is known that the damping ratio applied to the crane load is set at 10% critical damping. The crane load damping therefore is constant and independent of the frequency ω .

4.4.3. Example frequency response and phase shift

In section 4.1 it has been established that dynamic coupling will only influence roll (ϕ) and pitch (θ) motion, both angular displacements. Seen in figure 4.9 an example frequency response, figure 4.9a, accompanied with the phase shift, figure 4.9c is shown. The large peak in the frequency response, figure 4.9a, represents the resonance frequency with corresponding peak height representing the maximum motion at the resonant frequency. The maximum roll and pitch motion throughout the research may not be greater than 5° , any greater excitation is beyond the maximum operability excitation and secondly from section 4.2 it is known that for greater excitation the linearity assumptions are no longer valid.

Although the frequency shift through $\pm \frac{1}{2}$ would be the natural frequency, this research focuses on the highest peak within the frequency response, representing the resonance frequency. This is an important difference, hence due to damping the resonance frequency will be slightly different from the natural frequency. This effect is called resonance transmission. This effect can be seen in figures 4.9b representing a frequency response, accompanied by figure 4.9d representing the phase shift. Note that the x-axis shows a dimensionless scale, representing the frequency over the natural frequency (ω/ω_n). For an increasing damping ratio ζ , the resonance frequency increasingly differs from the natural frequency of the system. Similarly due to the damping the phase shift 'jump' becomes more gradual for increasingly large damping ratios.

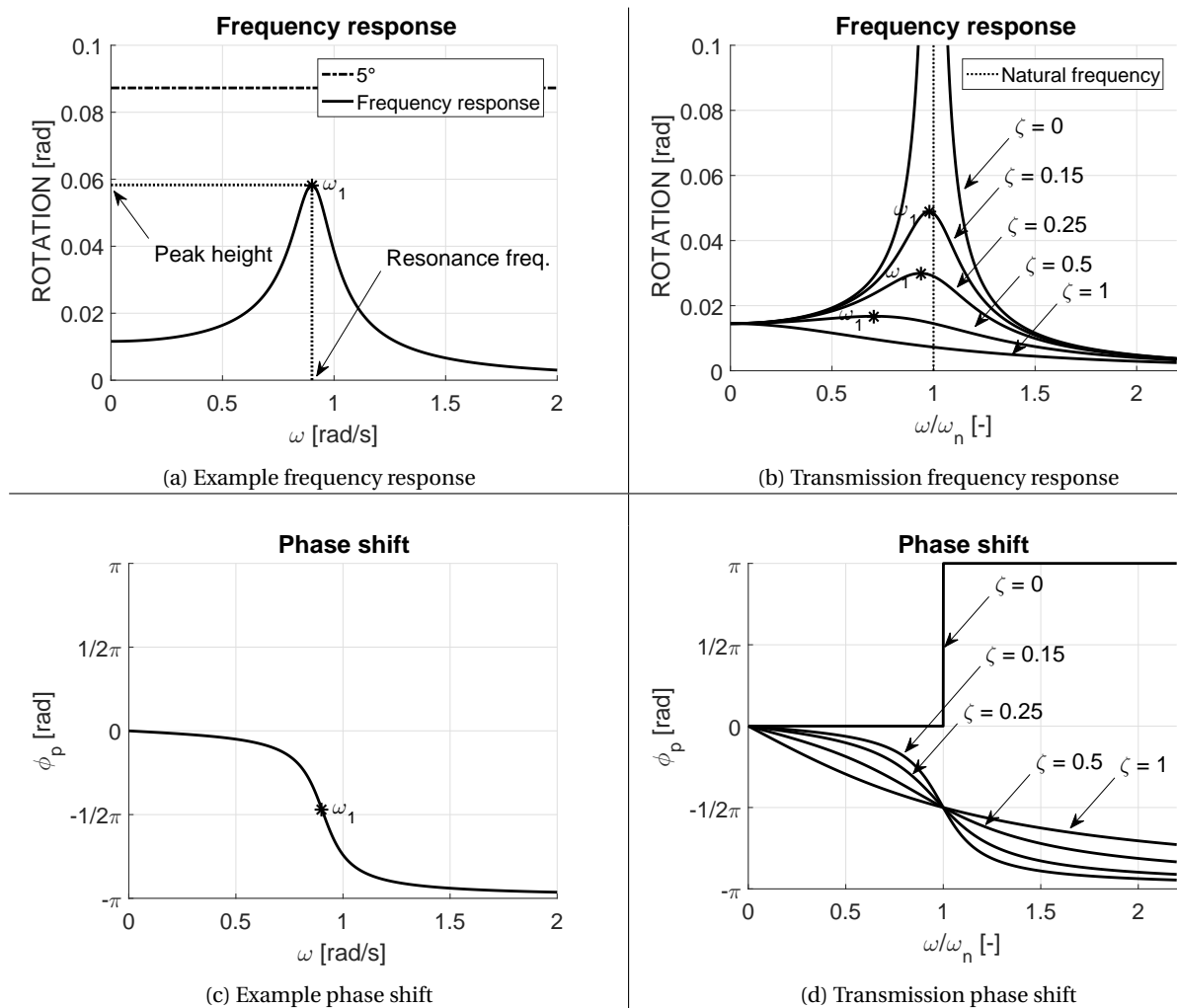


Figure 4.9: Example frequency response, transmission and phase shift

4.4.4. Sensitivity relations

Comparing frequency response graphs several relations can be made that give insight into the characteristics of the system. Seen in figure 4.10, four example frequency response graphs are set out to illustrate relations of interest.

The *frequency shift*, figure 4.10a, whilst comparing frequency responses gives insight into the transience of the resonance frequencies.

The *peak shift*, figure 4.10b, of two comparative frequency responses gives insight into the maximum motion at the resonance frequency of the system. Hence a higher peak implies a greater amplitude response of the system. Whenever the peak height increases substantially ($ROTATION \gg 0.1$ [rad]) one may conclude the vessel has disastrous resonance implying the vessel will 'tip over'.

If the system show dynamic *coupled motion*, the frequency response would show two resonance frequencies. I.e., the frequency response would display two prominent peaks, see figure 4.10c. This research focuses on the interaction of the vessel movement and the swaying of the crane load. It has already been shown in section 4.2.2 that a simple 2DOF system has two separate natural frequencies, ω_v and ω_p .

If the resonance frequencies of the coupled system converge towards each other, *strong dynamic coupled motion* will occur. This implies that only a single peak will become present. Although two natural frequencies may be present in the system, the frequency response will only show a single resonance frequency peak.

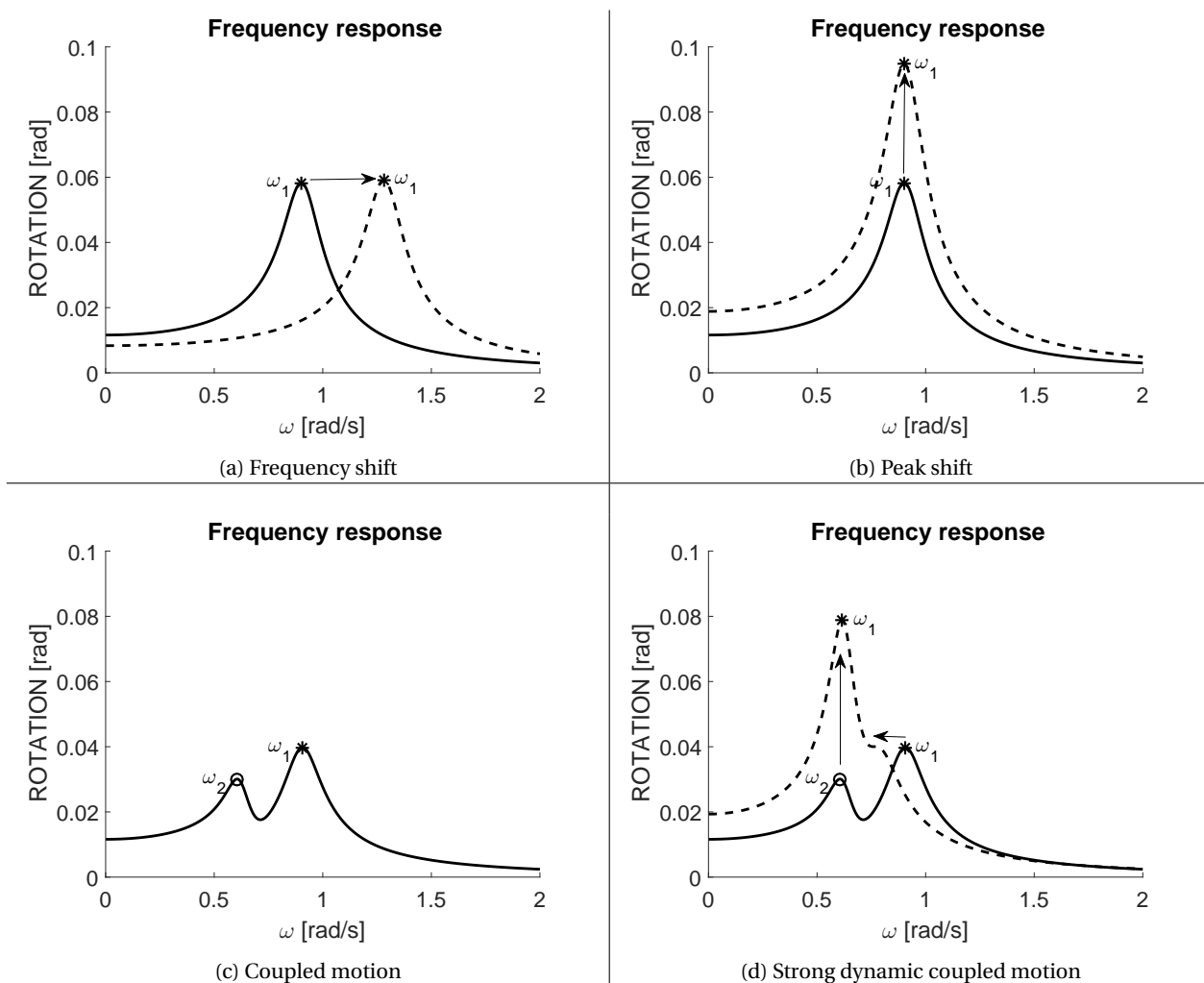


Figure 4.10: Frequency response function relations

4.4.5. Effective excitation, root mean square (RMS)

Although the frequency response relations give a good characterization of the system, it lacks the ability to describe how much the average motion will be. For example, given two separate frequency responses, as exemplified in figure 4.11, which of the two response figures will illustrate the most motion? It is known that the dashed frequency response will have a larger maximum response at the resonance frequency compared to the solid line frequency response, hence the peak height is greater. However, for most other frequencies the dashed frequency response is less than the solid frequency response. An extremely narrow banded sharply peaked frequency response could very well give a large excitation at the resonance frequency but very limited excitation at all other frequencies.

To define the effective excitation of the system, the root mean square or RMS of the system must be computed. The root mean square represents the quadratic average of the response function giving an effective excitation of the system. A greater RMS excitation implies that the average motion in effect is greater. The RMS value for a continuous function $f(x)$ over interval $x_1 \leq x \leq x_2$ is defined by equation 4.43.

$$f_{\text{RMS}} = \sqrt{\frac{\int_{x_1}^{x_2} f(x)^2 dx}{x_2 - x_1}} \quad (4.43)$$

The RMS value for the frequency response is defined by the dynamic frequency excitation (η_{dyn}) part. Hence, the static excitation does not illustrate the effect of the wave force acting upon the system. Regarding the dynamics of the system the static part therefore should not be taken into account. Since the frequency response is defined over the interval $0 \leq \omega \leq \omega_{\text{max}}$, the RMS of the system is defined by equation 4.44.

$$\eta_{\text{RMS}} = \sqrt{\frac{\int_0^{\omega_{\text{max}}} |\eta_{\text{dyn}}(\omega, \mu)|^2 d\omega}{\omega_{\text{max}}}} \quad (4.44)$$

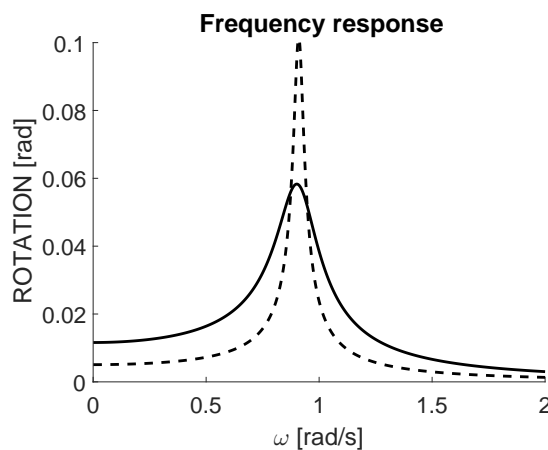


Figure 4.11: Example frequency responses

Subquestions

2. What induces crane load coupled motion on a crane vessel?

A crane system has got three degrees of freedom, the degree of freedom related to the elongation of the crane cable however has been proven to not exert any dynamic coupled motion. Even for an unrealistically small cable diameter and at great cable lengths the dynamic elongation motion does not influence the vessel motion. Dynamic coupled motion therefore will only be induced by the swaying of the crane load, namely swaying in either longitudinal- or perpendicular- direction of the vessel.

5

Base case analysis

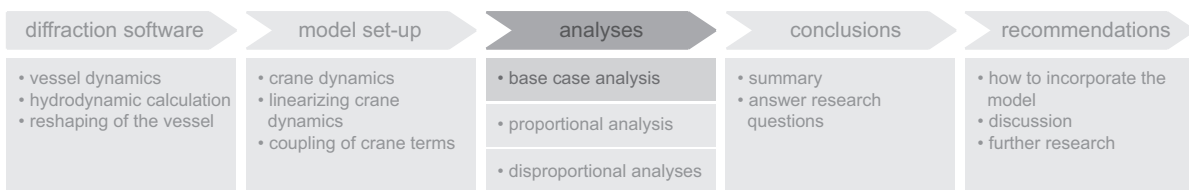


Figure 5.1: Research set-up

The base case scenario refers to the unaltered vessel, where all dimensional sensitivity multipliers are equal to 1.00, equation 5.1.

$$\underline{\lambda} = \begin{bmatrix} \lambda_X \\ \lambda_Y \\ \lambda_Z \end{bmatrix} = \begin{bmatrix} 1.00 \\ 1.00 \\ 1.00 \end{bmatrix} \quad (5.1)$$

The base case analysis, figure 5.1, will comparatively evaluate the lump loaded (6DOF) and coupled loaded (8DOF) system. If the effects of dynamic coupling in this case are noticeable, it will most likely have an effect throughout the sensitivity analyses. Established in chapter 4, the only degrees of freedom that exert coupled motion due to the swinging of the crane load are roll and pitch. To quantify the effect of dynamic coupling on the base case, the effect on the natural frequency, peak height and RMS excitation must be evaluated. If there would be a coupled effect due to the suspended crane load, the dynamic characteristics should be noticeably different compared to the current analysis of lump loading at the crane tip.

While discussing the results the roll governed motion, roll (ϕ) and perpendicular pendulum sway motion (β), will be discussed. Secondly the pitch governed motion, pitch (θ) and longitudinal pendulum sway motion (α), will be discussed.

In order to represent the data as clear as possible, the resonance frequency dependent on the vessel movement is referred to as ω_v and the resonance frequency dependent on the swaying of the pendulum is referred to as ω_p . This will be useful to distinguish the occurring resonance frequencies. It has been chosen to focus on the first resonance frequency due to the vessel movement.

In section 4.4 it has been shown that the frequency response depends on both the wave frequency (ω) and the wave encounter angle (μ). A total of 15 encounter angles are evaluated, however displaying 15 frequency response functions for both roll and pitch will become rather confusing. Therefore a single encounter angle that displays the effects of dynamic coupling best is chosen. Following and quartering seas give notoriously large vessel motion for both pitch and heave, therefore the quartering encounter angle of $\mu = 135^\circ$ has been chosen to exemplify the effect of dynamic coupling. Shifting to a more pitch governed vessel response encounter angles ($0^\circ < \mu < 45^\circ$ v $135^\circ < \mu < 180^\circ$), one would expect less coupled roll motion but an increased coupled pitch motion if present. Similarly, if the encounter angles would be shifted towards a more roll dominated encounter angle ($45^\circ < \mu < 135^\circ$) one would expect more coupled roll motion and less coupled pitch motion if present.

The relative effects of dynamic coupling appeared to be irrespective of the encounter angle, therefore an encounter angle of $\mu = 135^\circ$ will best exemplify the effects of dynamic coupling hence both roll and pitch will largely be present.

5.1. Roll governed motion

Looking at the roll motion frequency response, phase shift and damping ratio displayed in figure 5.2, it can be seen that the rolling characteristics for the 6DOF- and 8DOF- system are different. The displayed resonance frequency of the 6DOF system, figure 5.2a, appears to be at a lower frequency compared to the 8DOF resonance frequency related to the vessel motion ω_v . Lump loading the mass at the crane tip, the rotational moment of inertia is greater compared to suspending the crane load from the crane cable, resulting in a lower resonant frequency. The resonance frequency peak height, figure 5.2a, for the 6DOF system appears to be greater than the resonance frequency peak of the 8DOF system (ω_v). Lump loading the crane load at the tip of the crane will inadvertently make the system rather 'top heavy'.

Considering the 8DOF system, figure 5.2a, it can be observed that there is a prominent second resonance frequency peak (ω_p). This is exactly what one would expect with respect to dynamic coupled motion. The natural frequency of an 1DOF independent swaying pendulum system and the natural frequency of a vessel, seen in section 4.1.1, can be calculated using equation 5.2 and 5.3. Note that the 1DOF natural frequency related to the vessel motion ω_v is a function for a box shaped vessel. The Lewek Connector is nowhere near a box shaped vessel nor does this function incorporate the memory effect of the vessel, added mass is not present, therefore the natural frequency related to the roll motion of the vessel is an approximation.

$$\omega_p = \sqrt{\frac{g}{L_c}} = \sqrt{\frac{9.81}{25}} = 0.63 \text{ [rad/s]} \quad (5.2)$$

$$\omega_v \approx \sqrt{\frac{12 \cdot \left(\frac{1}{2} H_{pp} \left(\frac{T_{pp}}{H_{pp}} - 1 \right) + \frac{B_{pp}^2}{12 \cdot T_{pp}} \right) g}{H_{pp}^2 + B_{pp}^2}} = 0.91 \text{ [rad/s]} \quad (5.3)$$

Table 5.1: Natural/resonance roll frequencies, 1DOF, 2DOF and 8DOF

1DOF		2DOF		8DOF(@ $\mu = 135^\circ$)	
ω_p [rad/s]	ω_v [rad/s]	ω_p [rad/s]	ω_v [rad/s]	ω_p [rad/s]	ω_v [rad/s]
0.63	0.91	0.60	0.93	0.62	0.91

Comparing the natural/resonance frequencies, see table 5.1, for either the independent motion frequencies (1DOF), the highly simplified model defined by Vu et. al [10](2DOF) and the more complex model described in this research (8DOF), it can be seen that the natural frequency the 2DOF system compared to the resonance frequencies of the 8DOF system are rather similar to one another.

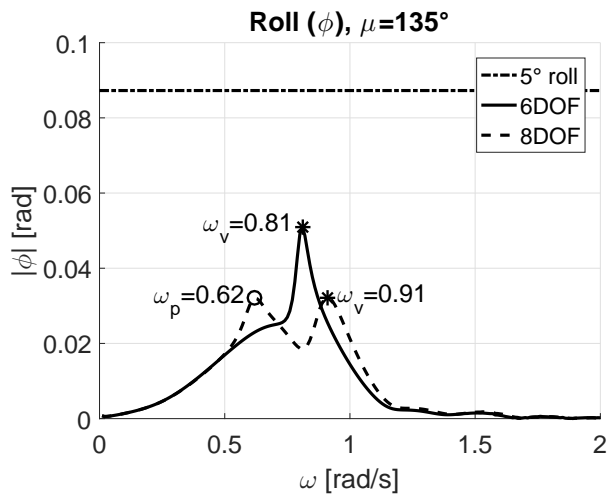
For the base case scenario, where the geometric properties have yet to be altered, the 2DOF system actually appears to have a rather good approximation in comparison to the resonance rolling frequencies of the 8DOF system. However, as explained in section 2.1 the 2DOF system is oversimplified and could give differences most likely as contribution of the simplification.

Comparing the effective roll motion defined by the RMS of the frequency response of both the 6DOF and 8DOF system in table 5.2, the 6DOF system will exert more roll effective roll motion. I.e., the 6DOF system will move more due to the incoming waves.

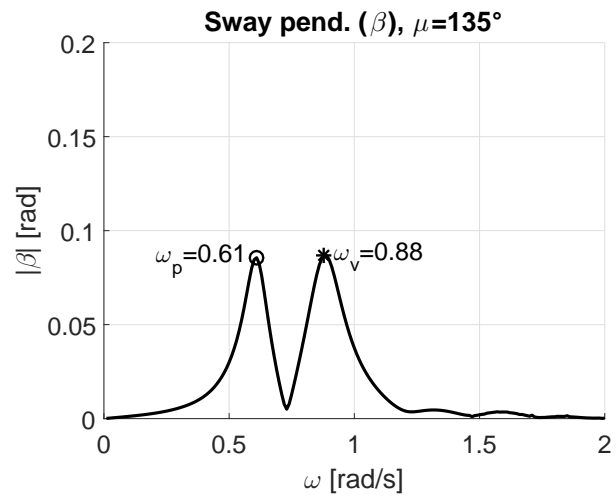
Table 5.2: RMS roll 6DOF vs. 8DOF

RMS roll 6DOF	RMS roll 8DOF	Difference
$1.48 \cdot 10^{-2}$ [rad]	$1.40 \cdot 10^{-2}$ [rad]	-5.9%

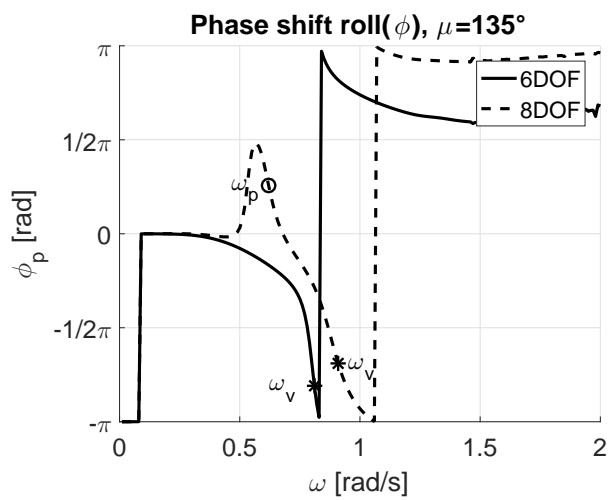
One would expect a similar coupled motion behavior regarding the resonance frequencies of the crane load motion. I.e., the pendulum would also exert multiple resonance frequencies. If the swaying crane load motion would not show dynamically coupled behavior with the vessel motion, the resonance frequency would be (largely) similar to the natural frequency of the independent swaying of a pendulum ($\omega_p = \sqrt{\frac{g}{L_c}}$).



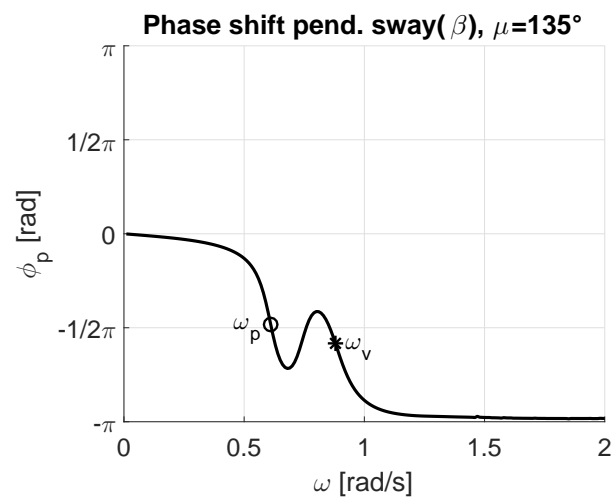
(a) Frequency response roll



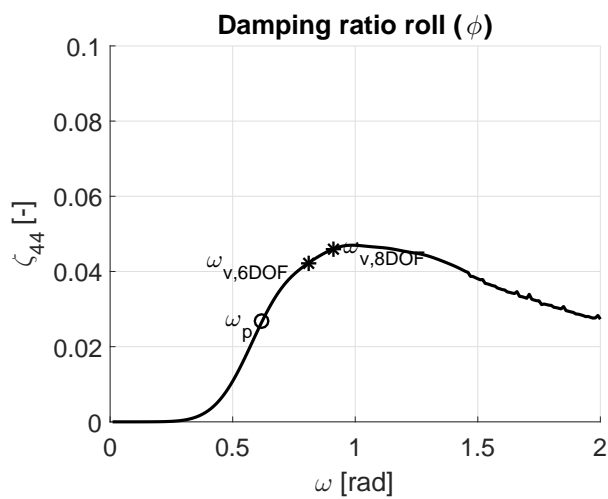
(b) Frequency response perpendicular sway



(c) Phase shift roll



(d) Phase shift perpendicular sway



(e) Damping ratio roll

Figure 5.2: Roll frequency response, phase shift and damping ratio base case, roll

Looking at the perpendicular pendulum swaying motion (β) frequency response and phase shift seen in figure 5.2b and 5.2d, there are two clear peaks visible related to the resonance frequency of either the swaying pendulum (ω_p) and the vessel motion (ω_v). This implies that the vessel shows dynamic coupled motion with the swaying of the pendulum. Regarding the peak height of the frequency response, figure 5.2b, both peaks appear to be approximately equal in height. The perpendicular swaying motion of the pendulum therefore is not dominated by a single motion.

5.2. Pitch governed motion

Considering the pitch motion frequency response, phase shift and damping ratio, figure 5.3, it can be concluded that the 8DOF system does not exert any different behavior compared to the 6DOF system. Both the shape of the frequency response, the occurring resonance frequency and phase shift are almost exactly the same. Moreover the longitudinal crane load swaying motion shows a single resonance frequency peak and therefore does not show any dynamic coupled motion.

Table 5.3: RMS pitch 6DOF vs. 8DOF

RMS pitch 6DOF	RMS pitch 8DOF	Difference
$1.03 \cdot 10^{-2}$ [rad]	$1.02 \cdot 10^{-2}$ [rad]	-1.1%

Moreover the RMS pitch excitation for both the 6DOF- and 8DOF- system, table 5.3, are almost similar. Therefore it may be concluded that for the base case, the swaying of the crane load does not have an effect on the pitch motion. I.e., dynamic coupled motion due to the crane load does not occur within pitch motion. This however does not imply dynamic coupled motion for pitch will not be present throughout the sensitivity analyses, hence whenever geometric properties of the vessel will be altered, the dynamic characteristics of the vessel inadvertently will be changed.

Seen in figure 5.3b, it can be seen that the swaying of the pendulum in longitudinal direction (α) shows a single large peak. This is exactly what would be expected when comparing this motion with the frequency response of the pitch motion, hence the 8DOF pitch motion also only exerts a single resonance frequency. However, the resonance frequency of the swaying pendulum is not dependent on the vessel motion but by the swaying of the pendulum itself. What this implies is that both the pitch motion and the longitudinal swaying motion of the pendulum are independent of on another.

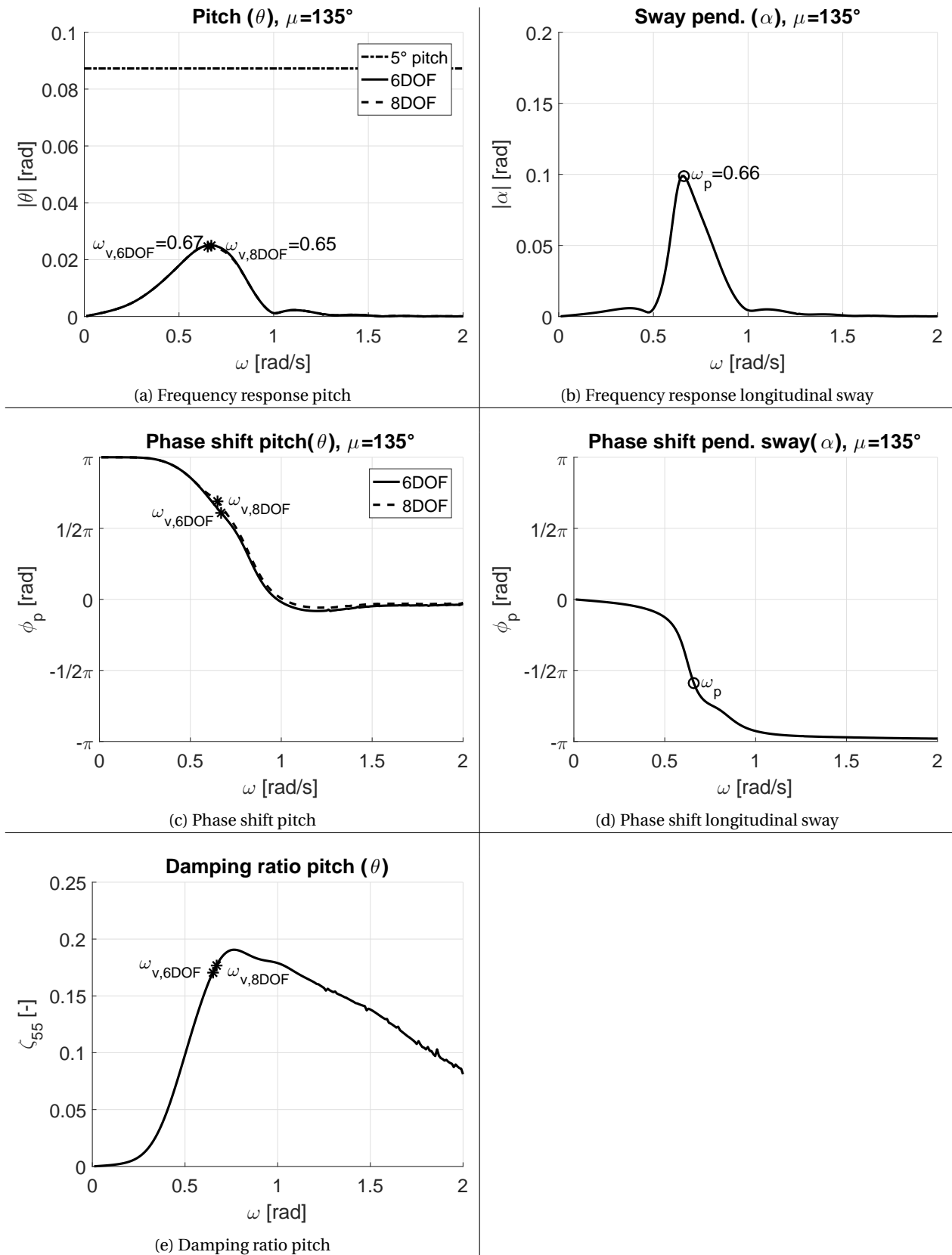


Figure 5.3: Frequency response, phase shift base case and damping ratio, pitch

5.3. Polar representation

As displayed in section 5.1 and 5.2, only a single encounter angle is shown to exemplify the effect of dynamic coupled motion. Another representation of the data is to polar plot ω_v and, if present, ω_p of all encounter angles. However, properties regarding the peak height, phase shift and the effective excitation (RMS excitation) is not known.

Due to the transverse symmetry of the vessel, there should not be any rolling excitation at encounter angles $\mu = 0^\circ$ and $\mu = 180^\circ$. The diffraction software WADAM will always have an extremely small error compiling the vessel from the geometry file. Therefore the vessel will be ever so slightly asymmetric in transverse direction. This asymmetry will therefore imply there would be rolling excitation for encounter angles $\mu = 0^\circ$ and $\mu = 180^\circ$. Looking at the data, the frequency response at both encounter angles give a maximum rolling excitation of $2.98 \cdot 10^{-19} \approx 0$ [rad]. This computational asymmetry error therefore may be neglected.

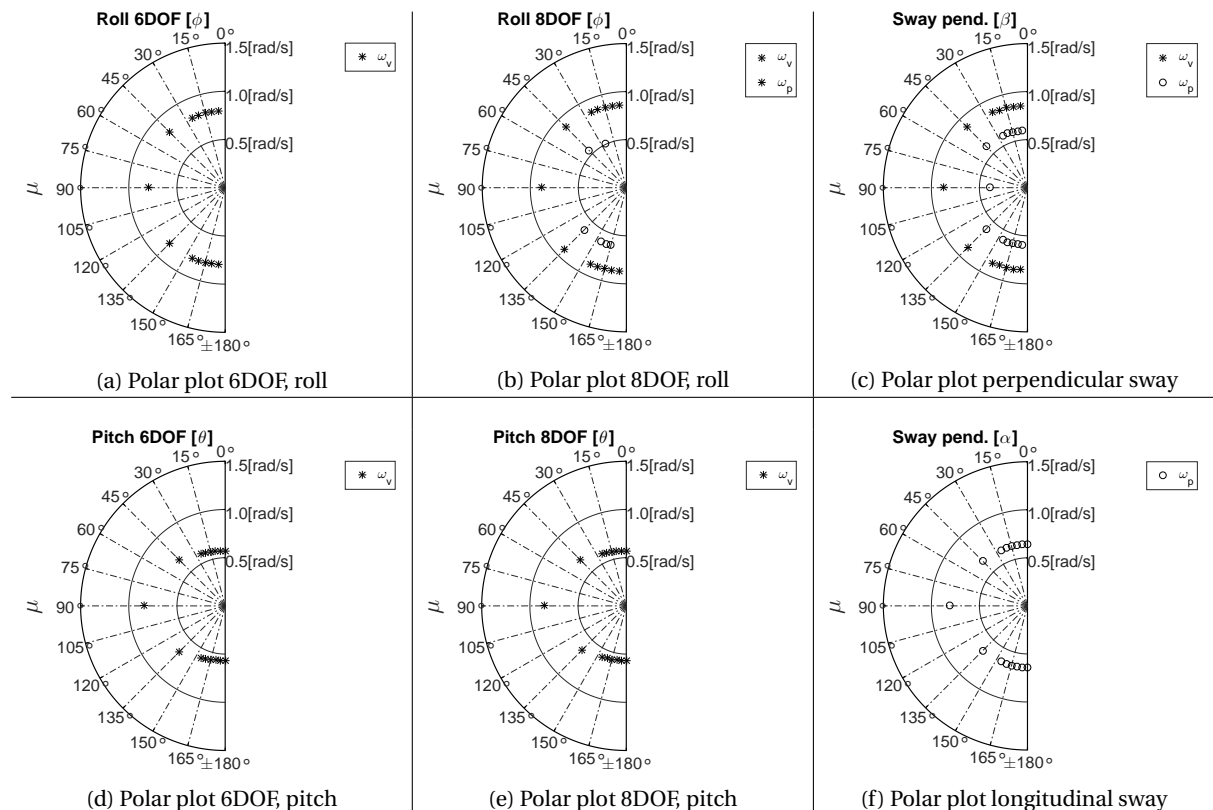


Figure 5.4: Polar plot base case

Seen in figure 5.4 both ω_v and ω_p are set out for roll, pitch and the two additional degrees of freedom caused by the swaying of the pendulum. Note that it has been chosen to display β in figure 5.4c first and α in figure 5.4f second. As previously stated rolling motion interacts with the perpendicular motion of the swinging crane load (β) and pitch motion interacts with the longitudinal motion of the swaying pendulum (α). Representing the data in this order, the interaction between either roll and perpendicular swaying motion or pitch and longitudinal swaying motion can be better evaluated.

Comparing the roll motion for the 6DOF system, figure 5.4a, with the rolling motion for the 8DOF system, figure 5.4b, it can be seen that the resonance frequencies are entirely different from one another. This is in consonance with the previous asserted notion that the rolling motion is dynamically coupled with the perpendicular swaying motion of the crane load.

Due to the asymmetric sagittal plane, the vessel rolling motion should induce pitching motion at mostly roll governed encounter angles ($45^\circ < \mu < 135^\circ$). This can clearly be seen in figure 5.4d and 5.4e. The natural frequency for pitch motion increases whenever roll motion becomes more dominant compared to pitch motion. I.e., at $\mu = 90^\circ$ the resonance frequency for pitch motion is equal to the resonance frequency of the rolling motion.

If the vessel would show dynamically coupled pitch motion, one would expect the frequency response to

have two resonance frequency peaks. This however is not the case regarding the pitch motion, no second resonance frequency related to the swaying of the pendulum can be seen. Similar to the pitch motion of the vessel the resonance frequency for the longitudinal swaying motion of the pendulum appears to be become more dependent on rolling motion at encounter angle $\mu = 90^\circ$.

5.4. Conclusion base case analysis

A first and rather important conclusion to be made is that the current representation EMAS considers to be correct (6DOF system) has its shortcomings in reflecting the true nature of a heavy lift offshore operation. Although motion for pitch motion is modeled almost correctly within this representation, for roll motion this model deviates from the coupled loaded (8DOF) system. Lump loading the load at the crane tip will make the vessel inherently unstable and increases the rotational moment of inertia, with consequences regarding the calculated vessel response. The 6DOF system misrepresents the occurring resonance frequencies, does not account for the resonance frequency related to the swaying of the pendulum, the effective motion is different compared to the the more complex 8DOF system. Therefore, the 6DOF system will no longer be evaluated in further sensitivity studies.

Subquestions

4. *Does dynamic crane load coupled motion occur during current operations and is this significant with respect to current method of analysis?*

It has been proven that the coupled system exerts different resonance rolling frequencies compared to the current set-up for the Lewek Connector. Within the roll governed motion of the coupled system (roll and perpendicular crane load swaying motion) there are two resonance frequencies present compared to the single resonance frequency of the current analysis. The resonance rolling frequency of the current system is only dependent on the vessel motion and will always be at a lower frequency compared to the resonance frequency of the coupled system.

Due to the allocation of the crane mass at the tip of the crane, the vessel is modeled as top heavy with negative consequences. The maximum exerted roll motion at the resonance frequency will therefore be greater compared to the coupled system. Similarly the effective motion of the current system is greater than the coupled system, implying the current system will exert more motion than the coupled system.

Summing up the differences between the current and coupled models, the current model has its shortcomings in reflecting the true nature of a heavy lift offshore operation. Firstly, the current system misrepresents the resonance frequencies. Secondly the maximum exerted motion at the resonance frequency for the current model is greater compared to the coupled model. Lastly the current model will exert more motion than the coupled system. Dynamic coupled crane load motion therefore is absolutely significant.

6

Proportional sensitivity analysis

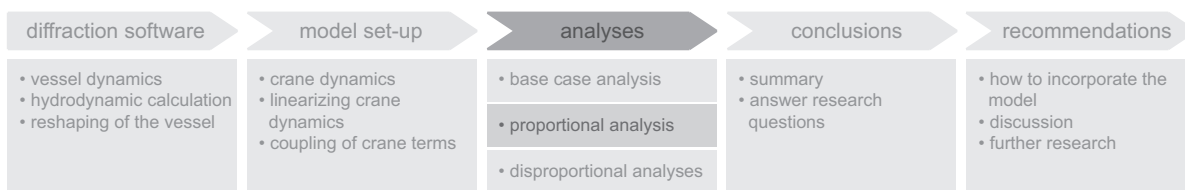


Figure 6.1: Research set-up

As explained in section 3.3, the proportionally sensitized vessel has equal sensitivity multipliers in either X-, Y- or Z- direction, equation 6.1. This implies that the relative geometric proportions are not altered throughout this sensitivity analysis. The vessel will be made smaller for $\lambda < 1.00$ and respectively larger for $\lambda > 1.00$.

$$\lambda_X = \lambda_Y = \lambda_Z = \lambda \quad (6.1)$$

$$\underline{\lambda} = \begin{bmatrix} \lambda_X \\ \lambda_Y \\ \lambda_Z \end{bmatrix} = \begin{bmatrix} 0.75 \\ 0.75 \\ 0.75 \end{bmatrix}, \quad \begin{bmatrix} 1.00 \\ 1.00 \\ 1.00 \end{bmatrix}, \quad \begin{bmatrix} 1.25 \\ 1.25 \\ 1.25 \end{bmatrix} \quad (6.2)$$

Established in chapter 5, the base case scenario already shows dynamically coupled rolling motion. Performing a proportional sensitivity study, figure 6.1, will evaluate whether the geometric properties of the vessel are of influence towards the dynamic coupled motion of the vessel. It is known that smaller vessels are more susceptible to excitation due to external forcing. Hence, by Newton's second law of motion the acceleration of an object is both dependent on the mass and the forcing applied. Not altering the properties related to the crane and the crane load will imply that the dynamic forcing, caused by the swaying of the crane load, relative to the mass of the vessel will in fact be more profound.

In chapter 5 it has been shown that the 6DOF system is considered to be an incorrect representation of reality. The 6DOF system will therefore not be included within this- and further sensitivity analyses. In Appendix C a similar analysis has been performed for a 6DOF- system showing an increase in inaccuracy for increasingly smaller vessels.

It has also been established that the base case pitch motion and longitudinal swaying motion of the pendulum do not show coupled motion behavior. If the pitch governed motion does not show coupled motion throughout the proportional sensitivity analysis, it may be concluded that pitch governed motion by no means will show dynamically coupled motion for the disproportional sensitivity analyses, hence the disproportional sensitivity analysis will only examine the effect of the dimensional properties of either the length, width and height of the vessel. The frequency response will be evaluated for two separate sensitized cases in comparison with the base case vessel, equation 6.2. Again the encounter angle of $\mu = 135^\circ$ has been chosen to exemplify the relations between the dynamic properties and the sensitivity multiplier λ . At this encounter angle the effects of dynamic coupled motion are most noticeable, the effects discussed appear to be mostly invariant to the encounter angle.

6.1. Roll governed motion

Seen in figure 6.2 the static relations with respect to the sensitivity multiplier λ can be seen. Looking at the static relations, it can be seen that a smaller vessel ($\lambda < 1.00$) will become increasingly less statically stable, hence the roll metacentric height of the vessel, figure 6.2b decreases. Both the mass, figure 6.2a, as well as the radii of gyration, figure 6.2c, are positively dependent on the sensitivity multiplier λ . A larger vessel will have a greater mass and a larger radii of gyration, both related to the moment of inertia of the vessel ($I = kx^2 \cdot M$).

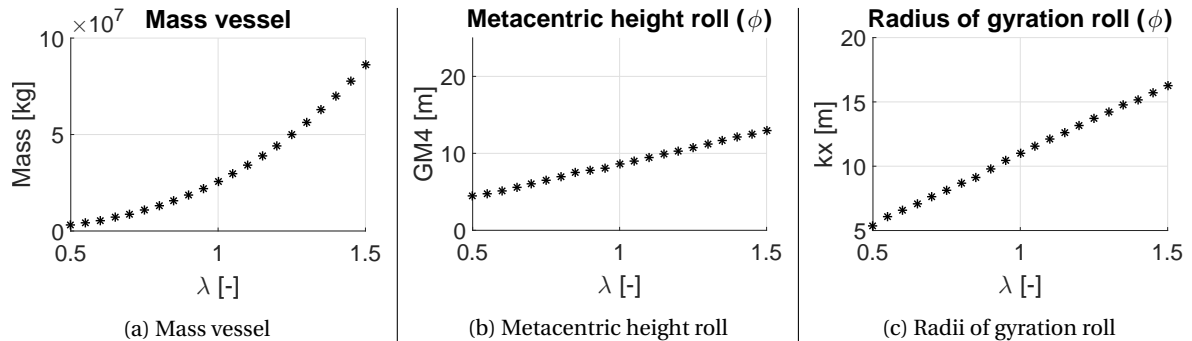


Figure 6.2: Static relations, roll

Looking at the frequency response of the 8DOF system, figure 6.3a, the two prominent peaks related to the resonance frequency of the rolling motion of the vessel and the swaying motion of the pendulum are noticeable. The resonance frequency related to the swaying of the pendulum (ω_p) appears to be invariant to the scaling multiplier and is roughly ($\omega_p \approx 0.60$ rad/s). The peak height however is negatively correlated to the sensitivity multiplier, the peak becomes greater for smaller vessels. This negative dependency will in fact cause the pendulum motion to become the dominant resonance frequency over the resonance frequency related to roll for smaller vessels¹. I.e., the peak height related to the pendulum motion ω_p will become greater for smaller vessels and therefore will be the most governing motion regarding the roll of the vessel. The resonance frequency related to the rolling motion of the vessel (ω_v), does appear to be negatively dependent to the sensitivity multiplier. Implying a higher resonance frequency for smaller vessels.

The peak height increase of the resonance frequency related to the swaying of the pendulum (ω_p) for the roll motion appears to be caused by the decrease of damping. Figure 6.3e shows that a smaller vessel in general exerts comparatively less critical damping than a larger vessel. This effect therefore has rather negative consequences on the maximum excitation at the resonance frequency.

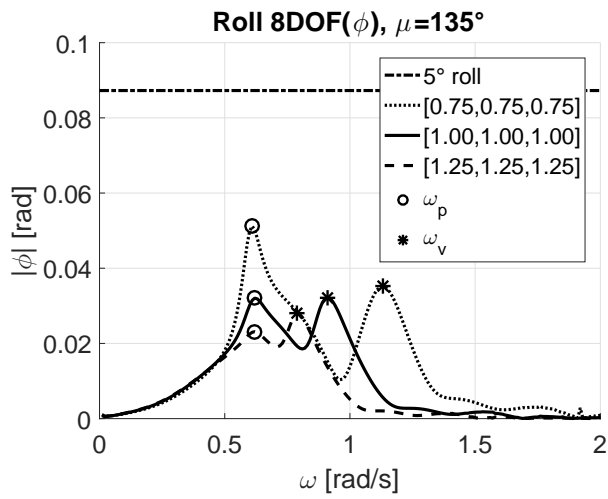
Within the perpendicular pendulum swaying motion frequency response, seen in figure 6.3b, two prominent resonance peaks are visible, again related to the swaying of the pendulum (ω_p) and the rolling of the vessel (ω_v). The resonance frequency related to the swaying of the pendulum, does not appear to differ throughout the sensitivity analysis. I.e., for larger vessels the resonance frequency related to the swaying of the pendulum appears to be similar to that of a smaller vessel. The resonance frequency related to the roll motion of the vessel however appears to be negatively related to the sensitivity multiplier. I.e., for larger vessels, the resonance frequency related to the roll motion of the vessel will be lower than the resonance frequency of a smaller vessel. The resonance frequency due to the rolling motion for the larger vessel appears to converge towards the resonance frequency of the pendulum motion.

The effective motion (RMS) for both the roll motion as well as the perpendicular swaying motion, table 6.1 show a negative dependency on the sensitivity multiplier λ . A larger vessel will effectively exert less motion than a comparatively smaller vessel.

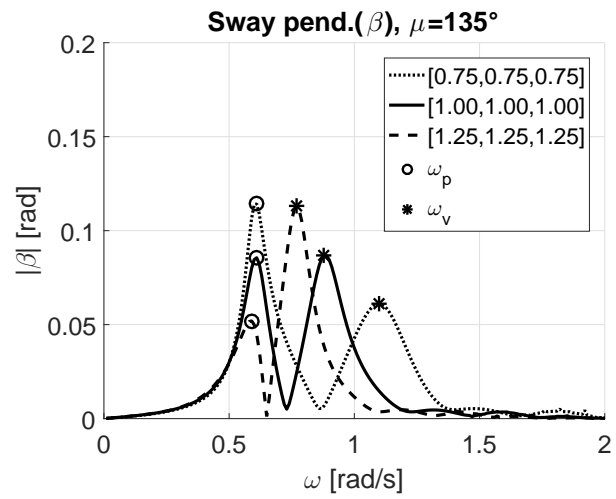
Table 6.1: RMS roll and perpendicular sway

λ	RMS roll	RMS perpendicular sway
[0.75; 0.75; 0.75]	$1.89 \cdot 10^{-2}$ [rad]	$3.32 \cdot 10^{-2}$ [rad]
[1.00; 1.00; 1.00]	$1.40 \cdot 10^{-2}$ [rad]	$3.01 \cdot 10^{-2}$ [rad]
[1.25; 1.25; 1.25]	$1.07 \cdot 10^{-2}$ [rad]	$2.92 \cdot 10^{-2}$ [rad]

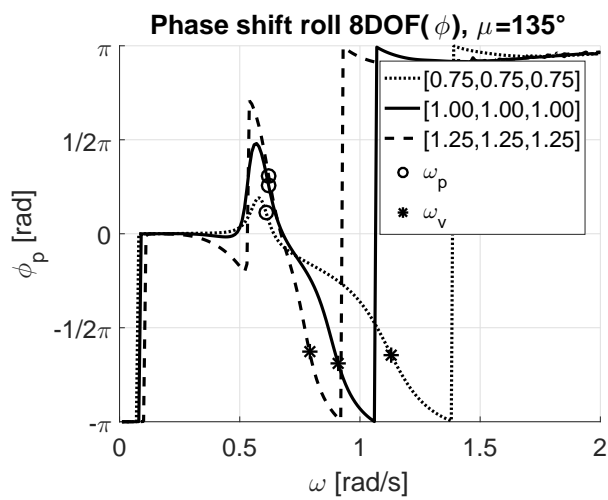
¹This will later be discussed when discussing figure 6.5



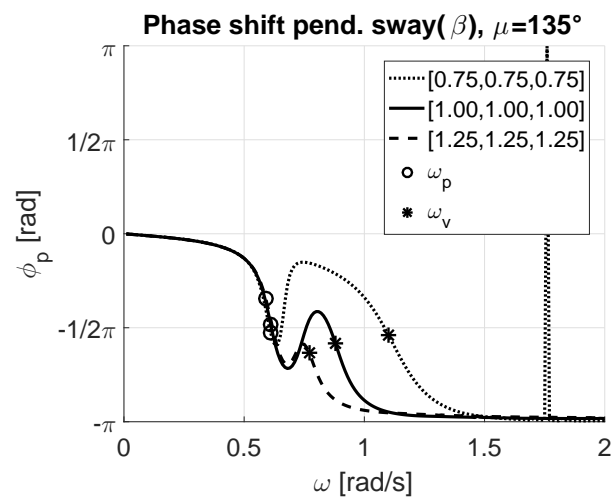
(a) Frequency response roll 8DOF



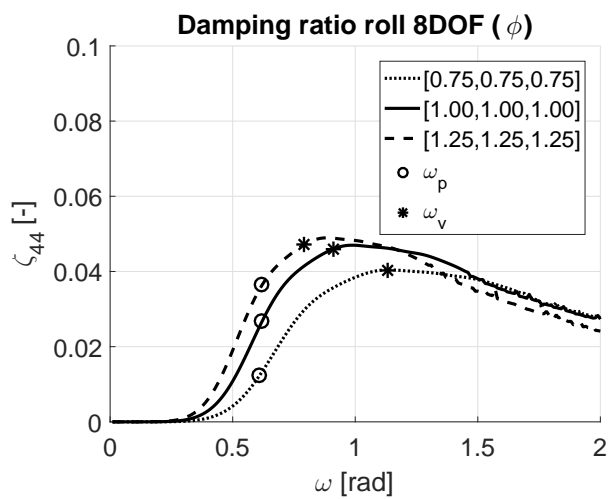
(b) Frequency response perpendicular sway



(c) Phase shift roll 8DOF



(d) Phase shift perpendicular sway



(e) Damping ratio roll 8DOF

Figure 6.3: Frequency response, phase shift and damping ratio roll governed motion

6.1.1. Frequency shift roll governed motion

To further justify the relations made regarding the frequency shift of the resonance frequency for the roll governed motion, the resonance frequency due to vessel motion (ω_v) and, if present, the resonance frequency due to the swaying of the pendulum (ω_p) are set out comparative to the sensitivity multiplier λ . Again encounter angle $\mu = 135^\circ$ is chosen to exemplify the resonance frequency relations. Representing the frequency shift in this manner however incapacitates the ability to see which of these two resonance frequencies is more dominant. Therefore, the peak shift of the two resonance frequency must subsequently be set out as function of the sensitivity multiplier λ .

Seen in figure 6.4 the resonance frequency due to the vessel movement and, if present, the resonance frequency due to the swaying pendulum are set out with relation to the sensitivity multiplier λ for roll motion and perpendicular crane load swaying motion. The horizontal axis displays the sensitivity multiplier and the vertical axis shows the resonance frequencies.

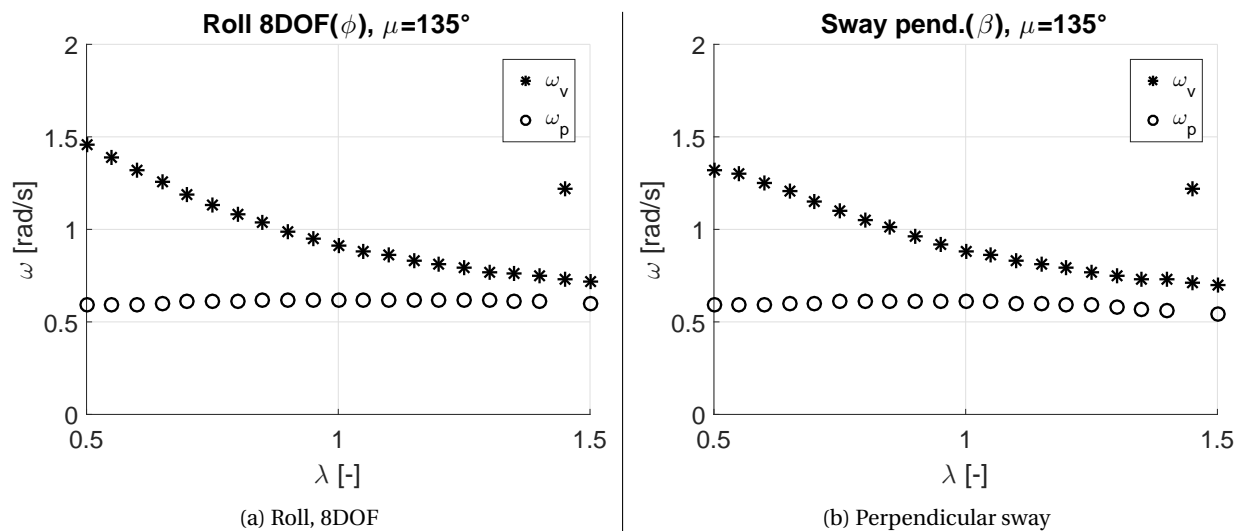


Figure 6.4: Frequency shift roll governed motion

Both the roll motion as well as the perpendicular swaying motion exert almost similar behavior regarding both resonance frequencies. The resonance frequency due to vessel motion appears to have a nonlinear negative dependency on the sensitivity multiplier λ . Thus, for smaller vessels ($\lambda < 1.00$) the resonance frequency due to the vessel motion will be greater. The resonance frequency due to the swaying of the pendulum (ω_p) is constant throughout all sensitivity multipliers.

6.1.2. Peak shift roll governed motion

Evaluating the peak height of both the resonance frequency due to the vessel movement (ω_v) and if present the resonance frequency due to the swaying of the pendulum (ω_p) will give insight into which of the two resonance frequencies is dominant and will give insight into the motion exerted at the resonance frequencies. Hence, a larger peak at the resonance frequency implies more motion. Figure 6.5 shows this relation with respect to the sensitivity multiplier λ . The horizontal axis displays the sensitivity multiplier and the vertical axis shows the resonance frequency peak values (I.e. the height of the peak in the frequency response function) representing the maximum motion at the resonance frequency.

As seen in the roll frequency response of figure 6.3a the peak height related to the pendulum swaying motion (ω_p) increases for increasingly smaller vessels. For vessels smaller than $\lambda \leq 0.90$ the resonance rolling frequency actually becomes dominated by the swaying of the pendulum motion, hence the peak height due to the resonance frequency of the pendulum is greater than the resonance frequency due to the vessel motion² ($\omega_p > \omega_v$). Even for a system that has considerable crane load damping, as like the system evaluated, the swaying of the pendulum becomes dominant for smaller vessels. The peak height increase related to the pendulum motion is clearly non linear, it increases significantly for increasingly smaller sensitivity mul-

²Note that this is dependent on the damping applied to the swaying of the crane load, whenever the damping becomes less, the swaying crane load motion becomes more dominant. Throughout this research the damping at the crane load is set at 10% critical damping. This amount of damping is considered rather large.

multipliers. For sensitivity multipliers less than $\lambda < 0.60$ the maximum exerted motion related to the crane load resonance frequency will in fact be greater than the maximum allowed 5° of roll motion. For vessel sizes smaller than $\lambda < 0.60$ this will imply the motion is too large and secondly the model is no longer valid hence the linear system no longer represents the true nature of the motion.

Contrary to the peak height related to the pendulum motion, the peak height related to the vessel motion clearly decreases nonlinearly for increasingly small sensitivity multipliers. Implying less motion due to vessel motion for increasingly smaller vessels.

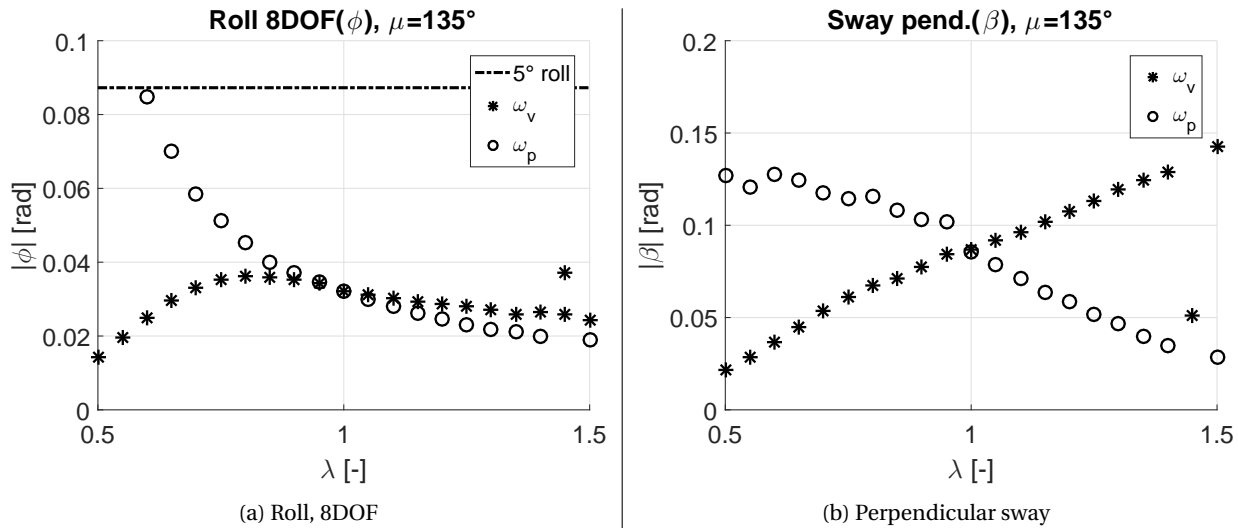


Figure 6.5: Peak height shift roll governed motion

The conclusion therefore can be made that for increasingly smaller vessel dimensions, the swaying of the pendulum will in fact become the dominant motion of the system. For increasingly smaller vessel geometry, the rolling motions will therefore be highly dependent on the movement of the suspended crane load.

The peak height related to the vessel motion for sensitivity multipliers greater than $\lambda > 1.00$ do not seem to decrease as significantly. For increasingly larger vessels the peak related to both the vessel and pendulum motion ever so slightly decrease, however the peak related to the swaying of the pendulum slightly decreases more than the peak related to the vessel motion. Implying the pendulum will have a decreasing effect on the vessel motion for increasingly large vessels.

Looking at the peak height sensitivity for the perpendicular pendulum sway motion, figure 6.5b, it does not exert similar behavior to the rolling motion of the 8DOF system. The peak height of the resonance frequency due to the vessel motion (ω_v) appears to be positive linearly dependent on the sensitivity multiplier and the peak height related to the swaying of the pendulum appears to be negatively dependent on the sensitivity multiplier. Implying the motion of the crane load will become more dominated by the resonance frequency related to the vessel motion for larger vessels. Similarly the crane load motion will become dominated by the resonance frequency related to the swaying of the pendulum for smaller vessels.

6.1.3. Roll damping ratio shift

Previously it has been established that both the damping ratio at the resonance frequency related to the vessel motion (ω_v) and, more importantly, the damping ratio at the resonance frequency related to the pendulum motion (ω_p) decreases. The damping ratio dependency on the sensitivity multiplier λ is in clear coalescence with that assertion, seen in figure 6.6. The damping ratio at the resonance frequency related to the pendulum motion (ω_p) decreases linearly for increasingly smaller vessels and approaches zero at $\lambda = 0.50$. This is in consonance with the peak height sensitivity seen in figure 6.5a, hence the peak height increases significantly for increasingly smaller vessels. Besides the decrease in damping, the decrease of the metacentric height, as seen back in figure 6.2b, also contributes to the increase of roll motion at the resonance frequency related to the crane load motion (ω_p) for increasingly smaller vessels.

Regarding the damping at the resonance frequency related to the vessel motion (ω_v), it can be seen that the damping ratio decreases more than linearly for increasingly smaller vessel sizes. Therefore, one would also expect a higher peak height at these sensitivity multipliers, as established in figure 6.5a, the peak height

related to the vessel motion actually decreases for increasingly smaller vessel sizes. This is all due to the frequency shift of the resonance frequency related to the vessel motion. Smaller vessels will have increasingly higher resonance frequencies related to the vessel motion. The wave force at higher frequencies is smaller and will therefore exert less motion.

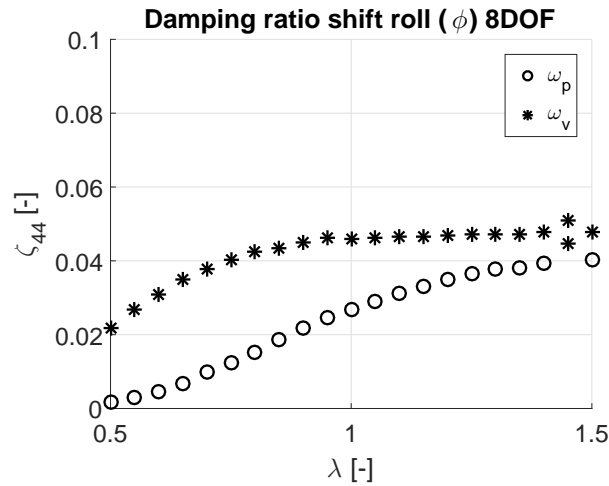


Figure 6.6: Damping ratio shift roll

6.1.4. Effective excitation (RMS) roll governed motion

The effective exerted roll motion, figure 6.7a has a clear nonlinear negative dependency to the sensitivity multiplier. This implies there will be more motion for smaller vessels, this is in consonance with the observed frequency response as seen in figure 6.3a and peak height shift seen in figure 6.5, hence for smaller vessels the frequency response appeared to be much broader and for smaller vessels the peak height increases due to the swaying of the pendulum. The effective exerted pendulum swaying motion, figure 6.7b, does not show a clear trend. The effective motion over all sensitivity multipliers appears to be rather constant and therefore invariant of the sensitivity multiplier λ .

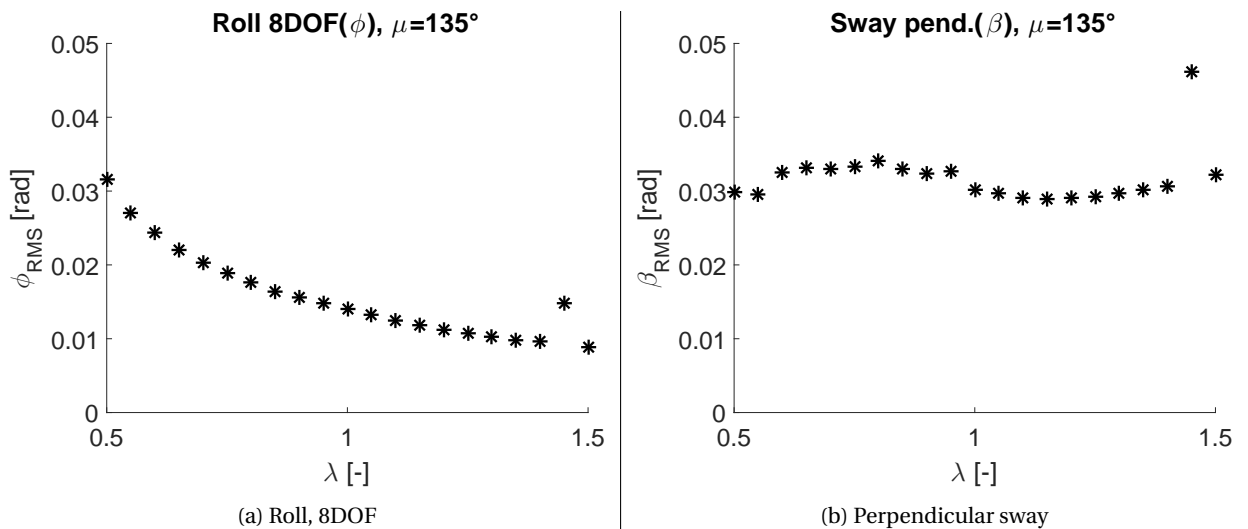


Figure 6.7: Root mean square roll governed motion

6.2. Pitch governed motion

Looking at the static pitch relations as seen in figure 6.8, it can be seen that both the pitch metacentric height, figure 6.8b, and pitch radius of gyration, figure 6.8c, are much greater compared to the roll motion. Pitch motion therefore is statically more stable than roll.

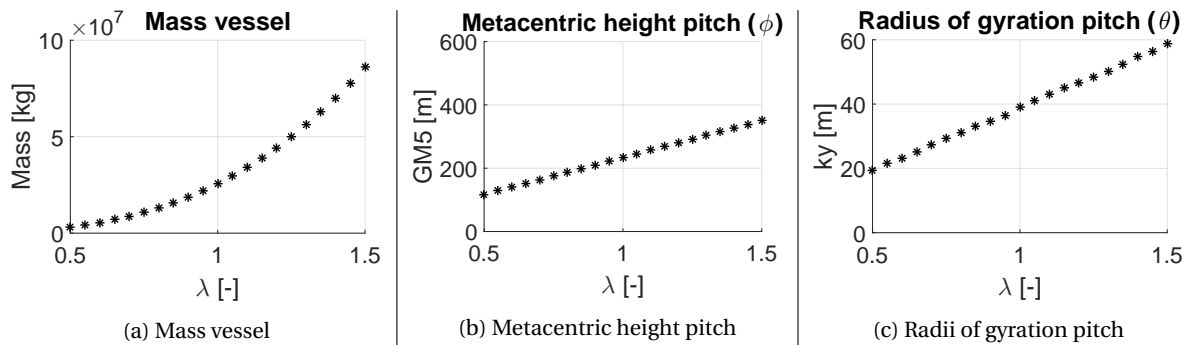


Figure 6.8: Static relations, pitch

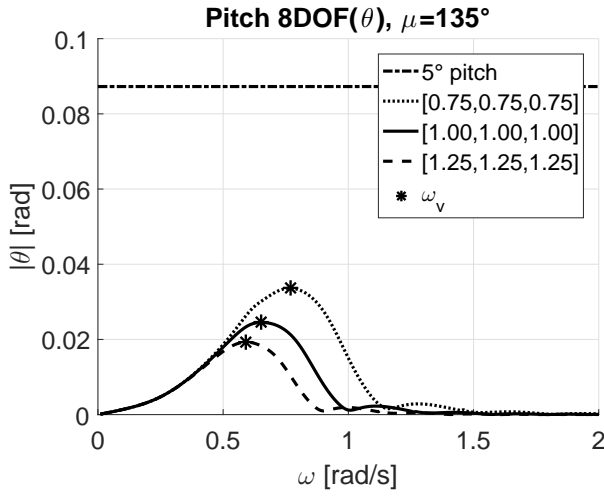
Seen in figure 6.9, the frequency response, phase shift for both pitch as well as longitudinal pitch motion and pitch damping ratio are illustrated.

Whilst discussing the frequency response for the pitch governed motion a first and rather essential observation must be made regarding the pitch motion, figure 6.9a. Neither the larger vessel $\lambda = 1.25$ nor the smaller vessel $\lambda = 0.75$ seems to exert any coupled motion behavior. Equally, the longitudinal crane load swaying motion, figure 6.9b, shows a single resonance frequency peak.

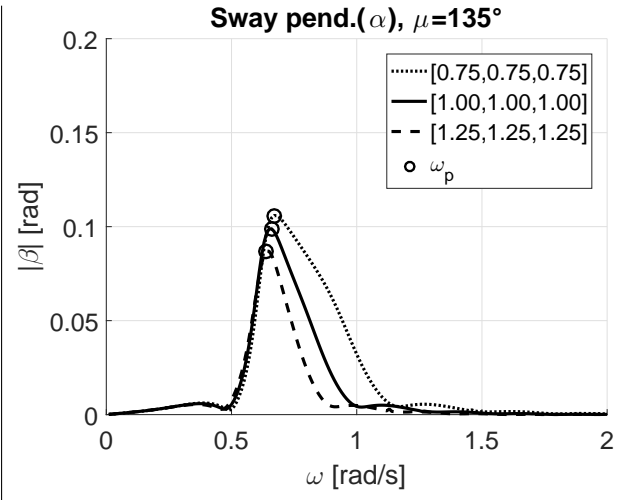
The effective exerted motion, table 6.2, show both a negative dependency for either the vessel motion and the longitudinal swaying motion. Implying more motion for smaller vessels and less motion for larger vessels.

Table 6.2: RMS pitch and longitudinal sway

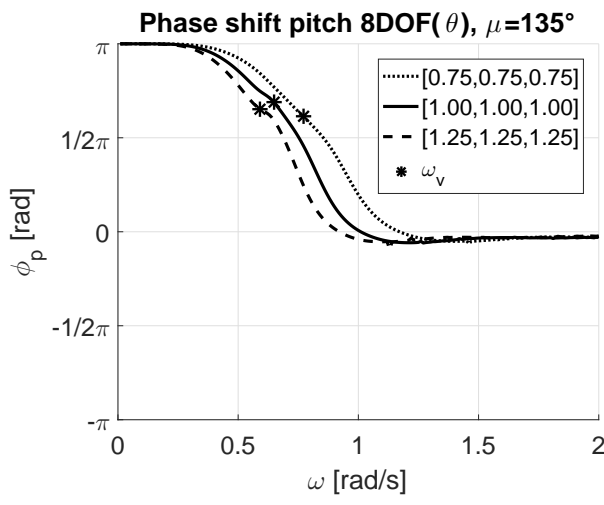
λ	RMS pitch	RMS longitudinal sway
[0.75; 0.75; 0.75]	$1.49 \cdot 10^{-2}$ [rad]	$3.69 \cdot 10^{-2}$ [rad]
[1.00; 1.00; 1.00]	$1.02 \cdot 10^{-2}$ [rad]	$2.87 \cdot 10^{-2}$ [rad]
[1.25; 1.25; 1.25]	$0.76 \cdot 10^{-2}$ [rad]	$2.26 \cdot 10^{-2}$ [rad]



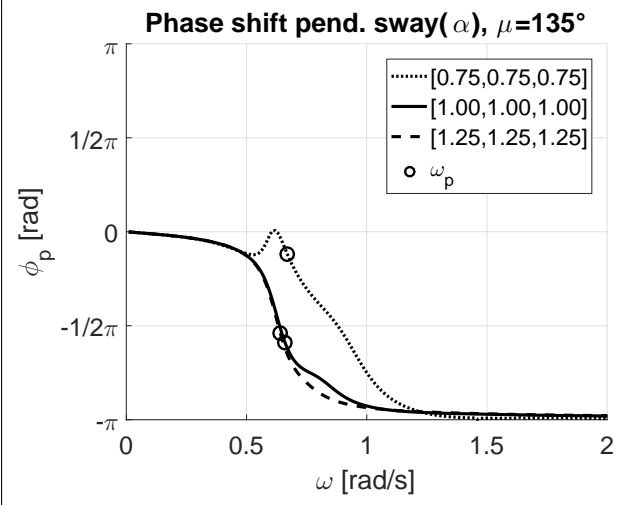
(a) Frequency response pitch 8DOF



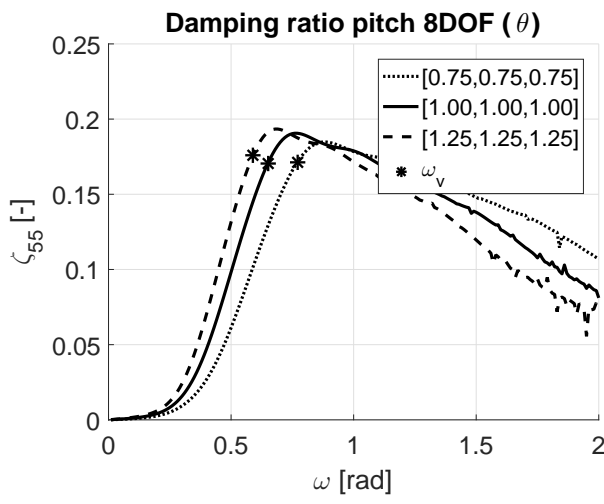
(b) Frequency response longitudinal sway



(c) Phase shift pitch 8DOF



(d) Phase shift longitudinal sway



(e) Damping ratio pitch 8DOF

Figure 6.9: Frequency response, phase shift and damping ratio pitch governed motion

6.2.1. Frequency shift pitch governed motion

Looking at the resonance frequency shift for the pitch motion, figure 6.10a, no additional resonance frequencies are noticeable for either larger sensitivity multipliers ($\lambda > 1.00$) nor for smaller sensitivity multipliers ($\lambda < 1.00$). Implying there is no dynamic coupling in pitch direction for any analyzed vessel size. The resonance frequency related to the vessel motion ω_v appears to have a negative dependency on the sensitivity multiplier λ . Similarly, the longitudinal swaying motion, figure 6.10b, stays absolutely monolithic throughout all sensitivity multipliers. Implying no dynamic coupled motion. The resonance frequency related to the crane load motion (ω_p) appears to remain rather constant throughout all sensitivity multipliers. Therefore it can be concluded that dynamic coupled motion just does not occur for pitch governed motion. The inertia forces generated by the longitudinal crane load swaying motion are just not great enough to generate any coupled motion behavior.

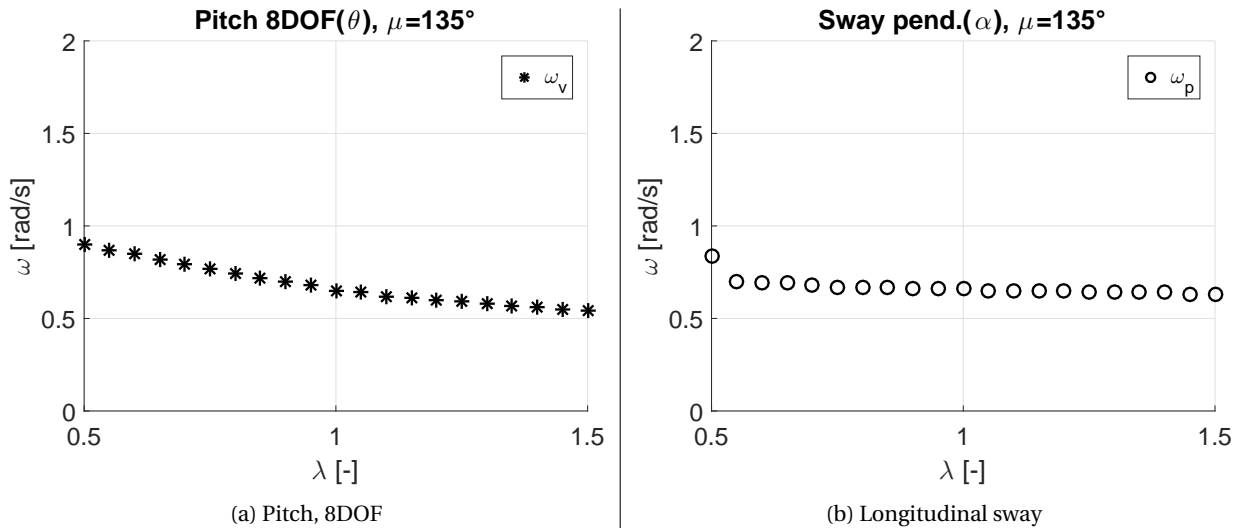


Figure 6.10: Frequency shift pitch governed motion

6.2.2. Static pitch excitation

Due to the placement of the crane at the aft of the vessel it is known that the vessel will exert static excitation. It can be seen in figure 6.11 that for increasingly smaller vessels the static response increases significantly. Therefore whenever one would design a new monohull heavy lift vessel, one should be more vigilant towards the static response compared to the unlikelihood possibility dynamic coupled pitch motion may occur.

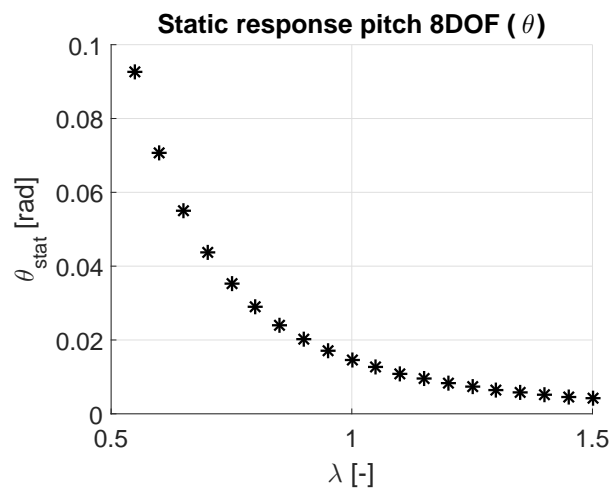


Figure 6.11: Static pitch response

6.3. Conclusion proportional sensitivity analysis

Table 6.3 summarizes all the relations observed in the proportional sensitivity study for the roll governed motion. Regarding the roll and perpendicular pendulum swaying motion it may be concluded that dynamic coupled motion definitely occurs and the motion of the crane load will dominate the response motion for both roll and perpendicular swaying motion whenever the vessel will become smaller. This assertion is highly dependent on the damping applied on the crane load, decreasing this damping would further increase the dominance of the swaying crane load.

For vessel sizes smaller than 0.60 times the original vessel size the maximum rolling motion exceeds the maximum allowed 5° roll excitation.

Table 6.3: Summary proportional sensitivity study roll governed motion

x	Not present			
✓	Present			
c	Constant			
d	Discontinuous			
↑	Increases			
↑↑	Increases more than linear			
↓	Decreases			
↓↓	Decreases more than linear			
ω_v	Resonance frequency related to the vessel motion			
ω_p	Resonance frequency related to the pendulum motion			
	Roll 8DOF		Perpendicular sway (β)	
	$\lambda < 1.00$	$\lambda > 1.00$	$\lambda < 1.00$	$\lambda > 1.00$
Coupled motion	✓	✓	✓	✓
Strong dynamic coupled motion	x	x	x	x
Effective motion (RMS)	↑↑	↓	c	c
Freq. shift	↑↑	↓	↑	↓
ω_v Peak height shift	↓↓	↓	↓	↑
Damping ratio	↓↓	c	c	c
Freq. shift	c	c	c	c
ω_p Peak height shift	↑↑	↓	↑	↓
Damping ratio	↓	↑	c	c

Regarding pitch motion, no dynamic coupled motion is noticeable throughout the proportional sensitivity analysis. The pitch motion remains monolithic in nature, no additional resonance frequencies contributed by the swaying of the crane load are observed. The longitudinal pendulum motion in turn also does not seem to exert any additional resonance frequency related to the vessel motion. It is known the coupled motion is highly dependent on the damping applied to the swaying of the pendulum. In appendix B a short sensitivity analysis illustrates the effect of decreasing the crane load damping, in order to force the system to show dynamically coupled behavior for pitch motion. It can be seen that for damping ratios nearing or equaling zero the crane system will in fact start to exert coupled motion behavior. However, this coupled motion behavior is at damping ratios of 1% or less. In one would be able to better define the damping acting upon the crane load, one could definitively exclude dynamic crane load pitch coupled motion. Considering the assumed 10% critical damping acting upon the crane load, further examination of dynamic coupling motion within pitch governed motion will no longer be examined in further sensitivity analyses.

Subquestions

3. In which degrees of freedom does dynamic crane load coupled motion occur?

The swaying of the crane load could effect both the roll and pitch motion of the vessel. Roll motion has been proven throughout all sensitivity analyses to show dynamic coupled behavior. However, whilst examining the results, no clear indication has been found regarding dynamic coupled motion in pitch motion. However, for crane load damping ratio approaching zero the pitch motion will start showing dynamic coupled behavior. Better defining the crane load damping could in fact help exclude dynamic pitch motion as an occurring phenomena. Under the assumption of 10% critical damping acting upon the crane load, one may exclude dynamic coupled pitch motion.

Static excitation in pitch motion due to the crane load however increases significantly for increasingly smaller vessels. This static excitation is due to the placement of the crane at the aft of the vessel.

6.4. Data errors

Although the diffraction software set-up shows very stable and mostly correct results, there have been some discrepancies using the diffraction software WADAM. As seen in most sensitivity figures, the results for $\underline{\lambda} = [1.45; 1.45; 1.45]$ appear to be not inline with the trends observed. Looking at the frequency response as seen in figure 6.12, at higher frequencies ($\omega \geq 1.00$ [rad/s]) the frequency response becomes rough and noisy. Diffraction software usually is used for low frequency hydrodynamic calculations, however the frequency bandwidth applied in this research should not induce this much noise. For all other sensitivity multipliers this error has not been observed.

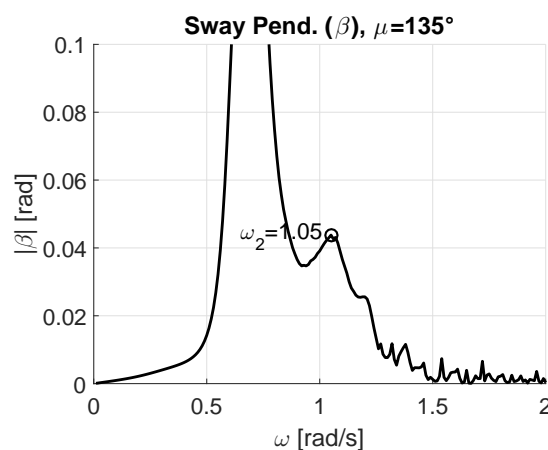


Figure 6.12: Error frequency response

The diffraction software input values are created through scripted commands, chapter 3, and seen in the static relations in figures 6.2-6.8 there does not seem to be a discrepancy at $\lambda = 1.45$. The numerical parametric calculation therefore most likely will not be the reason for the observed error.

Besides the scripted commands to calculate the input values for the diffraction software, scripted commands have been created to alter the geometric properties of the vessel according to the sensitivity multipliers. A visual inspection has been done to check if either the shape of the vessel or the shape of the bilge keels have been altered incorrectly. This however was not the case.

The last possible contributor to the observed error could be WADAM's ability to compile a closed vessel shape. WADAM compiles a closed vessel hull shape by means of large array of geometric data points [15]. A closed vessel hull basically implies that the vessel is watertight. If WADAM is not able to compile a closed vessel hull, strange effect will come into play hence fluid interactions will also act on the inside of the vessel. This could very well be the cause of the error.

Although the error gives very unsatisfying results it by now means compromises the outcome of the results, the trends observed do not seem to be affected by the error. During all sensitivity analyses performed the error has only been witnessed three times over a total of 336 cases calculated by WADAM. If anyone would ever incorporate the programmed calculation methods, one must be vigilant for the possible occurring errors.

7

Disproportional sensitivity analyses

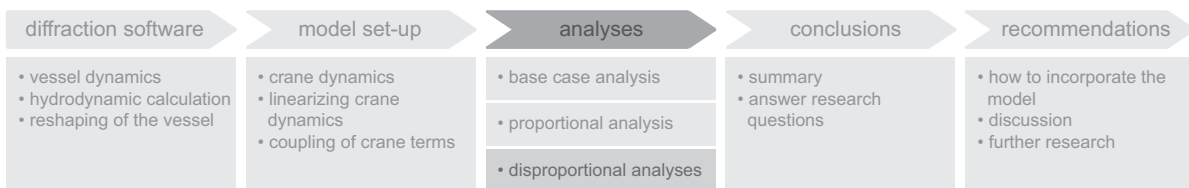


Figure 7.1: Research set-up

This chapter will discuss the last analyses, figure 7.1, related to the length, width and depth sensitivity of the system. Previously in chapter 6 it has been established that there is no noticeable dynamic coupled motion within the pitch governed motion (pitch and longitudinal crane load sway). Within the disproportional sensitivity analysis the pitch governed motion therefore will no longer be evaluated.

Concluding the dis-proportional sensitivity analysis will compare the effect of either the length, width and depth comparatively to on another. I.e., which of the dimensional properties has the least and most effect on the dynamic coupled behavior.

7.1. Length sensitivity

Seen in equation 7.1, the sensitivity vector $\underline{\lambda}$ is only dependent on the sensitivity multiplier in X-direction, λ_X . I.e. the vessel is elongated and compressed using these sensitivity multipliers, the width and depth of the vessel remain equal to the base case depth and width throughout the sensitivity analysis.

$$\underline{\lambda} = \begin{bmatrix} \lambda_X \\ \lambda_Y \\ \lambda_Z \end{bmatrix} = \begin{bmatrix} 0.75 \\ 1.00 \\ 1.00 \end{bmatrix}, \quad \begin{bmatrix} 1.00 \\ 1.00 \\ 1.00 \end{bmatrix}, \quad \begin{bmatrix} 1.25 \\ 1.00 \\ 1.00 \end{bmatrix} \quad (7.1)$$

Seen in figure 7.2, it can be seen that the mass of the vessel is the only static relation dependent on the sensitivity multiplier λ_X . The roll metacentric height, figure 7.2b, is constant for all sensitivity multipliers similarly the roll radius of gyration, figure 7.2c, remains constant throughout the sensitivity multipliers. From a simplified model as discussed in chapter 4, it is known that the vessel roll restoring force is proportional to the mass and the restoring force ($k_r \propto M, GM_4$). This however does not account for the added mass of the vessel.

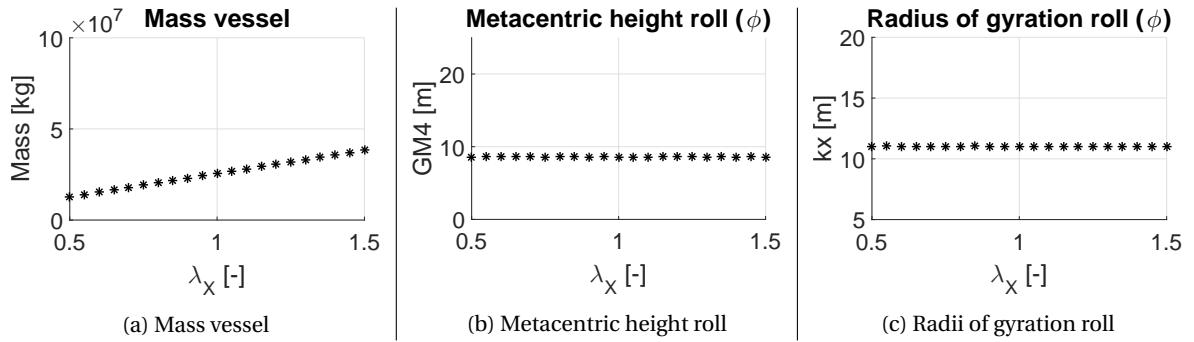


Figure 7.2: Static relations roll, length sensitivity

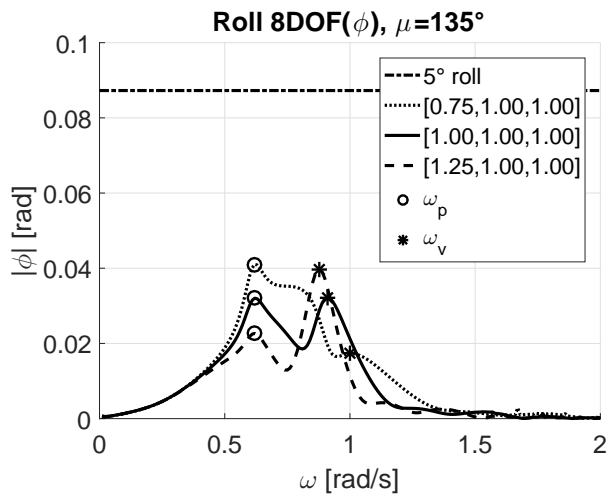
The frequency response, phase shift and roll damping, seen in figure 7.3, are on display for both roll and perpendicular crane load swaying motion. It can clearly be seen that both the resonance frequency related to the vessel motion (ω_v) and the resonance frequency related to the swaying of the pendulum (ω_p) are both present in the two separate degrees of freedom, figures 7.3a-7.3d. Similar to the proportional analysis, the resonance frequency related to the swaying of the pendulum (ω_p) is irrespective of the sensitivity multiplier λ_X . However, it can be seen that the peak height related to the swaying of the pendulum (ω_p) is negatively dependent on the sensitivity multiplier λ_X for both the roll motion as well as the perpendicular sway motion. This can be elucidated by the fact that the roll damping ratio at the resonance frequency related to the swaying of the pendulum, seen in figure 7.3e, is less for the shorter vessel.

Looking at the shape of the frequency response of the roll motion, figure 7.3a, the shorter vessel ($\lambda_X = 0.75$) is clearly different than the other sensitized cases. The shape gets skewed, this is a clear sign that both the roll motion and the crane load swaying motion have strong dynamic coupled motion.

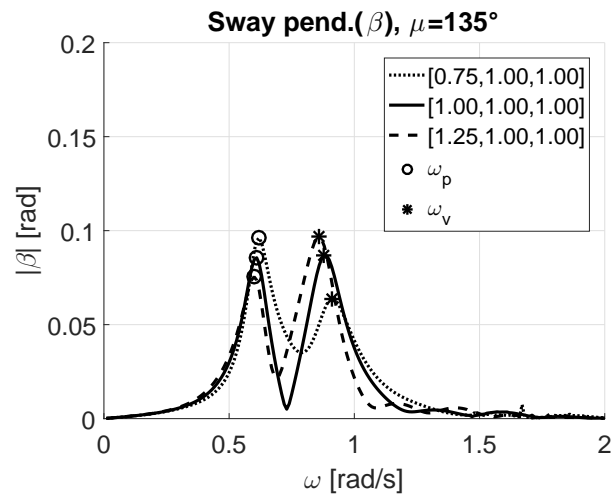
In table 7.1, it can be seen that the effective roll motion decreases for larger sensitivity multipliers λ_X . The perpendicular swaying motion however does not show a clear trend and appears to be rather constant. The vessel will exert more roll motion for shorter vessels and will exert less motion for longer vessels.

Table 7.1: RMS roll and perpendicular crane load sway, length sensitivity

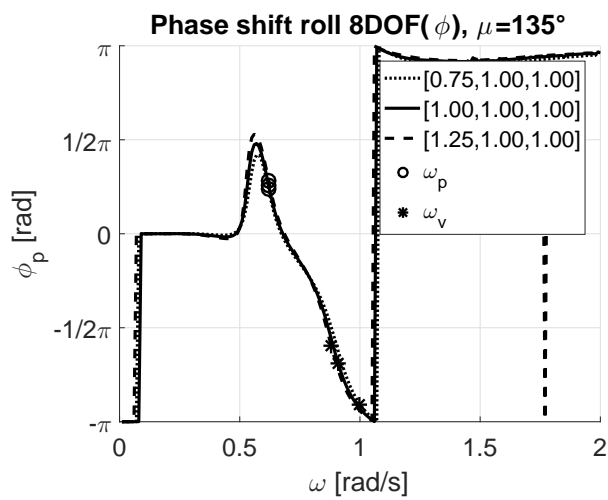
λ	RMS roll	RMS perpendicular sway
[0.75;1.00;1.00]	$1.66 \cdot 10^{-2}$ [rad]	$3.02 \cdot 10^{-2}$ [rad]
[1.00;1.00;1.00]	$1.40 \cdot 10^{-2}$ [rad]	$3.01 \cdot 10^{-2}$ [rad]
[1.25;1.00;1.00]	$1.24 \cdot 10^{-2}$ [rad]	$3.12 \cdot 10^{-2}$ [rad]



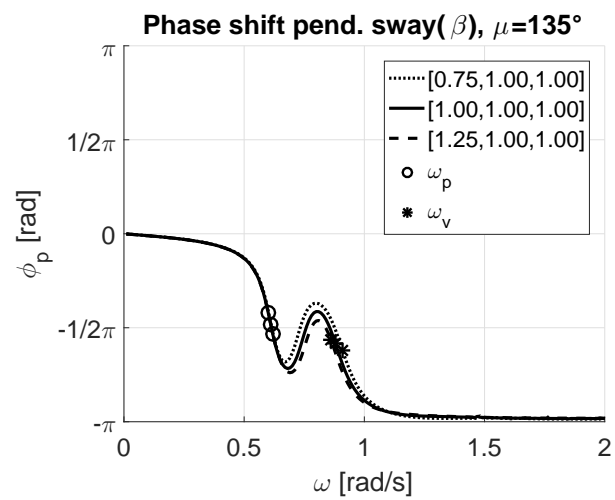
(a) Frequency response roll 8DOF



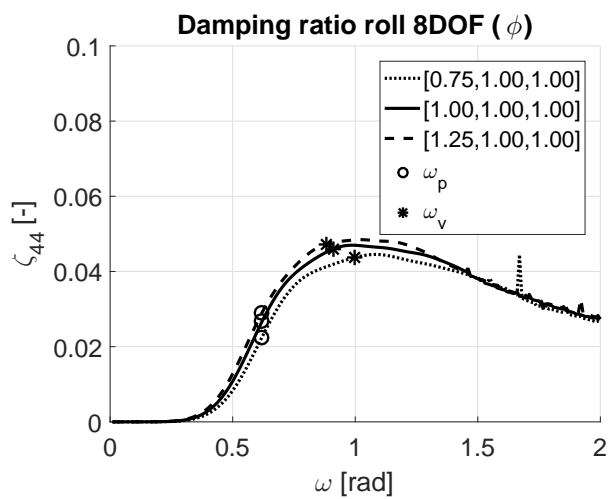
(b) Frequency response perpendicular sway



(c) Phase shift roll 8DOF



(d) Phase shift perpendicular sway



(e) Damping ratio roll 8DOF

Figure 7.3: Frequency response and phase shift roll governed motion, length sensitivity

7.1.1. Frequency shift

Seen in figure 7.4, the resonance frequency is set out with respect to the sensitivity multiplier in X-direction λ_X . It can clearly be seen that the resonance frequency related to the crane load swaying motion (ω_p) is constant throughout the sensitivity multipliers for both roll motion, figure 7.4a, and perpendicular crane load swaying motion, figure 7.4b. Regarding the roll resonance frequency, there is a clear discontinuity for the resonance frequency related to the vessel motion (ω_v) at approximately $\lambda_X < 0.75$. This is a clear sign of strong coupled motion in figure 7.5. What this implies is that the frequency response for shorter vessels will be increasingly skewed due to strong coupled motion between the vessel motion and the swaying of the crane load.

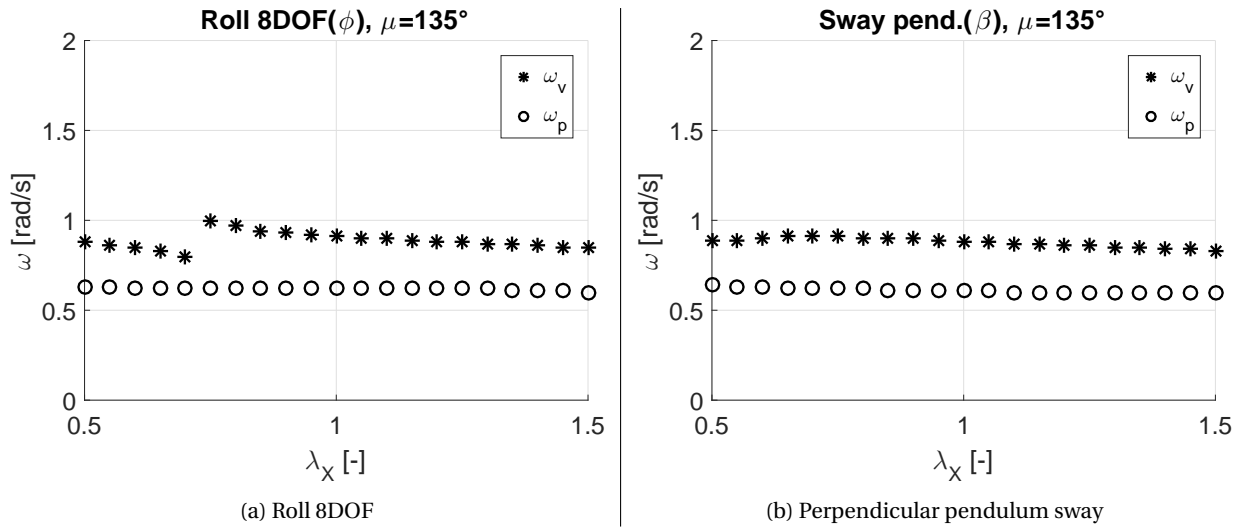


Figure 7.4: Frequency shift, length sensitivity

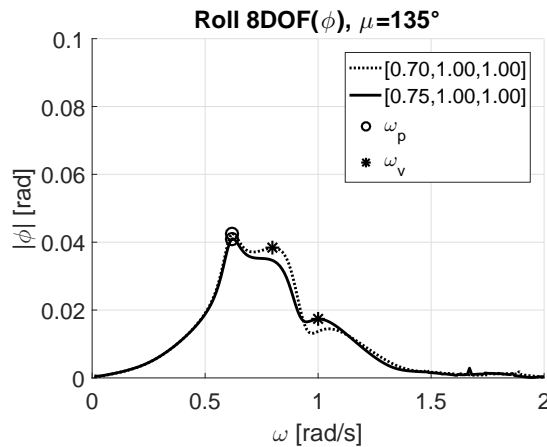


Figure 7.5: Strong coupled motion

7.1.2. Peak shift

The previous asserted notion that for increasingly shorter vessels strong coupled motion will skew the frequency response can also clearly be seen in the roll motion peak shift, figure 7.6a. The discontinuity occurs at the previous stated interval of $\lambda_X = 0.70$ and $\lambda_X = 0.75$. Roll motion peak height related to the swaying of the pendulum (ω_p) appears to have a negative linear dependency on the sensitivity multiplier λ_X . The swaying crane load motion therefore will have an increased influence on shorter vessels and a decreased influence on longer vessels.

Looking at the peak height shift for the perpendicular swaying motion, figure 7.6b, the peak height related to the swaying of the pendulum (ω_p) shows a negative linear dependency on the sensitivity multiplier. The

peak height related to the vessel motion (ω_v) however does not show a clear dependency on the sensitivity multiplier. The peak height appears to have a positive parabolic dependency for shorter vessels and a negative parabolic dependency for longer vessels.

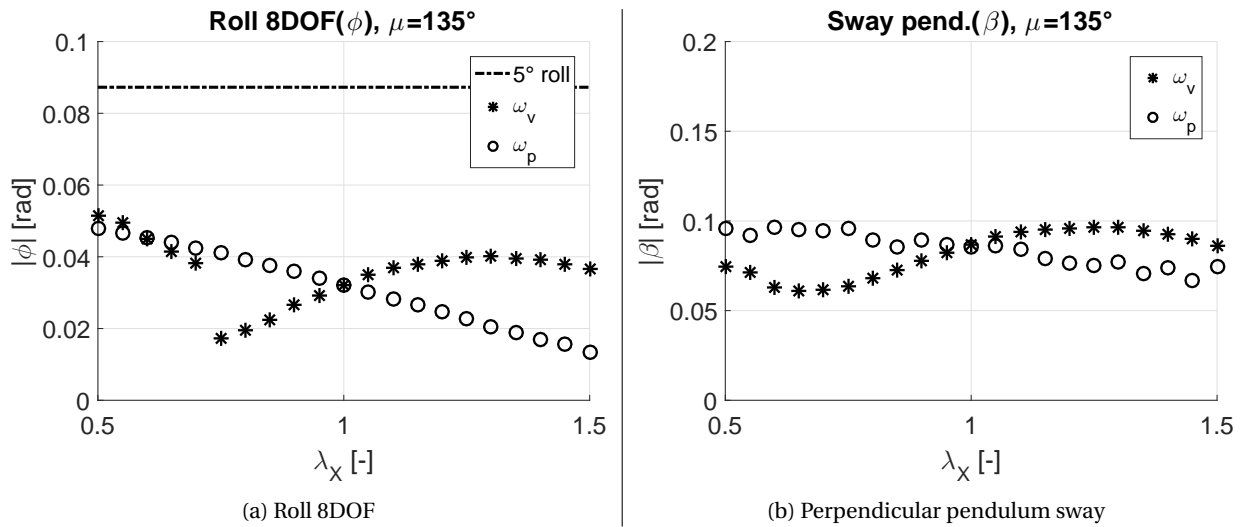


Figure 7.6: Peak shift, length sensitivity

7.1.3. Roll damping ratio shift

Seen in figure 7.7, the roll damping ratio at both the resonance frequency related to the vessel motion (ω_v) and the resonance frequency related to the pendulum swaying motion (ω_p) have a positive linear dependency on the sensitivity multiplier. Due to the strong coupled motion for shorter vessels the vessel damping ratio shows a discontinuity.

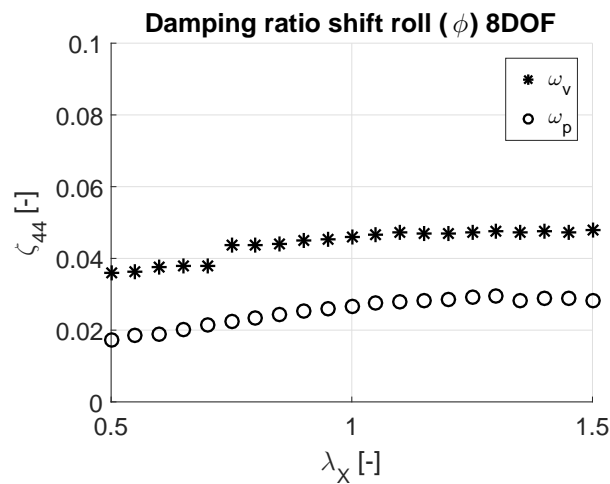


Figure 7.7: Damping ratio shift roll, length sensitivity

7.1.4. Effective excitation (RMS) roll governed motion

The effective roll motion excitation as seen in figure 7.8a, increases more than linearly for increasingly shorter vessels ($\lambda_X < 1.00$) and decreases approximately linearly for increasingly longer vessels ($\lambda_X > 1.00$). The vessel therefore will exert increasingly more motion for ever shorter vessels and less motion for longer vessels.

Regarding the effective crane load swaying motion, figure 7.8b, the crane load will exert more motion for increasingly smaller vessels ($\lambda_X < 1.00$). The swaying of the pendulum will however exert rather constant motion for increasingly longer vessel ($\lambda_X > 1.00$).

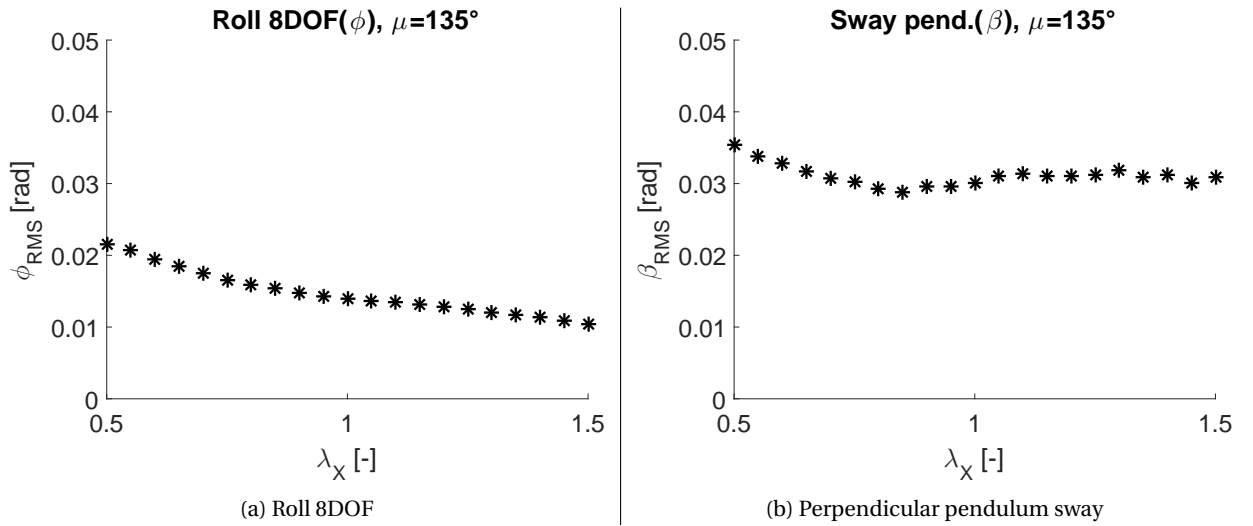


Figure 7.8: Root mean square, length sensitivity

7.1.5. Conclusion length sensitivity analysis

Summarized in table 7.2 the effects of elongation and shortening of the vessel are set out. The most important conclusion for the X-sensitivity study is the fact that for shorter vessels the swaying of the pendulum and the vessel motion will have strong coupled motion. Due to this strong coupled motion a clear discontinuity regarding the resonance frequency related to the vessel motion is observable throughout the sensitivity multipliers. The vessel will become more dominated by the swaying of the crane load for increasingly shorter vessels and less dependent on the swaying of the crane load for longer vessels. The crane load in turn will start to increasingly sway for ever shorter vessels but will not really decrease in motion for increasing vessel lengths.

Table 7.2: Summary length sensitivity, roll governed motion

x	Not present
✓	Present
c	Constant
d	Discontinuous
↑	Increases
↑↑	Increases more than linear
↓	Decreases
↓↓	Decreases more than linear
ω_v	Resonance frequency related to the vessel motion
ω_p	Resonance frequency related to the pendulum motion

	Roll 8DOF		Perpendicular sway (β)	
	$\lambda_X < 1.00$	$\lambda_X > 1.00$	$\lambda_X < 1.00$	$\lambda_X > 1.00$
Coupled motion	✓	✓	✓	✓
Strong dynamic coupled motion	✓	x	x	x
Effective motion (RMS)	↑↑	↓	↑	c
Freq. shift	d↑	↓	c	↓
ω_v Peak height shift	d↓	c	↓	↑
Damping ratio	d↓	↑	c	c
Freq. shift	c	c	c	c
ω_p Peak height shift	↑	↓	↑	↓
Damping ratio	↓	c	c	c

7.2. Width sensitivity

Seen in equation 7.2, the sensitivity vector $\underline{\lambda}$ is only dependent on the sensitivity multiplier in Y-direction, λ_Y . I.e. the vessel is broadened and made narrower using these sensitivity multipliers, the length and depth of the vessel remain equal throughout the sensitivity analysis.

$$\underline{\lambda} = \begin{bmatrix} \lambda_X \\ \lambda_Y \\ \lambda_Z \end{bmatrix} = \begin{bmatrix} 1.00 \\ 0.75 \\ 1.00 \end{bmatrix}, \quad \begin{bmatrix} 1.00 \\ 1.00 \\ 1.00 \end{bmatrix}, \quad \begin{bmatrix} 1.00 \\ 1.25 \\ 1.00 \end{bmatrix} \quad (7.2)$$

Seen in figure 7.9, both the mass, roll metacentric height and roll radius of gyration are all positively dependent on the sensitivity multiplier λ_Y . Regarding the roll metacentric height, figure 7.9b, for an increasingly slender vessel geometry the metacentric height approaches zero. A negative metacentric height implies that the vessel is statically unstable. This decrease of metacentric height will make the vessel less statically stable.

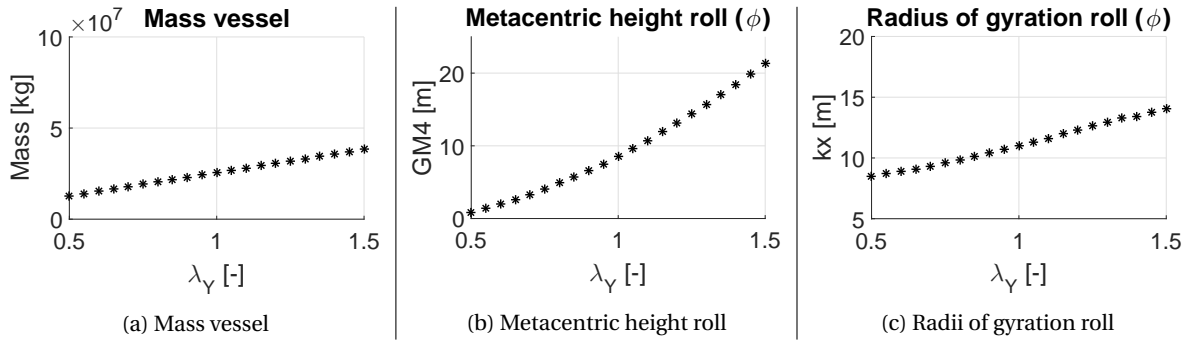


Figure 7.9: Static relations roll, width sensitivity

Comparing the frequency response for roll motion, figure 7.10a, it can be seen that the narrower vessel ($\lambda_Y = 0.75$) is much more peaked than the base case vessel ($\lambda_Y = 1.00$) and even more so compared to the wider vessel ($\lambda_Y = 1.25$). This change in shape appears to be dictated by the roll damping. Looking at figure 7.10e it can clearly be seen that the roll damping for the more narrow vessel is much less. This decrease in roll damping is a logical effect of making the vessel more slender. Hence the roll damping in effect is determined by the torque arm the friction terms are able to generate. Making the vessel more slender, the arm decreases implying the roll damping will be inherently lower. This results in less damped roll motion for more narrow vessels and more damped roll motion for wider vessels. This decrease in damping is most noticeable at the resonance frequency related to the swaying of the pendulum (ω_p). For increasingly narrower vessels the roll damping ratio at the resonance frequency related to the pendulum motion approaches zero, implying almost no damping at the resonance frequency. This results in an increase of motion hence the more peaked nature of the frequency response. Seen in table 7.3 both the roll motion as well as the perpendicular swaying motion exert more motion at smaller sensitivity multipliers ($\lambda_Y < 1.00$) and less motion at greater sensitivity multipliers ($\lambda_Y > 1.00$). This is in consonance with the fact that the narrower vessel is less damped and the wider vessel is more damped.

Table 7.3: RMS roll and perpendicular crane load sway, width sensitivity

λ	RMS roll	RMS perpendicular sway
[1.00;0.75;1.00]	$1.85 \cdot 10^{-2}$ [rad]	$3.70 \cdot 10^{-2}$ [rad]
[1.00;1.00;1.00]	$1.40 \cdot 10^{-2}$ [rad]	$3.01 \cdot 10^{-2}$ [rad]
[1.00;1.25;1.00]	$1.10 \cdot 10^{-2}$ [rad]	$2.21 \cdot 10^{-2}$ [rad]

7.2.1. Frequency shift

Looking at the resonance frequency dependent on the sensitivity multiplier, as seen in figure 7.11 it can be seen that the resonance frequency related to the vessel motion (ω_v) remains constant over all sensitivity multipliers. I.e., the width of the vessel does not change the resonance frequency related to the vessel motion. Looking at the resonance frequency related to the pendulum swaying motion (ω_p) it can clearly be seen the

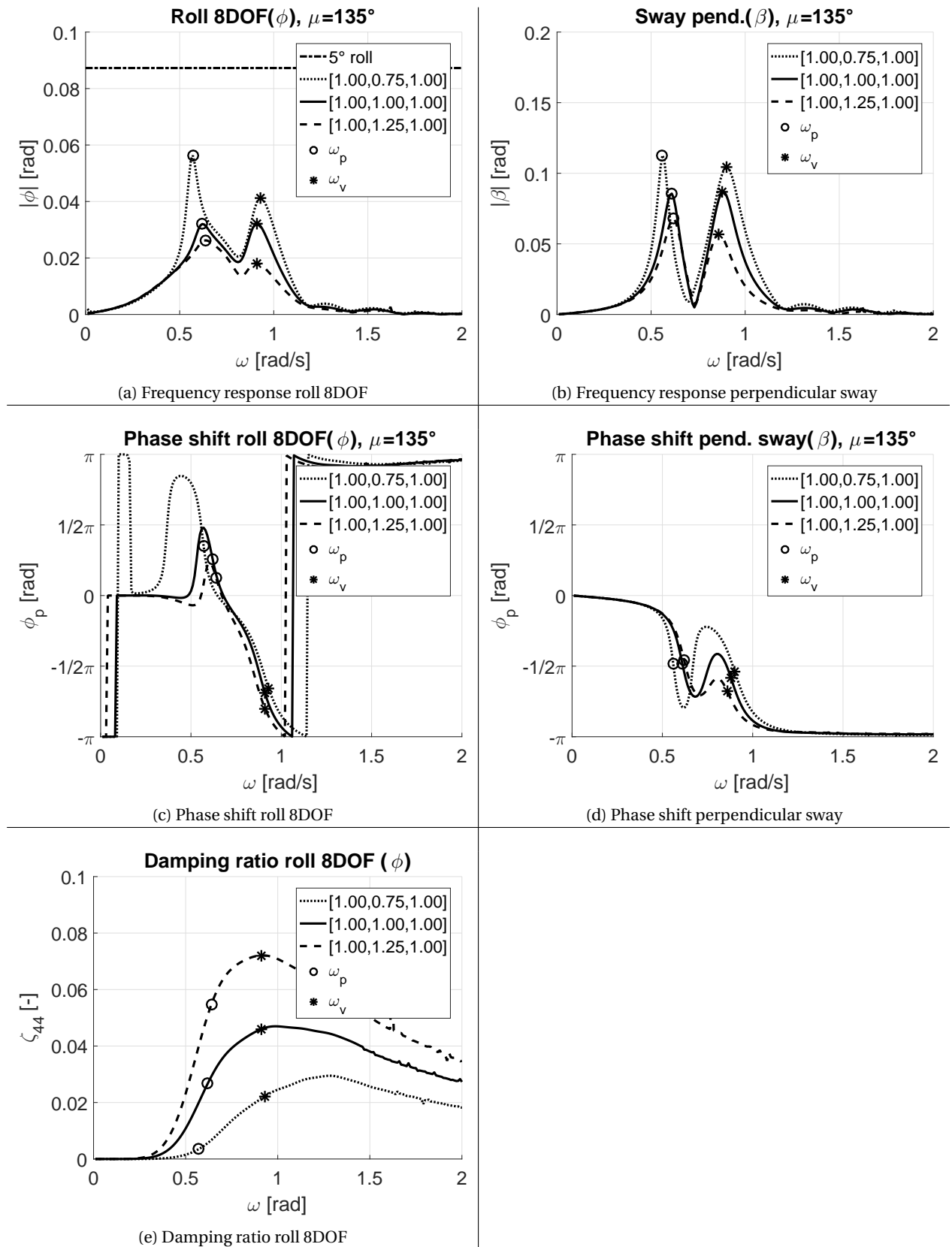


Figure 7.10: Frequency response and phase shift roll governed motion, width sensitivity

resonance frequency sharply decreases for increasingly narrow vessels. These observation both applies for the roll motion, figure 7.11a, as well as the perpendicular swaying motion of the crane load, figure 7.11b.

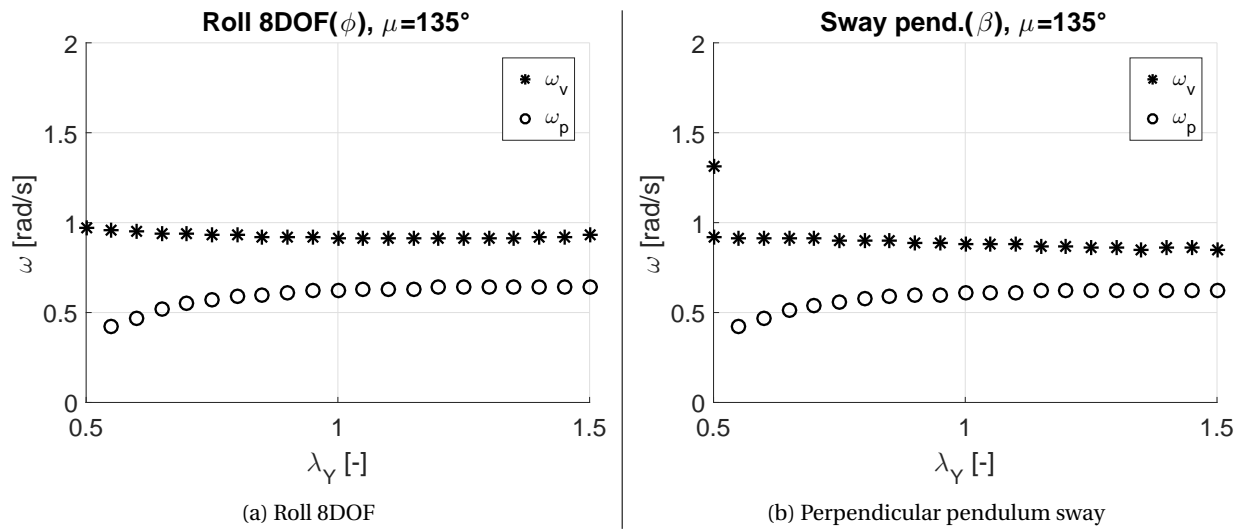


Figure 7.11: Frequency shift, width sensitivity

7.2.2. Peak shift

Looking at the peak height shift as seen in figure 7.12 it can be seen that the width of the vessel has a rather significant effect on the maximum occurring motion. The vessel roll motion, 7.12a, becomes increasingly dominated by the swaying of the crane load (ω_p) for increasingly narrower vessel dimensions. This relation is nonlinear and is attributed to the decrease of metacentric height combined with the decrease of damping. This implies that the motion at the resonance frequency related to the swaying of the crane load (ω_p) will be much greater for increasingly narrow vessel dimensions. For vessels widths narrower than $\lambda_Y < 0.70$ the maximum roll excitation exceeds the maximum 5° .

Regarding the peak height shift of the resonance frequency related to the vessel motion (ω_v), it can be seen there is a negative dependency on the sensitivity multiplier. That is, for wider vessels the motion related to the resonance frequency of the vessel will become less and for narrower vessels the motion will become greater. However, regarding sensitivity multipliers less than $\lambda_Y < 0.75$ this relation no longer holds.

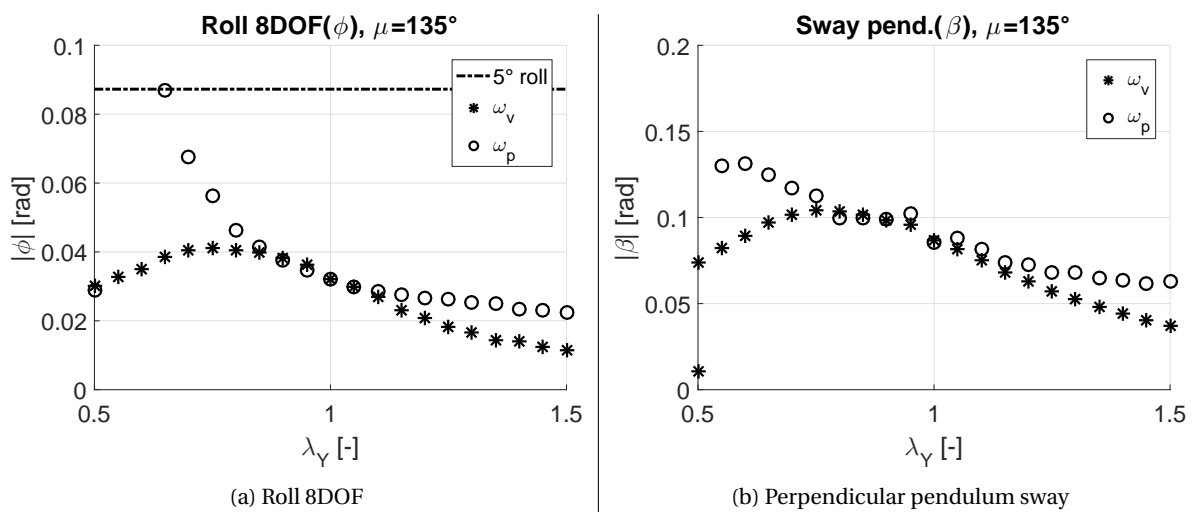


Figure 7.12: Peak shift, width sensitivity

7.2.3. Roll damping ratio shift

As previously stated the roll damping ratio at the resonance frequency related to the pendulum motion (ω_p) decreases for increasingly narrow vessels. This relation is clearly seen in figure 7.10e. The roll damping at the pendulum swaying resonance frequency approaches zero at approximately $\lambda_Y < 0.70$. Considering the roll damping for the frequency related to the vessel motion (ω_v), it can be seen that the damping ratio decreases for narrower vessels ($\lambda_Y < 1.00$). For increasingly narrower vessels ($\lambda_Y < 0.70$) the damping will significantly increase again. This increase in damping is in consonance with the observed resonance frequency peak as seen in figure 7.12a. Hence the peak height related to the vessel motion (ω_v) increases for increasingly narrower vessels but become less again for sensitivity multipliers $\lambda_Y < 0.75$. Considering the fact that the roll damping at the resonance frequency related to the swaying of the crane load (ω_p) is equal to zero at very narrow vessels ($\lambda_Y > 0.70$). The peak height of the frequency response did not appear to go to infinity. The vessel therefore is damped due to the applied crane load damping (10% critical damping).

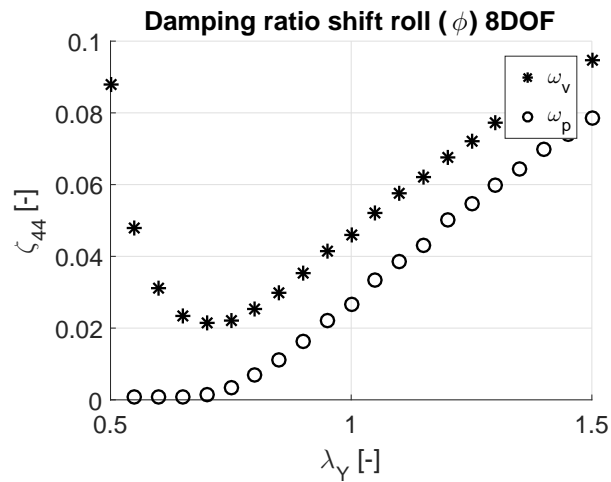


Figure 7.13: Damping ratio shift roll, width sensitivity

7.2.4. Effective excitation (RMS) roll governed motion

The effective roll excitation (RMS), figure 7.14a, increases more than linearly for ever narrower vessel widths. Implying that the vessel will exert more motion for increasingly slender vessels. Similarly, for wider vessels there will be less excited motion. Looking at the perpendicular swaying motion, figure 7.14b, one cannot define a clear trend regarding the total exerted motion in comparison to the sensitivity multiplier λ_Y . In general a narrower vessel will exert more perpendicular swaying motion and a wider vessel will exert less perpendicular swaying motion.

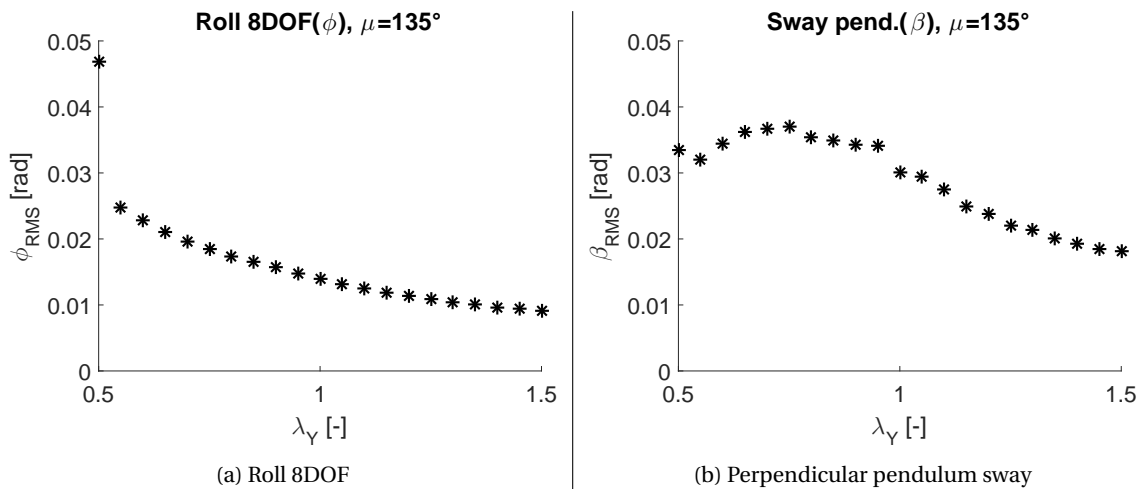


Figure 7.14: Root mean square, width sensitivity

7.2.5. Conclusion width sensitivity analysis

The most important conclusion regarding the width sensitivity of the vessel is that due to the decrease of the roll damping and decrease of the metacentric height, the roll motion will become increasingly dominated by the swaying of the crane load for increasingly narrower vessels. I.e., the maximum exerted roll motion at the resonance frequency related to the pendulum swaying motion will become greater for increasingly narrower vessels. The effective excitation therefore will also increase significantly for ever narrower vessels implying that more narrow vessels will move more.

The second conclusion regarding the width sensitivity of the vessel is that the resonance frequency related to the swaying of the crane load decreases sharply for increasingly slender vessel geometries. The resonance frequency related to the crane load therefore is cannot be assumed to be similar to its independent natural frequency ($\omega_n = \sqrt{\frac{g}{L_c}}$). The dynamic characteristics related to the width sensitivity are listed in table 7.4.

Table 7.4: Summary width sensitivity, roll governed motion

x	Not present			
✓	Present			
c	Constant			
d	Discontinuous			
↑	Increases			
↑↑	Increases more than linear			
↓	Decreases			
↓↓	Decreases more than linear			
ω_v	Resonance frequency related to the vessel motion			
ω_p	Resonance frequency related to the pendulum motion			
	Roll 8DOF		Perpendicular sway (β)	
	$\lambda_Y < 1.00$	$\lambda_Y > 1.00$	$\lambda_Y < 1.00$	$\lambda_Y > 1.00$
Coupled motion	✓	✓	✓	✓
Strong dynamic coupled motion	x	x	x	x
Effective motion (RMS)	↑↑	↓	↑	↓
Freq. shift	c	c	c	c
ω_v Peak height shift	↓	↓	↓	↓
Damping ratio	↓	↑	c	c
Freq. shift	↓↓	c	↓↓	c
ω_p Peak height shift	↑↑	↓	↑	↓
Damping ratio	↓	↑	c	c

7.3. Depth sensitivity

Seen in equation 7.3, the sensitivity vector $\underline{\lambda}$ is only dependent on the sensitivity multiplier in Z-direction λ_Z . I.e., the vessel depth is elevated or lowered using these sensitivity multipliers whilst the length and the width of the vessel remain equal throughout the sensitivity analysis.

$$\underline{\lambda} = \begin{bmatrix} \lambda_X \\ \lambda_Y \\ \lambda_Z \end{bmatrix} = \begin{bmatrix} 1.00 \\ 1.00 \\ 0.75 \end{bmatrix}, \begin{bmatrix} 1.00 \\ 1.00 \\ 1.00 \end{bmatrix}, \begin{bmatrix} 1.00 \\ 1.00 \\ 1.25 \end{bmatrix} \quad (7.3)$$

Compared to the mass of the vessel, figure 7.15a, and roll radius of gyration, figure 7.15c, the roll metacentric height, figure 7.15b, is negatively dependent on the sensitivity multiplier λ . Implying the vessel becomes less statically stable for increased vessel depths.

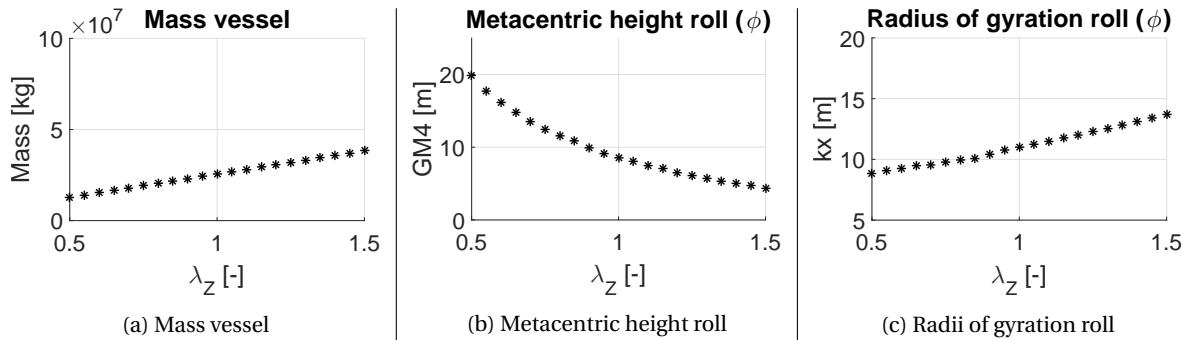
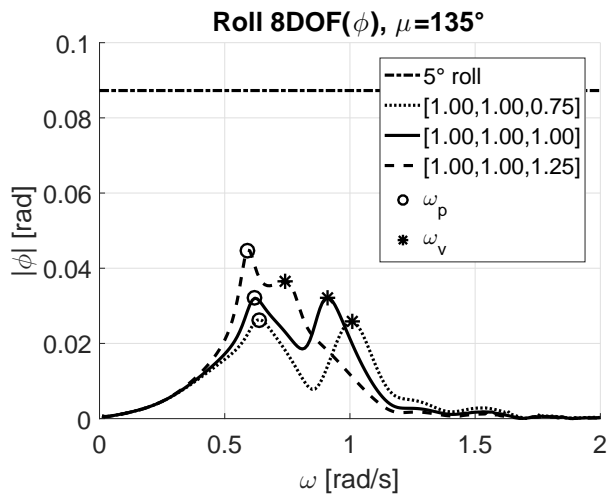


Figure 7.15: Static relations roll, depth sensitivity

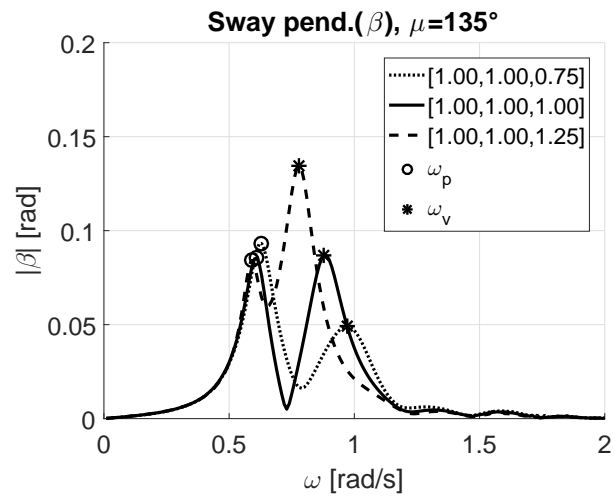
Seen in figure 7.16, the frequency response, phase shift and roll damping are on display for both the rolling motion as well as the perpendicular swaying motion. Looking at the rolling motion of the vessel, figure 7.16a, it can be seen that the resonance frequency related to the vessel motion (ω_v) is negatively dependent on the sensitivity multiplier. A vessel with less depth will exert a higher resonance frequency related to the vessel motion and a larger depth vessel will exert a lower resonance frequency related to the vessel motion. For increasing vessel depths geometries, strong dynamic coupling of both the resonance frequency related to the vessel motion (ω_v) and the resonance frequency related to the swaying of the pendulum (ω_p) comes into play, resulting in a single large peak. Looking at the roll damping ratio, figure 7.16e, it can be seen that the roll damping ratio for vessels with increased depth is less compared to less depth vessels. The effect of decreased roll damping can be seen in the roll frequency response in figure 7.16a. Due to a decreased damping for larger depth vessels, the peak height of both the roll motion and the perpendicular crane load swaying motion increases. Regarding the effective excitation (RMS) for both the roll and perpendicular crane load sway motion, table 7.5, it can be seen both the roll motion as well as the perpendicular swaying motion will exert more motion for increased vessel depths, this is in consonance with the fact that the vessel is less damped for vessels with a larger depth.

Table 7.5: RMS roll and perpendicular crane load sway, depth sensitivity

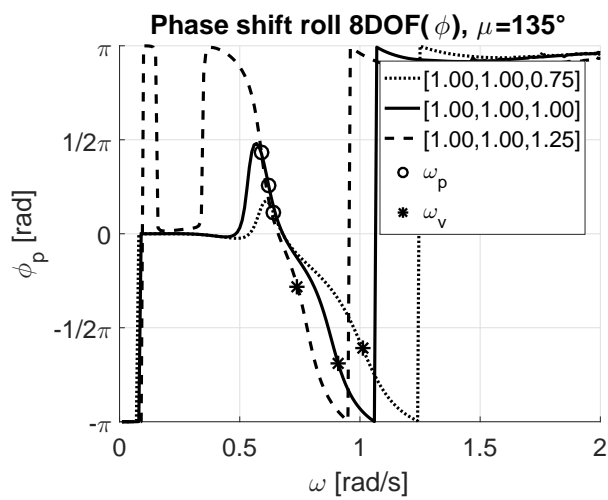
$\underline{\lambda}$	RMS roll	RMS perpendicular sway
[1.00;1.00;0.75]	$1.16 \cdot 10^{-2}$ [rad]	$2.75 \cdot 10^{-2}$ [rad]
[1.00;1.00;1.00]	$1.40 \cdot 10^{-2}$ [rad]	$3.01 \cdot 10^{-2}$ [rad]
[1.00;1.00;1.25]	$1.59 \cdot 10^{-2}$ [rad]	$3.93 \cdot 10^{-2}$ [rad]



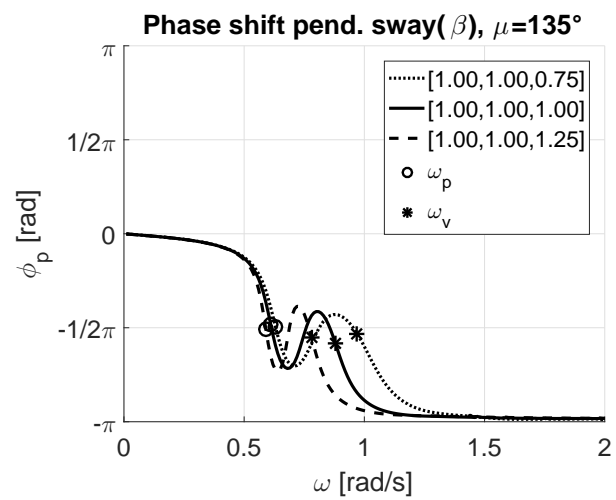
(a) Frequency response roll 8DOF



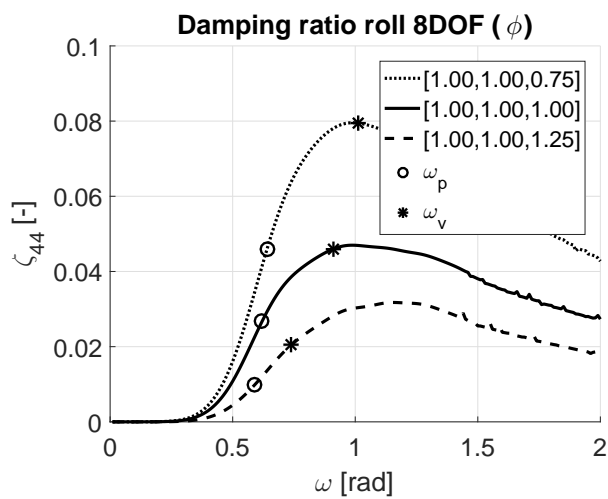
(b) Frequency response perpendicular sway



(c) Phase shift roll 8DOF



(d) Phase shift perpendicular sway



(e) Damping ratio roll 8DOF

Figure 7.16: Frequency response and phase shift roll governed motion, depth sensitivity

7.3.1. Frequency shift

Seen in figure 7.17, the resonance frequencies of both ω_v and ω_p are set out with respect to the sensitivity multiplier λ_Z for both the roll motion as well as the perpendicular crane load swaying motion. The resonance frequency related to the vessel motion (ω_v) is clearly negatively dependent on the sensitivity multiplier λ_Z . Due to strong dynamic coupled motion, the resonance roll frequency related to the vessel motion is discontinuous. That is, between $1.10 < \lambda_Z < 1.20$ only a single peak frequency is noticeable for roll motion related to the swaying of the crane load (ω_p). This strong dynamic coupled motion can be seen in figure 7.18.

The resonance frequency related to the crane load swaying motion (ω_p) for increasingly tall vessels ($\lambda_Z > 1.00$) appears to decrease ever so slightly. This effect however is rather marginal. Again the resonance frequency related to the crane load is dependent on the vessel geometry and cannot be assumed to be equal to the independent natural frequency related to a swaying pendulum ($\omega_n = \sqrt{\frac{g}{L_c}}$).

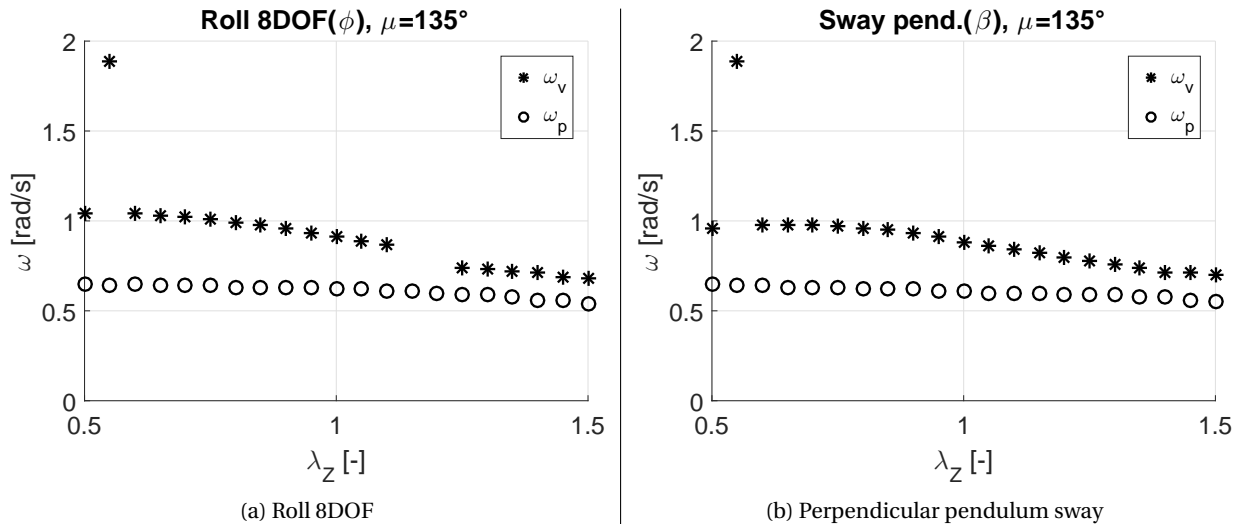


Figure 7.17: Frequency shift, depth sensitivity

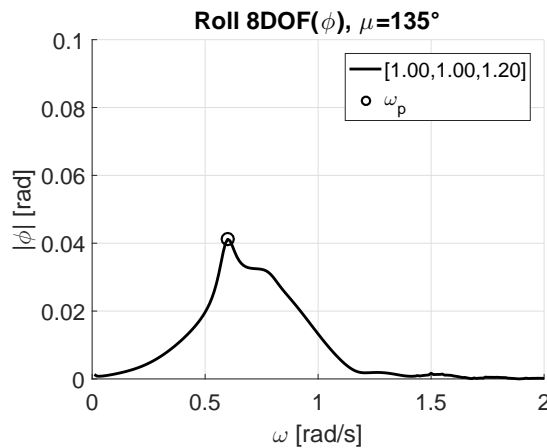


Figure 7.18: Strong coupled motion

7.3.2. Peak shift

Looking at the roll motion peak height shift as seen in figure 7.19a it can be seen that the peak height related to the pendulum swaying motion (ω_p) increases more than linearly for greater sensitivity multipliers ($\lambda_Z > 1.00$). Implying that the vessel roll motion will exert increasingly more motion at the resonance frequency related to the swaying of the crane load (ω_p) for larger vessel depths. The vessel depths greater than $\lambda_Z > 1.45$ the maximum roll motion will be greater than the maximum 5° allowed. Due to strong dynamic coupled

motion, the roll motion is discontinuous with respect to the resonance frequency related to the vessel motion (ω_v).

Looking at the perpendicular swaying motion, figure 7.19b, it can clearly be seen that for lower depth vessels the peak height related to the crane load motion (ω_p) is constant. For increasingly tall vessel sizes, the peak height related to the crane load motion however appears to increase more than linear. The peak height related to the vessel motion (ω_v) appears to have a more than linear dependency on the sensitivity multiplier λ_z . The crane load swaying motion therefore is dominated by the resonance frequency related to the crane load motion (ω_p) for lower depth vessels and is dominated by the vessel motion (ω_v) for increasingly larger depth vessels.

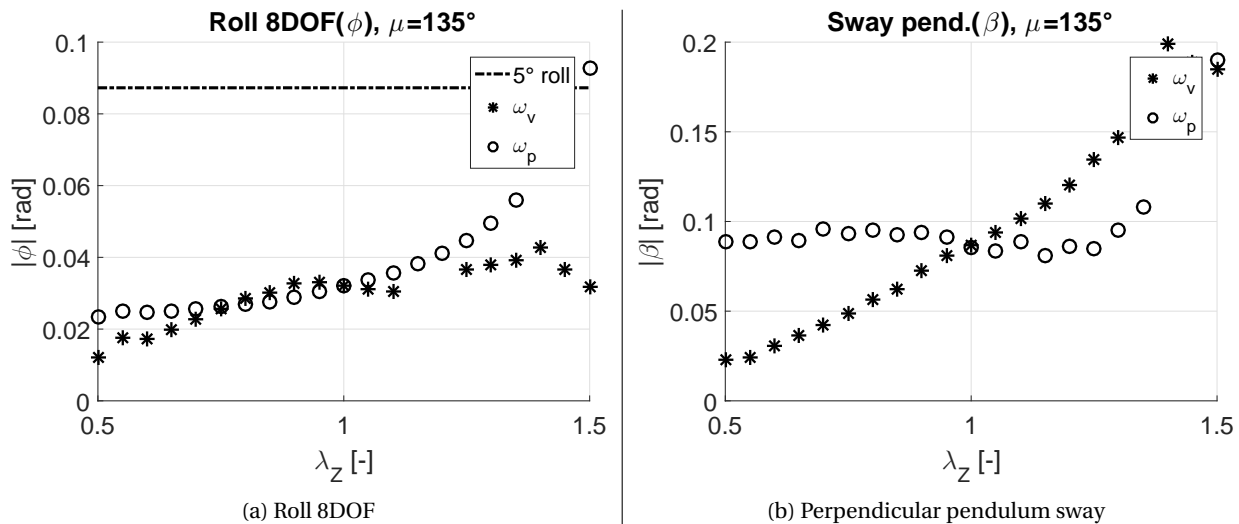


Figure 7.19: Peak shift, depth sensitivity

7.3.3. Roll damping ratio shift

The peak height increase of both the roll motion as well as the perpendicular swaying motion are largely dependent on the fact that the roll damping decreases for increasingly large vessel depths, seen in figure 7.20. Both the roll damping ratio at the resonance frequency related to the vessel motion ω_v and the resonance frequency related to the crane load swaying motion ω_p appear to decrease significantly for increasingly large vessel depth geometries.

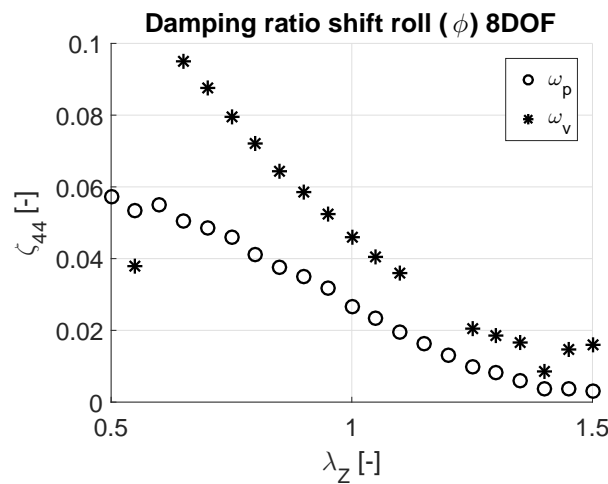


Figure 7.20: Damping ratio shift roll, depth sensitivity

7.3.4. Effective excitation (RMS) roll governed motion

It can be seen that the effective roll motion, figure 7.21a, is positively linear dependent on the sensitivity multiplier λ_Z . Implying that the vessel will exert more rolling motion for taller vessels and less rolling motion for lower vessels.

Regarding the effective motion of the perpendicular crane load sway as seen in figure 7.21b it can be seen that there is a clearly positive nonlinear dependency on the sensitivity multiplier. Implying that for ever taller vessels the crane load will exert more motion.

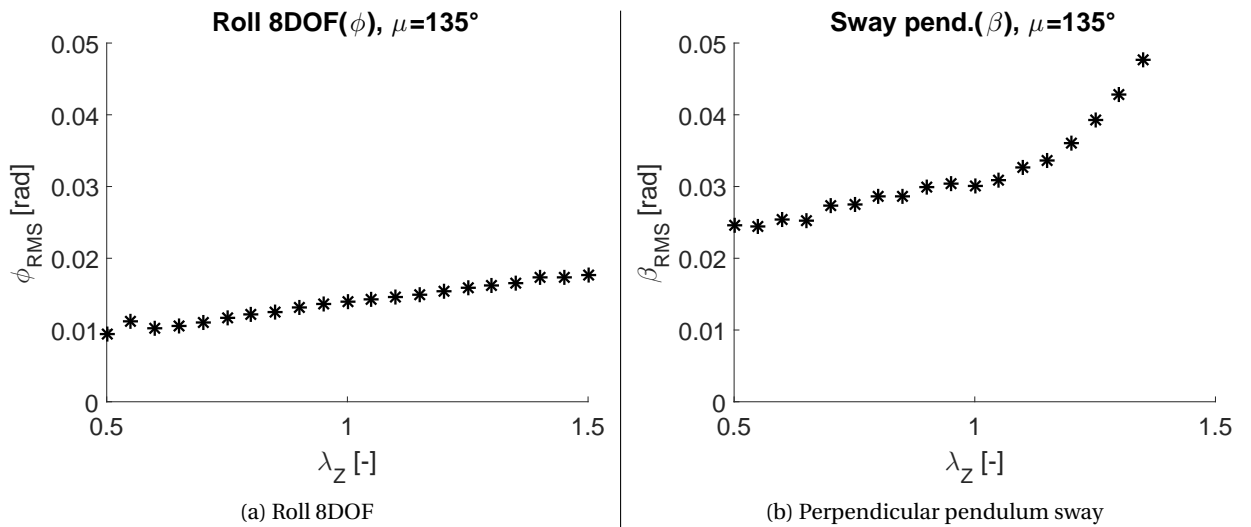


Figure 7.21: Root mean square, depth sensitivity

7.3.5. Conclusion depth sensitivity analysis

Compared to the length and width sensitivity analyses the dynamic characteristics for the depth sensitivity appear to have an opposite dependency on the sensitivity multiplier. Increasing the depth of a vessel will increase motion and secondly it will increase the maximum exerted motions at the resonance frequencies. What this implies is that for a taller, heavier and therefore more costly vessel the dynamic response motions for both the roll motion as well as the perpendicular swaying motion are less favorable. This dependency therefore is contrary to the relations of the length and the width of the vessel, implying that for longer and wider vessels the dynamic characteristics improve. One may ask why the base case vessel has the set vessel depth in the first place, wouldn't it be more reasonable to decrease the vessel depth? This research has focused on the dynamic characteristics of the vessel, however, effects like free-boarding are not taken into account. Simply stating that a vessel will have better motion response, oversimplifies the criteria a vessel has to comply with.

Table 7.6: Summary depth sensitivity, roll governed motion

x	Not present				
✓	Present				
c	Constant				
d	Discontinuous				
↑	Increases				
↑↑	Increases more than linear				
↓	Decreases				
↓↓	Decreases more than linear				
ω_v	Resonance frequency related to the vessel motion				
ω_p	Resonance frequency related to the pendulum motion				
		Roll 8DOF		Perpendicular sway (β)	
		$\lambda_Z < 1.00$	$\lambda_Z > 1.00$	$\lambda_Z < 1.00$	$\lambda_Z > 1.00$
Coupled motion		✓	✓	✓	✓
Strong dynamic coupled motion		x	✓	x	✓
Effective motion (RMS)		↓	↑	↓	↑↑
	Freq. shift	↑	d↓	↑	↓
ω_v	Peak height shift	↓	d↑	↓	↑↑
	Damping ratio	↑	d↓	c	c
	Freq. shift	c	↓	c	↓
ω_p	Peak height shift	↓	↑↑	c	↑↑
	Damping ratio	↑	↓	c	c

7.4. Comparative peak shift

In the separate sensitivity analyses the shift in either resonance frequency, peak height, damping ratio and effective exerted motion has been set out in comparison to the sensitivity multipliers. The resonance frequencies related to either the crane load motion (ω_p) and vessel motion (ω_v) have been proven to change for different vessel lengths, widths and heights. To compare which of the geometrical properties, either length, width or depth, has got the most influence on the motion behavior of the vessel the peak height shift will be compared for both the resonance frequency related to the pendulum (ω_p) and the resonance frequency related to the vessel motion (ω_v).

Within figure 7.22 four figures illustrating the peak height shift related to the pendulum motion (ω_p), figure 7.22a and 7.22b, and the peak height shift related to the vessel motion (ω_v), figure 7.22c and 7.22d, are seen for both the X-, Y- and Z- sensitivity. Just giving the figures a quick glance shows there is a significant difference between either sensitivity analysis.

Regarding the roll motion of the vessel, figure 7.22a and 7.22c, it can be seen that the maximum motion is both highly dependent on the crane load resonance frequency (figure 7.22a) and both the width and depth sensitivity. I.e., the maximum occurring roll motion for narrower (Y-sens) or larger depth (Z-sens) vessel geometries will be increasingly dominated by the swaying of the crane load. Although the roll motion peak height also changes for the resonance frequency related to the vessel motion (figure 7.22c), the maximum occurring motion throughout all sensitivity analyses is more dependent on the swaying of the crane load.

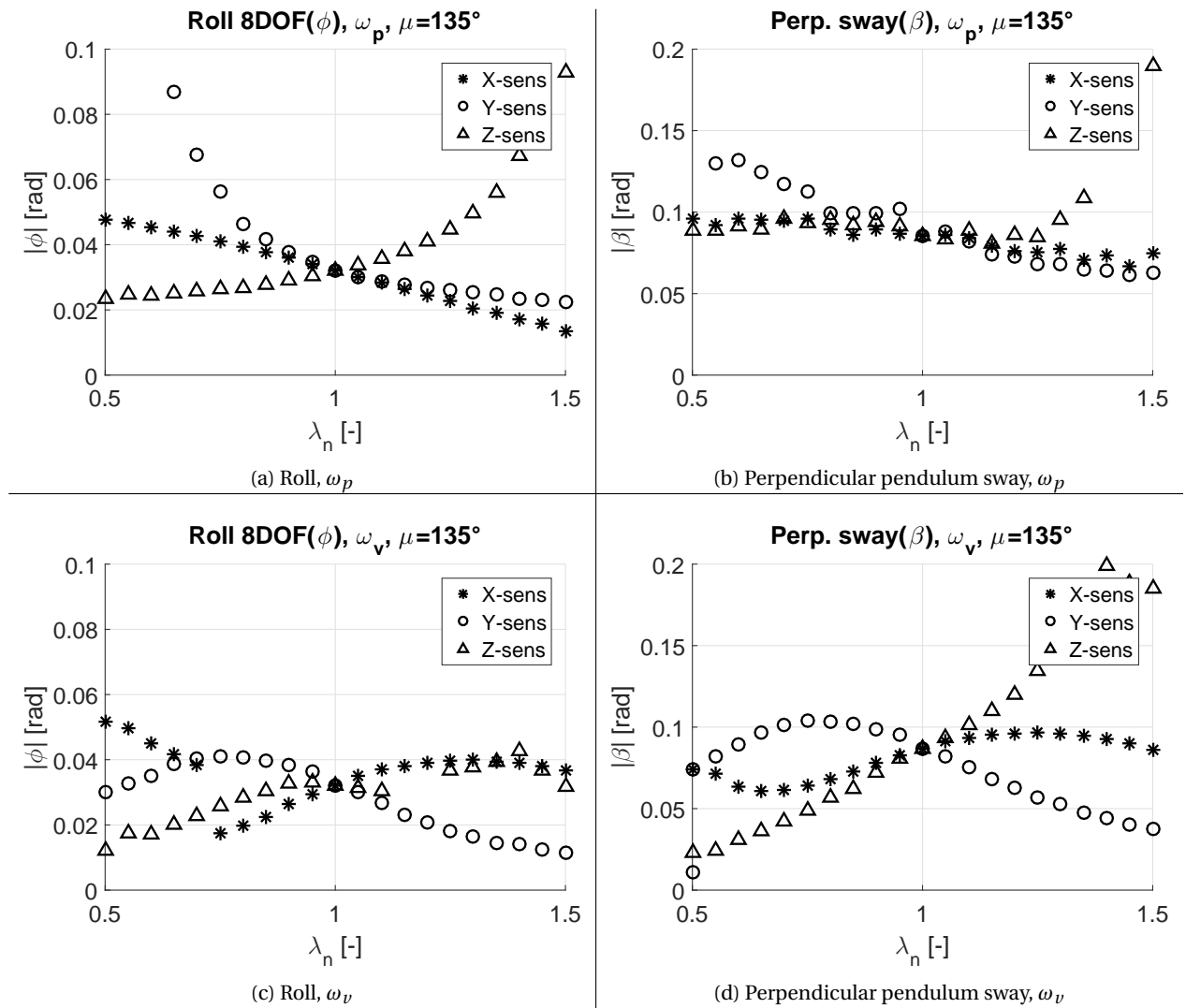


Figure 7.22: Comparative peak height

Contrarily, the maximum occurring motion for the crane load swaying motion, figure 7.22b and 7.22d, is mostly dependent on the vessel motion (figure 7.22d). Especially the depth sensitivity (Z-sens) will make the crane load swing increasingly more for increasingly taller vessels.

Looking at all figures it may be concluded that both the width (Y-sens) and depth (Z-sens) sensitivity have the most influence on the maximum occurring motion both considering the roll and perpendicular crane load swaying motion. The maximum roll motion is mostly dependent on the width sensitivity, second by the depth sensitivity and lastly by the length sensitivity.

7.5. Comparative effective motion (RMS)

Seen in figure 7.23 the effective motion shift of both length-, width and depth- sensitivity analyses are shown for both the roll motion and perpendicular pendulum swaying motion.

It can clearly be seen that the depth sensitivity (Z-sens) has an opposite relation to the sensitivity multiplier compared to the length- (X-sens) and width- (Y-sens) sensitivity. Implying that the motion of both the roll motion as well as the perpendicular swaying motion increases for vessels with increasing depth. Decreasing the vessel depth would therefore give better dynamic characteristics, less effective motion and less maximum exerted movement at the resonance frequency. However decreasing the vessel depth will most likely compromise other characteristics besides the dynamic response. Therefore one cannot make the assertion that decreasing the vessel depth will only see positive improvements. Other conditions must be taken into account.

Looking at the comparative effective roll motion, figure 7.23a, it can be seen that the exerted rolling motion is mostly dependent on the width of the vessel (Y-sens). For smaller sensitivity multipliers ($\lambda_n < 1.00$) the effective motion for the Y-sensitivity analysis changes the most compared to decreasing the length (X-sens) or increasing the depth (Z-sens).

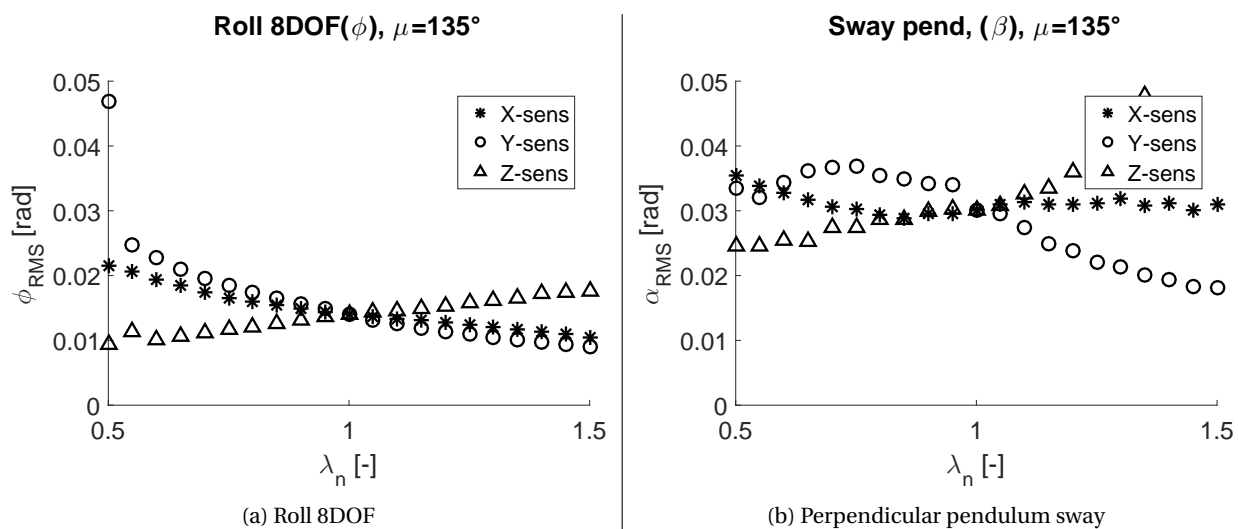


Figure 7.23: Comparative RMS shift

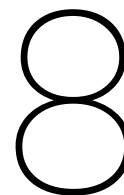
Subquestions

5. Which geometrical vessel parameters have the most influence on dynamic crane load coupled motion?

The size of the vessel has a significant influence on the dynamic coupled motion of the vessel, in general one may conclude the swinging of the crane load has an increased influence on the dynamic coupled motion behavior for increasingly smaller vessels. Oppositely, for larger vessels the vessel motion is the absolute dominant motion within the system, implying the crane load motion will influence the vessel motion less and less for increasingly larger vessels.

Both the vessel roll resonance frequency as well as the perpendicular swaying resonance frequency are highly dependent on either the length, width or depth of the vessel. The length sensitivity of the vessel will only change the resonance frequency related to the vessel motion whereas the width- (Y-sens) and depth- (Z-sens) sensitivity show a resonance frequency shift for both the resonance frequency related to the vessel motion as well as the resonance frequency related to the swaying of the crane load. Implying that changing the vessel length will only change the resonance frequency related to the vessel motion whereas changing the width or the height will in turn also change the resonance frequency related to the crane load motion.

The maximum exerted motion at the resonance frequencies are mostly dependent on the width and depth of the vessel. Implying that either a narrower vessel as well as larger depth vessels will both increase the maximum roll motion as well as the maximum perpendicular crane load swaying motion. Similarly the effective motion is mostly dependent on the width and depth of the vessel, implying that a narrower- or larger depth-vessel will exert more motion.



Conclusions



Figure 8.1: Research set-up

Concluding the research, figure 8.1, a short summary with respect to the evaluated model is given followed by the answered research questions. The subquestions have been answered throughout the research, this chapter therefore is reiteration and recital of all subquestions.

8.1. Summary

The model presented in this research incorporates both the hydrodynamic calculations needed to describe the vessel motion as well as the the coupled motion due to the crane load. Implementing the additional degrees of freedom due to the swaying of the crane load, has been proven to be a viable method of analysis. The model is able to reconfigure any existing vessel, with respect to its length, width or depth. Moreover the model is able to reconfigure all geometry based components like bilge keels, outputting smooth frequency response figures. Throughout most sensitivity analyses the obtained results show predictability and stability. Some data errors, section 6.4, have been observed but they by no means compromise the data trends. However, due to these discrepancies, if one would incorporate the model in future works one must be vigilant towards possible misrepresented calculated characteristics.

8.2. Research questions

In order to conclude the research the research question and subsequently the subquestions as seen in chapter 1 must be answered.

"What is the effect of vessel geometry on dynamic crane load coupling?"

In general, the swaying of the crane load will have an increasing effect on increasingly smaller vessels. The influence of the swinging crane load on the motion behavior is highly governed by both the length, width and depth of the vessel. However, both the width and depth of the vessel have proven to have to most effect on the dynamic coupled characteristics.

1. What is dynamic coupled motion?

A coupled dynamical system is one composed of subsystems, that is, the states of certain subsystems affect the time-evolution of others [11]. The system researched is respectively the vessel system and secondly the crane system, i.e., the effect of the vessel motion on the crane load motion and vice versa.

2. *What induces crane load coupled motion on a crane vessel?*

A crane system has got three degrees of freedom, the degree of freedom related to the elongation of the crane cable however has been proven to not exert any dynamic coupled motion. Even for an unrealistically small cable diameter and at great cable lengths the dynamic elongation motion does not influence the vessel motion. Dynamic coupled motion therefore will only be induced by the swaying of the crane load, namely swaying in either longitudinal- or perpendicular- direction of the vessel.

3. *In which degrees of freedom does dynamic crane load coupled motion occur?*

The swaying of the crane load could effect both the roll and pitch motion of the vessel. Roll motion has been proven throughout all sensitivity analyses to show dynamic coupled behavior. However, whilst examining the results, no clear indication has been found regarding dynamic coupled motion in pitch motion. However, for crane load damping ratio approaching zero the pitch motion will start showing dynamic coupled behavior. Better defining the crane load damping could in fact help exclude dynamic pitch motion as an occurring phenomena. Under the assumption of 10% critical damping acting upon the crane load, one may exclude dynamic coupled pitch motion.

Static excitation in pitch motion due to the crane load however increases significantly for increasingly smaller vessels. This static excitation is due to the placement of the crane at the aft of the vessel.

4. *Does dynamic crane load coupled motion occur during current operations and is this significant with respect to current method of analysis?*

It has been proven that the coupled system exerts different resonance rolling frequencies compared to the current set-up for the Lewek Connector. Within the roll governed motion of the coupled system (roll and perpendicular crane load swaying motion) there are two resonance frequencies present compared to the single resonance frequency of the current analysis. The resonance rolling frequency of the current system is only dependent on the vessel motion and will always be at a lower frequency compared to the resonance frequency of the coupled system.

Due to the allocation of the crane mass at the tip of the crane, the vessel is modeled as top heavy with negative consequences. The maximum exerted roll motion at the resonance frequency will therefore be greater compared to the coupled system. Similarly the effective motion of the current system is greater than the coupled system, implying the current system will exert more motion than the coupled system.

Summing up the differences between the current and coupled models, the current model has its shortcomings in reflecting the true nature of a heavy lift offshore operation. Firstly, the current system misrepresents the resonance frequencies. Secondly the maximum exerted motion at the resonance frequency for the current model is greater compared to the coupled model. Lastly the current model will exert more motion than the coupled system. Dynamic coupled crane load motion therefore is absolutely significant.

5. *Which geometrical vessel parameters have the most influence on dynamic crane load coupled motion?*

The size of the vessel has a significant influence on the dynamic coupled motion of the vessel, in general one may conclude the swinging of the crane load has an increased influence on the dynamic coupled motion behavior for increasingly smaller vessels. Oppositely, for larger vessels the vessel motion is the absolute dominant motion within the system, implying the crane load motion will influence the vessel motion less and less for increasingly larger vessels.

Both the vessel roll resonance frequency as well as the perpendicular swaying resonance frequency are highly dependent on either the length, width or depth of the vessel. The length sensitivity of the vessel will only change the resonance frequency related to the vessel motion whereas the width- (Y-sens) and depth- (Z-sens) sensitivity show a resonance frequency shift for both the resonance frequency related to the vessel motion as well as the resonance frequency related to the swaying of the crane load. Implying that changing the vessel length will only change the resonance frequency related to the vessel motion whereas changing the width or the depth will in turn also change the resonance frequency related to the crane load motion.

The maximum exerted motion at the resonance frequencies are mostly dependent on the width and depth of the vessel. Implied that either a narrower vessel as well as larger depth vessels will both increase the maximum roll motion as well as the maximum perpendicular crane load swaying motion. Similarly the effective motion is mostly dependent on the width and depth of the vessel, implying that a narrower- or larger depth-vessel will exert more motion.

9

Recommendations



Figure 9.1: Research set-up

This chapter, figure 9.1, will discuss how the model could be implemented in future works or analysis.

Several recommendations regarding the research have been made. The recommendations have been subdivided into two categories, first certain recommendations regarding the implementation of the model will be discussed and secondly recommendations regarding the improvement of the research will be set out.

9.1. Implementation

If one would like to design a new vessel based on the geometry of an existing vessel this model will be able to redefine the geometric properties of the existing vessel. The model uses the WADAM diffraction software to create the reshaped vessels.

If the vessel is programmed correctly within the diffraction software and if the supplemented crane characteristics are known (height, crane cable length, crane load) the model will output frequency response and static response graphs from which conclusions can be made regarding the dynamic and static characteristics of the reshaped vessel.

A crude manner of analysis therefore could be, reshape a vessel with respect to its length, width and/or depth, evaluate the characteristics of the output graphs and define whether the newly designed vessel complies with the predetermined boundary conditions. In order to better evaluate the optimum vessel geometry/crane ratio, limiting boundaries must be determined and subsequently evaluated. A few example boundary conditions could be:

- Maximum or minimum displacement
- Maximum or minimum length/width/depth
- Maximum or minimum metacentric heights
- Maximum exerted motion at resonance frequencies
- Maximum effective exerted motion

Using the model as defined in this research an optimization tool could be created defining a vessel that has the most optimum geometric properties that will comply with all the limiting boundaries set.

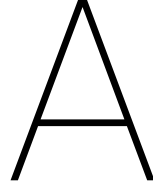
This research has focused on the sensitivity of both the size (proportional sensitivity analysis) and length, width or depth (disproportional sensitivity analyses) sensitivity of the vessel response. The optimum vessel geometry however could very well be one that has rather strange geometric proportion. An optimization tool would therefore be convenient in determining the optimum geometric properties. An optimization tool could use different algorithms to determine the best geometric properties. Easiest but most time consuming would be creating a data set with of reshaped vessel geometries and evaluating each and every geometry and finding the optimum vessel geometry. A single diffraction software run approximately has a duration of 30 minutes to complete. This research has performed 336 diffraction software runs, culminating to an approximate analysis time of 8400 minutes or exactly 7 days continuous calculating time. If one would create a large data set of geometrically altered vessel sizes the total run time would be tremendous. Therefore a better defined algorithm would be much better.

9.2. Recommendations for implementation

1. **Implement the coupled system:** A rudimentary 2DOF system as described by Vu et. al. [10] as well as the 6DOF system have seen their shortcomings in representing the true nature of vessel motion during heavy lift offshore operations. Therefore it is highly recommend to implement this higher degree of freedom system.
2. **Ask DNV GL to implement higher degree of freedom coupled terms:** As of now, the WADAM HydroD package provided by DNV GL does not include the ability to implement additional terms related to coupled systems. If DNV GL would enable the implementation of higher degree of freedom (>6DOF) coupled systems, one could implement any coupled system of interest. This would drastically decrease the external programming needed to define the influence of coupled systems. Due to the fact that the additional crane terms were not implementable within the diffraction software, all results had to be obtained externally using Matlab. If the additional coupled terms were implemented within WADAM, the results could have been computed much more easily without the need of any external programming. The best solution would be an easy user interface within HydroD, were the user could easily define the additional coupled terms.
3. **Ask DNV GL to increase the evaluation frequency range:** A great problem throughout creating the different analyses has been the coarseness of the output values. Due to limited evaluated frequency increments, the results at first were rather coarse in nature. In able to create the smooth frequency response functions as seen throughout the research, multiple runs had to be created and subsequently put together to improve the coarseness of the results. This is a time consuming process and could easily be avoided by increasing the frequency mesh from a maximum of 50 evaluated frequencies to at least 200 evaluated frequencies.
4. **Implement sensitivity programming:** The defined model is able to reshape any existing vessel with respect to its length, width or depth including all related properties. Implementing this programming related to the vessel dimensions will enable the user to research different vessel dimensions of interest. One can choose to implement the crane terms or disregard the crane terms.
5. **Better define other vessels within WADAM:** Additionally the research was posed to research the effect of dynamic coupling on a different vessel, namely the Lewek Champion, however this vessel was not modeled as accurately in WADAM as one would want, making it impossible to use the built programming. One of the main problems with respect to the inability to use the Lewek Champion was that the vessel geometry file, used to describe the hull of the vessel, was not set up accurately within the preferred reference frame. Using the manual HydroD user interface this has never been a problem, but through the scripted commands this has been proven to be a great struggle.

9.3. Recommendation for future research

1. **Better determine damping terms:** One of the parameters that has the most influence on the results is the applied damping upon the crane load. Within this research the crane load damping is set at a reasonably high 10% critical damping. It has been established that decreasing the crane load damping towards ever smaller damping ratios the pitch motion would as well show dynamic coupled motion behavior. If one would be able to define the damping acting upon the crane load correctly it will give different results. Damping terms related to the swinging crane load could be due to structural damping, frictional damping and viscous damping. Secondly the diffraction software is not able to calculate the quadratic damping terms related to the vessel, these damping terms must be defined through experimental tow tank testing.
2. **Create time domain analysis:** This research has focused on the frequency response functions, time domain analysis will give insight into the actual occurring motion. The time domain analysis will also give a better insight into the statistical operability of the vessel and the maximum occurring motion. Within the time domain analysis one should vary the environmental conditions.
3. **Motion reduction systems:** During operation the vessel will have several controlled systems managing the motion of the vessel and crane load. The coupled system is set-up in such a way that the crane load is able to freely swing from the suspended crane cable. In reality a crane operator will not allow the mass to exert large motion. Therefore a restoring force due to the crane operator will impact the results. Similarly the roll motion will be controlled using active ballast tanks, gyroscopes, active fin stabilizers or any other stabilizing system. These systems have not been modeled within this research.
4. **Research different crane configurations:** This research has focused on a heavy lift vessel configuration with a single large crane operating at the aft of the vessel. This has implied that the vessel remained transversely symmetric. Replacing the crane, or altering the dimensions of the crane will have an influence on the motion response of the vessel. Using the formulation and the programming developed this can easily be done.
5. **CFD research into crane load:** Within this research the crane load modeled did not have any attributed physical properties. If the crane load would have some sort of attributed physical properties one could in fact define environmental forces (wind, hydrodynamic etc.) acting upon the load. This could be done by CFD modeling of the apparatus being installed
6. **Towing tank tests:** To validate the presented model one must perform actual towing tank tests. Hence all the vessels evaluated throughout the sensitivity analyses are imaginary, there is no method besides performing towing tests to compare and validate the results. Validating the system through towing tank research will also help define the quadratic roll damping terms.



Euler Lagrangian calculations

In chapter 4, three different dynamic systems are defined. Either the simplified 2DOF system representing roll motion (ϕ) and perpendicular pendulum swaying motion (β), the 6DOF vessel system and lastly the more complex 8DOF system incorporating the swaying motion of the pendulum in both longitudinal (β) and perpendicular (β) direction. This appendix will show how these equation of motion are determined.

The vessel system remains within the frequency domain, therefore the coupled matrices must be linear. The defined matrices will be super-positioned to the matrices related to the vessel dynamics. Both the 6DOF system as well as the 8DOF system have super-positioned dynamic matrices, these matrices first have to be determined using the Euler Lagrangian method.

The Euler Lagrangian method examines both the potential and kinetic energy in the system and is an alternative to the Newtonian approach. This method is especially useful for multiple independent degrees of freedom but is restricted to holonomic systems [8] (The number of generalized displacement variables used to the describe the system is equal to the number of degrees of freedom).

The Lagrangian is defined as the kinetic energy (T) minus the potential energy (V).

$$\mathcal{L} \equiv T - V \tag{A.1}$$

The Euler Lagrangian equation is defined as the partial derivative as seen in A.2. This is equal to the equation of motion of variable j .

$$\text{EOM}_j: \frac{d}{dt} \frac{\partial \mathcal{L}}{\partial \dot{\eta}_j} - \frac{\partial \mathcal{L}}{\partial \eta_j} = 0 \tag{A.2}$$

A.1. Euler Lagrangian calculations 2DOF

The simplified 2DOF system, figure A.1, representing the roll motion and perpendicular sway motion has got two degrees of freedom. First of all, the transitional location of the crane mass M_2 must be defined, seen in equation A.3 - A.5.

$$y_2(t) = H_0 \sin(\phi(t)) + L_c \sin(\beta(t)) \tag{A.3}$$

$$z_2(t) = H_0 \cos(\phi(t)) - L_c \cos(\beta(t)) \tag{A.4}$$

$$\Delta z_2(t) = -H_0(1 - \cos(\phi(t))) + L_c(1 - \cos(\beta(t))) \tag{A.5}$$

The velocity of the crane load mass is defined as the Pythagorean term of both the velocity in y and z direction, equation A.6.

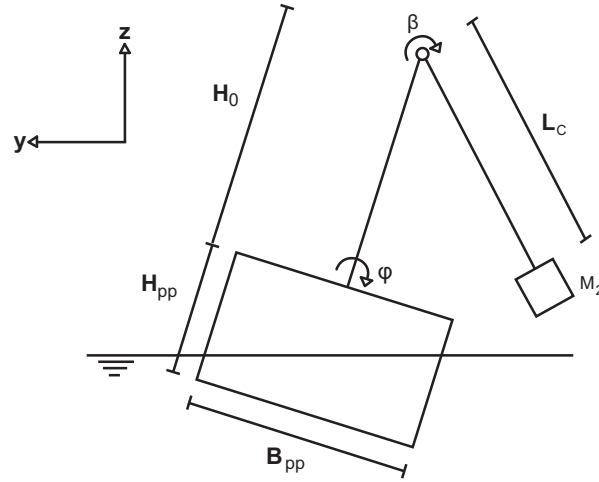


Figure A.1: 2DOF system

$$v_2(t) = \sqrt{\left(\frac{d}{dt}y_2(t)\right)^2 + \left(\frac{d}{dt}z_2(t)\right)^2} \quad (\text{A.6})$$

$$= \sqrt{2H_0L_c \left(\frac{d}{dt}\phi(t)\right) \cos(\phi(t)) \left(\frac{d}{dt}\beta(t)\right) \cos(\beta(t)) \dots} \\ \dots - 2H_0L_c \left(\frac{d}{dt}\phi(t)\right) \left(\frac{d}{dt}\beta(t)\right) \sin(\phi(t)) \sin(\beta(t)) + H_0^2 \left(\frac{d}{dt}\phi(t)\right)^2 + L_c^2 \left(\frac{d}{dt}\beta(t)\right)^2} \quad (\text{A.7})$$

The total Lagrangian potential energy term is defined as the potential energy of the crane load and the spring term (k_r) related to the geometric height of the vessel, equation A.8.

$$V = M_2g\Delta z_2(t) + \frac{1}{2}k_r\phi(t)^2 \\ = M_2g(-H_0(1 - \cos(\phi(t))) + L_c(1 - \cos(\beta(t)))) + \frac{1}{2}k_r(\phi(t))^2 \quad (\text{A.8})$$

The total kinetic energy is defined as the quadratic velocity terms multiplied with their corresponding mass term, equation A.9. Note that $\phi(t)$ is an angular motion and therefore the mass is defined as the moment of inertia of the vessel J_1 .

$$T = \frac{1}{2}J_1\frac{d}{dt}\phi(t)^2 + \frac{1}{2}M_2v_2(t)^2 \\ = \frac{1}{2}J_1\left(\frac{d}{dt}\phi(t)\right)^2 + \frac{1}{2}M_2\left(2H_0L_c\left(\frac{d}{dt}\phi(t)\right)\cos(\phi(t))\left(\frac{d}{dt}\beta(t)\right)\cos(\beta(t))\dots\right. \\ \left.\dots - 2H_0L_c\left(\frac{d}{dt}\phi(t)\right)\left(\frac{d}{dt}\beta(t)\right)\sin(\phi(t))\sin(\beta(t)) + H_0^2\left(\frac{d}{dt}\phi(t)\right)^2 + L_c^2\left(\frac{d}{dt}\beta(t)\right)^2\right) \quad (\text{A.9})$$

The Lagrangian is defined as the kinetic term minus the potential term.

$$\mathcal{L} \equiv T - V \quad (\text{A.10})$$

The independent equation of motion, either the rolling motion or the pendulum swaying motion, are defined by equation A.11 - A.12.

$$\begin{aligned}
\text{EOM1: } \frac{d}{dt} \left(\frac{\partial \mathcal{L}}{\partial \dot{\phi}} \right) - \frac{\partial \mathcal{L}}{\partial \phi} &= 0 \\
&- H_0 L_c M_2 \cos(\phi(t)) \left(\frac{d}{dt} \beta(t) \right)^2 \sin(\beta(t)) - H_0 L_c M_2 \left(\frac{d}{dt} \beta(t) \right)^2 \cos(\beta(t)) \sin(\phi(t)) \dots \\
&\dots + H_0 L_c M_2 \cos(\phi(t)) \cos(\beta(t)) \frac{d^2}{dt^2} \beta(t) - H_0 L_c M_2 \sin(\phi(t)) \sin(\beta(t)) \frac{d^2}{dt^2} \beta(t) \dots \\
&\dots + H_0^2 M_2 \frac{d^2}{dt^2} \phi(t) - M_2 g H_0 \sin(\phi(t)) + J_1 \frac{d^2}{dt^2} \phi(t) + k_r \phi(t) = 0
\end{aligned} \tag{A.11}$$

$$\begin{aligned}
\text{EOM2: } \frac{d}{dt} \left(\frac{\partial \mathcal{L}}{\partial \dot{\beta}} \right) - \frac{\partial \mathcal{L}}{\partial \beta} &= 0 \\
&- M_2 L_c \left(H_0 \left(\frac{d}{dt} \phi(t) \right)^2 \cos(\phi(t)) \sin(\beta(t)) + H_0 \left(\frac{d}{dt} \phi(t) \right)^2 \cos(\beta(t)) \sin(\phi(t)) \dots \right. \\
&\dots - H_0 \cos(\phi(t)) \cos(\beta(t)) \frac{d^2}{dt^2} \phi(t) + H_0 \sin(\phi(t)) \sin(\beta(t)) \frac{d^2}{dt^2} \phi(t) \dots \\
&\left. \dots - L_c \frac{d^2}{dt^2} \beta(t) - \sin(\beta(t)) g \right) = 0
\end{aligned} \tag{A.12}$$

$$\mathbf{M}\ddot{\underline{\eta}} + \mathbf{C}\dot{\underline{\eta}} + \mathbf{K}\underline{\eta} = \underline{F} \tag{A.13}$$

$$\text{Where: } \underline{\eta} = \begin{bmatrix} \phi(t) \\ \beta(t) \end{bmatrix}$$

A.1.1. Non linear system

The non linear terms in the mass, damping and stiffness matrices as well as the force vector now can be compiled, equation A.14 - A.17. Note that within the force vector terms related to the motion of both ϕ and β are listed. These terms are the complex nonlinear terms, these are better represented within the force vector notation.

$$\mathbf{M} = \begin{bmatrix} H_0^2 M_2 + J_1 & H_0 L_c M_2 (\cos(\phi(t)) \cos(\beta(t)) - \sin(\phi(t)) \sin(\beta(t))) \\ H_0 L_c M_2 (\cos(\phi(t)) \cos(\beta(t)) - \sin(\phi(t)) \sin(\beta(t))) & M_2 L_c^2 \end{bmatrix} \tag{A.14}$$

$$\mathbf{C} = \begin{bmatrix} 0 & 0 \\ 0 & 0 \end{bmatrix} \tag{A.15}$$

$$\mathbf{K} = \begin{bmatrix} k_r & 0 \\ 0 & 0 \end{bmatrix} \tag{A.16}$$

$$\underline{F} = \begin{bmatrix} H_0 L_c M_2 (\cos(\phi(t)) \sin(\beta(t)) + \cos(\beta(t)) \sin(\phi(t))) \dot{\beta}(t)^2 + M_2 g H_0 \sin(\phi(t)) \\ H_0 L_c M_2 (\cos(\phi(t)) \sin(\beta(t)) + \cos(\beta(t)) \sin(\phi(t))) \dot{\phi}(t)^2 - M_2 g L_c \sin(\beta(t)) \end{bmatrix} \tag{A.17}$$

A.1.2. Linearization

Linearizing the system will get rid of the nonlinear terms and simplify the system. The linearization assumptions are listed in equation A.18 - A.20.

$$\sin(\phi(t)) = \phi(t), \quad \sin(\beta(t)) = \beta(t) \tag{A.18}$$

$$\cos(\phi(t)) = 1 - \frac{\phi(t)^2}{2} \approx 1, \quad \cos(\beta(t)) = 1 - \frac{\beta(t)^2}{2} \approx 1 \tag{A.19}$$

$$\dot{\phi}(t)^2 = 0, \quad \dot{\beta}(t)^2 = 0 \tag{A.20}$$

The linearized mass, damping and stiffness matrices as well as the linearized force vector can now be compiled, equation A.21 - A.24. Note that the force vector now is empty, no external forces are present and the highly complex nonlinear terms are gotten rid of during the linearization.

$$\mathbf{M} = \begin{bmatrix} H_0^2 M_2 + J_1 & H_0 L_c M_2 \\ H_0 L_c M_2 & M_2 L_c^2 \end{bmatrix} \quad (\text{A.21})$$

$$\mathbf{C} = \begin{bmatrix} 0 & 0 \\ 0 & 0 \end{bmatrix} \quad (\text{A.22})$$

$$\mathbf{K} = \begin{bmatrix} -M_2 g H_0 + k_r & 0 \\ 0 & M_2 L_c g \end{bmatrix} \quad (\text{A.23})$$

$$\underline{F} = \begin{bmatrix} 0 \\ 0 \end{bmatrix} \quad (\text{A.24})$$

A.2. Euler Lagrangian calculations 6DOF

The lump loaded 6DOF system, figure A.2, is used to compile the superposition mass, damping and stiffness matrix as well as the static force vector. Similarly to the 2DOF system seen in section A.1, the Lagrangian method is used to determine the dynamic matrices. The Cartesian crane tip locations are respectively x_{ct} , y_{ct} and z_{ct} .

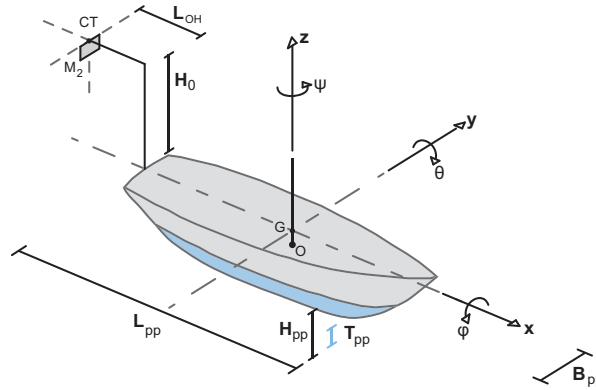


Figure A.2: 6DOF system

The time dependent displacement of the mass M_2 is defined as seen in equation A.25 - A.27.

$$x_2(t) = x(t) + x_{ct} - y_{ct} \psi(t) + z_{ct} \theta(t) \quad (\text{A.25})$$

$$y_2(t) = y(t) + x_{ct} \psi(t) + y_{ct} - z_{ct} \phi(t) \quad (\text{A.26})$$

$$z_2(t) = z(t) - x_{ct} \theta(t) + y_{ct} \phi(t) + z_{ct} \quad (\text{A.27})$$

Again the velocity of the mass M_2 is defined as the Pythagorean of the velocity in both x, y and z direction, equation A.29.

$$v_2(t) = \sqrt{\left(\frac{d}{dt}x_2(t)\right)^2 + \left(\frac{d}{dt}y_2(t)\right)^2 + \left(\frac{d}{dt}z_2(t)\right)^2} \quad (\text{A.28})$$

$$\begin{aligned} &= \sqrt{\left(\frac{d}{dt}\psi(t)\right)^2 x_{ct}^2 + \left(\frac{d}{dt}\psi(t)\right)^2 y_{ct}^2 - 2\left(\frac{d}{dt}\psi(t)\right)\left(\frac{d}{dt}\theta(t)\right)y_{ct}z_{ct}\dots} \\ &\quad \dots - 2\left(\frac{d}{dt}\psi(t)\right)\left(\frac{d}{dt}\phi(t)\right)x_{ct}z_{ct} + \left(\frac{d}{dt}\theta(t)\right)^2 x_{ct}^2 + \left(\frac{d}{dt}\theta(t)\right)^2 z_{ct}^2 - 2\left(\frac{d}{dt}\theta(t)\right)\left(\frac{d}{dt}\phi(t)\right)x_{ct}y_{ct}\dots} \\ &\quad \dots + \left(\frac{d}{dt}\phi(t)\right)^2 y_{ct}^2 + \left(\frac{d}{dt}\phi(t)\right)^2 z_{ct}^2 - 2\left(\frac{d}{dt}x(t)\right)\left(\frac{d}{dt}\psi(t)\right)y_{ct} + 2\left(\frac{d}{dt}x(t)\right)\left(\frac{d}{dt}\theta(t)\right)z_{ct}\dots} \\ &\quad \dots + 2\left(\frac{d}{dt}\psi(t)\right)\left(\frac{d}{dt}y(t)\right)x_{ct} - 2\left(\frac{d}{dt}\theta(t)\right)\left(\frac{d}{dt}z(t)\right)x_{ct} - 2\left(\frac{d}{dt}y(t)\right)\left(\frac{d}{dt}\phi(t)\right)z_{ct}\dots} \\ &\quad \dots + 2\left(\frac{d}{dt}\phi(t)\right)\left(\frac{d}{dt}z(t)\right)y_{ct} + \left(\frac{d}{dt}x(t)\right)^2 + \left(\frac{d}{dt}y(t)\right)^2 + \left(\frac{d}{dt}z(t)\right)^2 \end{aligned} \quad (\text{A.29})$$

The potential energy of the Lagrangian is defined in A.30. Note that because there is no additional degree of freedom (no stiffness terms) the term related to the potential energy is rather short.

$$\begin{aligned} V &= M_2 g z_2(t) \\ &= M_2 g (z(t) - x_{ct}\theta(t) + y_{ct}\phi(t) + z_{ct}) \end{aligned} \quad (\text{A.30})$$

The kinetic energy terms are calculated using equation A.31.

$$\begin{aligned} T &= \frac{1}{2} M_2 v_2(t)^2 \\ &= \frac{1}{2} M_2 \left(\left(\frac{d}{dt}\psi(t)\right)^2 x_{ct}^2 + \left(\frac{d}{dt}\psi(t)\right)^2 y_{ct}^2 - 2\left(\frac{d}{dt}\psi(t)\right)\left(\frac{d}{dt}\theta(t)\right)y_{ct}z_{ct} - 2\left(\frac{d}{dt}\psi(t)\right)\left(\frac{d}{dt}\phi(t)\right)x_{ct}z_{ct}\dots \right. \\ &\quad \dots + \left(\frac{d}{dt}\theta(t)\right)^2 x_{ct}^2 + \left(\frac{d}{dt}\theta(t)\right)^2 z_{ct}^2 - 2\left(\frac{d}{dt}\theta(t)\right)\left(\frac{d}{dt}\phi(t)\right)x_{ct}y_{ct} + \left(\frac{d}{dt}\phi(t)\right)^2 y_{ct}^2 \dots \\ &\quad \dots + \left(\frac{d}{dt}\phi(t)\right)^2 z_{ct}^2 - 2\left(\frac{d}{dt}x(t)\right)\left(\frac{d}{dt}\psi(t)\right)y_{ct} + 2\left(\frac{d}{dt}x(t)\right)\left(\frac{d}{dt}\theta(t)\right)z_{ct} + 2\left(\frac{d}{dt}\psi(t)\right)\left(\frac{d}{dt}y(t)\right)x_{ct}\dots \\ &\quad \dots - 2\left(\frac{d}{dt}\theta(t)\right)\left(\frac{d}{dt}z(t)\right)x_{ct} - 2\left(\frac{d}{dt}y(t)\right)\left(\frac{d}{dt}\phi(t)\right)z_{ct}\dots \\ &\quad \left. \dots + 2\left(\frac{d}{dt}\phi(t)\right)\left(\frac{d}{dt}z(t)\right)y_{ct} + \left(\frac{d}{dt}x(t)\right)^2 + \left(\frac{d}{dt}y(t)\right)^2 + \left(\frac{d}{dt}z(t)\right)^2 \right) \end{aligned} \quad (\text{A.31})$$

Again the equations of motion can be calculated using the Lagrangian, seen in equation A.33 - A.38.

$$\mathcal{L} \equiv T - V \quad (\text{A.32})$$

$$\begin{aligned} \text{EOM1: } \frac{d}{dt}\left(\frac{\partial \mathcal{L}}{\partial \dot{x}}\right) - \frac{\partial \mathcal{L}}{\partial x} &= 0 \\ -M_2 \left(y_{ct} \frac{d^2}{dt^2}\psi(t) - z_{ct} \frac{d^2}{dt^2}\theta(t) - \frac{d^2}{dt^2}x(t) \right) &= 0 \end{aligned} \quad (\text{A.33})$$

$$\begin{aligned} \text{EOM2: } \frac{d}{dt}\left(\frac{\partial \mathcal{L}}{\partial \dot{y}}\right) - \frac{\partial \mathcal{L}}{\partial y} &= 0 \\ -M_2 \left(z_{ct} \frac{d^2}{dt^2}\phi(t) - x_{ct} \frac{d^2}{dt^2}\psi(t) - \frac{d^2}{dt^2}y(t) \right) &= 0 \end{aligned} \quad (\text{A.34})$$

$$\mathbf{K} = \begin{bmatrix} 0 & 0 & 0 & 0 & 0 & 0 \\ 0 & 0 & 0 & 0 & 0 & 0 \\ 0 & 0 & 0 & 0 & 0 & 0 \\ 0 & 0 & 0 & 0 & 0 & 0 \\ 0 & 0 & 0 & 0 & 0 & 0 \\ 0 & 0 & 0 & 0 & 0 & 0 \end{bmatrix} \quad (\text{A.42})$$

$$\underline{F}_{\text{stat}} = M_2 g \begin{bmatrix} 0 \\ 0 \\ -1 \\ x_{ct} \\ y_{ct} \\ 0 \end{bmatrix} \quad (\text{A.43})$$

A.3. Euler Lagrangian calculations 8DOF

The coupled loaded 8DOF system, figure A.3, is used to compile the superpositioning mass, damping and stiffness matrix as well as the static force vector. This system incorporates the two additional degrees of freedom related to the swaying of the pendulum. Similarly to the 2DOF and 6DOF system as seen in section A.1 and A.2, the Lagrangian method is used to determine the dynamic matrices. The Cartesian crane tip locations are respectively x_{ct} , y_{ct} and z_{ct} . This system also incorporates a crane cable with length L_c and two corresponding degrees of freedom α and β . During Lagrangian method approach the linearization steps are skipped, hence showing the nonlinear terms to this system would give way more equations than need be. Similarly the full equations are not written down.

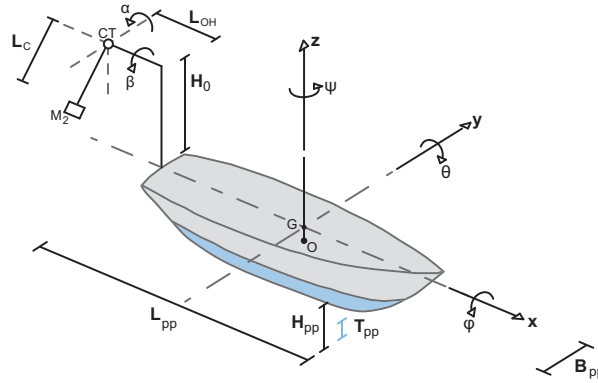


Figure A.3: 6DOF system

The time dependent displacement of the mass M_2 is defined as seen in A.44 - A.46. Note that compared to the 6DOF system the location of the mass is also dependent on the crane cable length and motion.

$$x_2(t) = x(t) + x_{ct} - y_{ct} \psi(t) + z_{ct} \theta(t) + L_c \sin(\alpha(t)) \quad (\text{A.44})$$

$$y_2(t) = y(t) + x_{ct} \psi(t) + y_{ct} - z_{ct} \phi(t) + L_c \sin(\beta(t)) \quad (\text{A.45})$$

$$z_2(t) = z(t) - x_{ct} \theta(t) + y_{ct} \phi(t) + z_{ct} - L_c \cos(\alpha(t)) \cos(\beta(t)) \quad (\text{A.46})$$

Again the velocity of the mass M_2 is defined as the Pythagorean of the velocity in both x, y and z direction, equation A.47.

$$v_2(t) = \sqrt{\left(\frac{d}{dt} x_2(t)\right)^2 + \left(\frac{d}{dt} y_2(t)\right)^2 + \left(\frac{d}{dt} z_2(t)\right)^2} \quad (\text{A.47})$$

The Lagrangian energy of the system is defined as seen in equation A.48.

$$V = M_2 g z_2(t) \quad (\text{A.48})$$

The Lagrangian kinetic energy of the system is defined as seen in equation A.49.

$$T = \frac{1}{2} M_2 v_2(t)^2 \quad (\text{A.49})$$

The (linearized) equation of motion can be seen equation A.50 - A.57.

$$\text{EOM1: } -M_2 \left(-L_c \frac{d^2}{dt^2} \alpha(t) - z_{ct} \frac{d^2}{dt^2} \theta(t) + y_{ct} \frac{d^2}{dt^2} \psi(t) - \frac{d^2}{dt^2} x(t) \right) = 0 \quad (\text{A.50})$$

$$\text{EOM2: } -M_2 \left(-L_c \frac{d^2}{dt^2} \beta(t) + z_{ct} \frac{d^2}{dt^2} \phi(t) - x_{ct} \frac{d^2}{dt^2} \psi(t) - \frac{d^2}{dt^2} y(t) \right) = 0 \quad (\text{A.51})$$

$$\text{EOM3: } M_2 \left(y_{ct} \frac{d^2}{dt^2} \phi(t) - x_{ct} \frac{d^2}{dt^2} \theta(t) + \frac{d^2}{dt^2} z(t) + g \right) = 0 \quad (\text{A.52})$$

$$\begin{aligned} \text{EOM4: } M_2 \left(-L_c \left(\frac{d^2}{dt^2} \beta(t) \right) z_{ct} + \left(\frac{d^2}{dt^2} \phi(t) \right) y_{ct}^2 + \left(\frac{d^2}{dt^2} \phi(t) \right) z_{ct}^2 - \left(\frac{d^2}{dt^2} \theta(t) \right) x_{ct} y_{ct} \dots \right. \\ \left. \dots - \left(\frac{d^2}{dt^2} \psi(t) \right) x_{ct} z_{ct} - \left(\frac{d^2}{dt^2} y(t) \right) z_{ct} + \left(\frac{d^2}{dt^2} z(t) \right) y_{ct} + g y_{ct} \right) = 0 \end{aligned} \quad (\text{A.53})$$

$$\begin{aligned} \text{EOM5: } -M_2 \left(-L_c \left(\frac{d^2}{dt^2} \alpha(t) \right) z_{ct} + \left(\frac{d^2}{dt^2} \phi(t) \right) x_{ct} y_{ct} - \left(\frac{d^2}{dt^2} \theta(t) \right) x_{ct}^2 - \left(\frac{d^2}{dt^2} \theta(t) \right) z_{ct}^2 \dots \right. \\ \left. \dots + \left(\frac{d^2}{dt^2} \psi(t) \right) y_{ct} z_{ct} - \left(\frac{d^2}{dt^2} x(t) \right) z_{ct} + \left(\frac{d^2}{dt^2} z(t) \right) x_{ct} + g x_{ct} \right) = 0 \end{aligned} \quad (\text{A.54})$$

$$\begin{aligned} \text{EOM6: } M_2 \left(-L_c \left(\frac{d^2}{dt^2} \alpha(t) \right) y_{ct} + L_c \left(\frac{d^2}{dt^2} \beta(t) \right) x_{ct} - \left(\frac{d^2}{dt^2} \phi(t) \right) x_{ct} z_{ct} - \left(\frac{d^2}{dt^2} \theta(t) \right) y_{ct} z_{ct} \dots \right. \\ \left. \dots + \left(\frac{d^2}{dt^2} \psi(t) \right) x_{ct}^2 + \left(\frac{d^2}{dt^2} \psi(t) \right) y_{ct}^2 + \left(\frac{d^2}{dt^2} y(t) \right) x_{ct} - \left(\frac{d^2}{dt^2} x(t) \right) y_{ct} \right) = 0 \end{aligned} \quad (\text{A.55})$$

$$\text{EOM7: } M_2 L_c \left(L_c \frac{d^2}{dt^2} \alpha(t) + z_{ct} \frac{d^2}{dt^2} \theta(t) - y_{ct} \frac{d^2}{dt^2} \psi(t) + \alpha(t) \frac{d^2}{dt^2} z(t) + \alpha(t) g + \frac{d^2}{dt^2} x(t) \right) = 0 \quad (\text{A.56})$$

$$\text{EOM8: } M_2 L_c \left(L_c \frac{d^2}{dt^2} \beta(t) + \beta(t) \frac{d^2}{dt^2} z(t) + \beta(t) g - z_{ct} \frac{d^2}{dt^2} \phi(t) + x_{ct} \frac{d^2}{dt^2} \psi(t) + \frac{d^2}{dt^2} y(t) \right) = 0 \quad (\text{A.57})$$

The mass, damping and stiffness matrices as well as the static force vector now can be compiled. Equation A.59 - A.62. It can be seen the mass matrix for the 6DOF- and 8DOF- system are almost entirely similar except for the two additional degrees of freedom related to the swaying of the pendulum. Note that due to the swaying of the pendulum an additional restoring forces are present, equation A.61. No damping has (yet) been specified and therefore the damping matrix are all zeros.

$$\mathbf{M}\ddot{\underline{\eta}} + \mathbf{C}\dot{\underline{\eta}} + \mathbf{K}\underline{\eta} = \underline{F} \quad (\text{A.58})$$

$$\text{Where: } \underline{\eta} = \begin{bmatrix} x(t) \\ y(t) \\ z(t) \\ \phi(t) \\ \theta(t) \\ \psi(t) \\ \alpha(t) \\ \beta(t) \end{bmatrix}$$

$$\mathbf{M} = M_2 \begin{bmatrix} 1 & 0 & 0 & 0 & z_{ct} & -y_{ct} & L_c & 0 \\ 0 & 1 & 0 & -z_{ct} & 0 & x_{ct} & 0 & L_c \\ 0 & 0 & 1 & y_{ct} & -x_{ct} & 0 & 0 & 0 \\ 0 & -z_{ct} & y_{ct} & (y_{ct}^2 + z_{ct}^2) & -x_{ct}y_{ct} & -x_{ct}z_{ct} & 0 & -L_cz_{ct} \\ z_{ct} & 0 & -x_{ct} & -x_{ct}y_{ct} & (x_{ct}^2 + z_{ct}^2) & -y_{ct}z_{ct} & L_cz_{ct} & 0 \\ -y_{ct} & x_{ct} & 0 & -x_{ct}z_{ct} & -y_{ct}z_{ct} & (x_{ct}^2 + y_{ct}^2) & -L_cy_{ct} & L_cx_{ct} \\ L_c & 0 & 0 & 0 & L_cz_{ct} & -L_cy_{ct} & L_c^2 & 0 \\ 0 & L_c & 0 & -L_cz_{ct} & 0 & L_cx_{ct} & 0 & L_c^2 \end{bmatrix} \quad (\text{A.59})$$

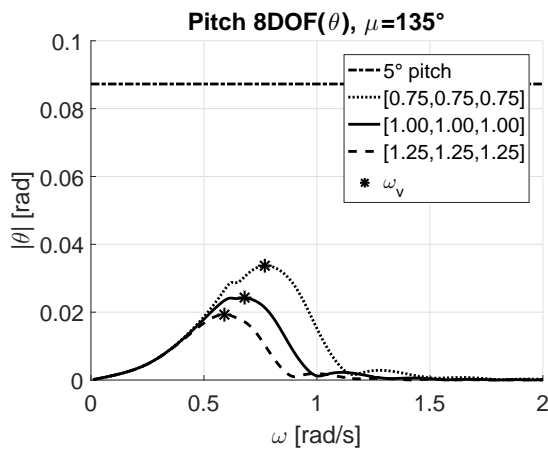
$$\mathbf{C} = \begin{bmatrix} 0 & 0 & 0 & 0 & 0 & 0 & 0 & 0 & 0 \\ 0 & 0 & 0 & 0 & 0 & 0 & 0 & 0 & 0 \\ 0 & 0 & 0 & 0 & 0 & 0 & 0 & 0 & 0 \\ 0 & 0 & 0 & 0 & 0 & 0 & 0 & 0 & 0 \\ 0 & 0 & 0 & 0 & 0 & 0 & 0 & 0 & 0 \\ 0 & 0 & 0 & 0 & 0 & 0 & 0 & 0 & 0 \\ 0 & 0 & 0 & 0 & 0 & 0 & 0 & 0 & 0 \\ 0 & 0 & 0 & 0 & 0 & 0 & 0 & 0 & 0 \end{bmatrix} \quad (\text{A.60})$$

$$\mathbf{K} = M_2 \begin{bmatrix} 0 & 0 & 0 & 0 & 0 & 0 & 0 & 0 & 0 \\ 0 & 0 & 0 & 0 & 0 & 0 & 0 & 0 & 0 \\ 0 & 0 & 0 & 0 & 0 & 0 & 0 & 0 & 0 \\ 0 & 0 & 0 & 0 & 0 & 0 & 0 & 0 & 0 \\ 0 & 0 & 0 & 0 & 0 & 0 & 0 & 0 & 0 \\ 0 & 0 & 0 & 0 & 0 & 0 & 0 & 0 & 0 \\ 0 & 0 & 0 & 0 & 0 & 0 & L_cg & 0 & 0 \\ 0 & 0 & 0 & 0 & 0 & 0 & 0 & L_cg & 0 \end{bmatrix} \quad (\text{A.61})$$

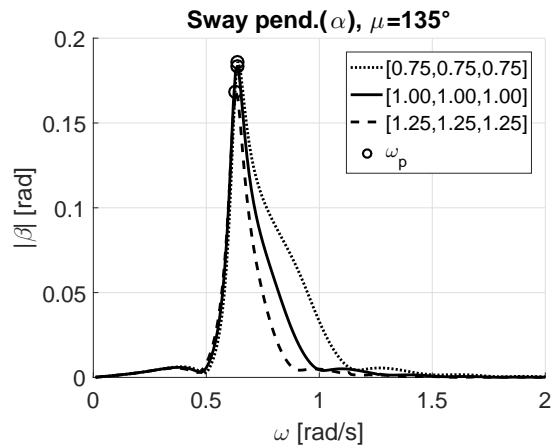
$$\underline{F} = M_2 g \begin{bmatrix} 0 \\ 0 \\ -1 \\ -y_{ct} \\ x_{ct} \\ 0 \\ 0 \\ 0 \end{bmatrix} \quad (\text{A.62})$$

B

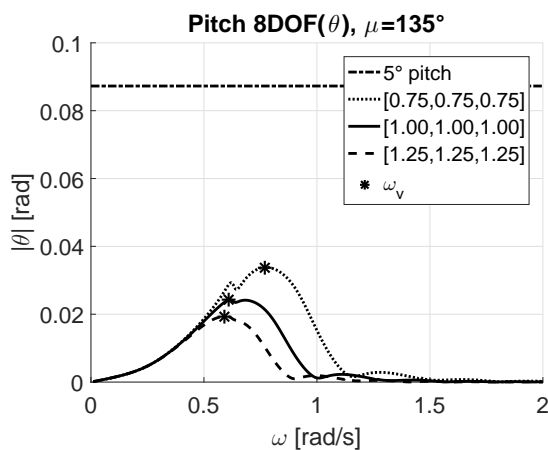
Damping sensitivity, pitch governed motion



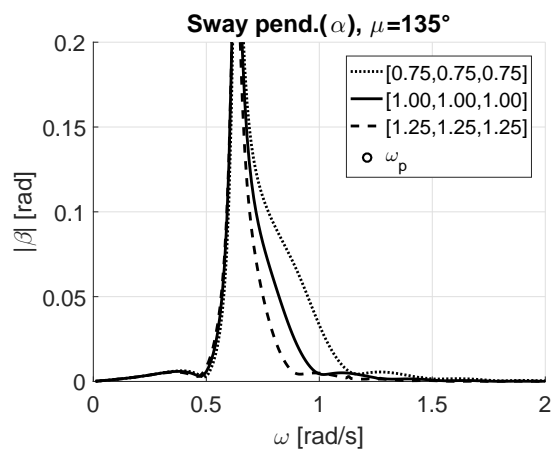
(a) Frequency response pitch 8DOF, 5% critical damping



(b) Frequency response longitudinal sway, 5% critical damping

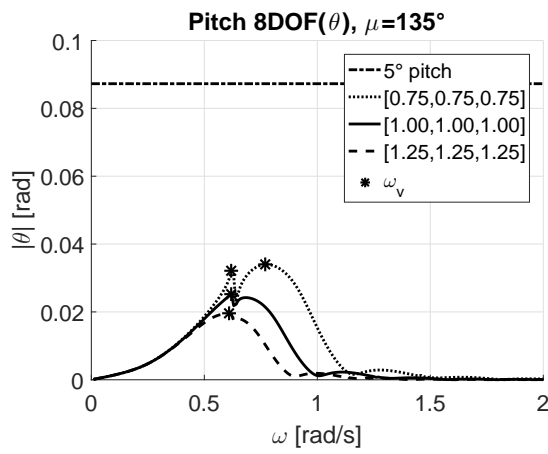


(c) Frequency response pitch 8DOF, 3% critical damping

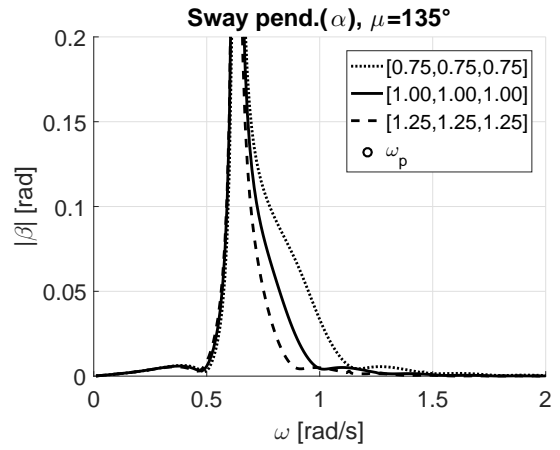


(d) Frequency response longitudinal sway, 3% critical damping

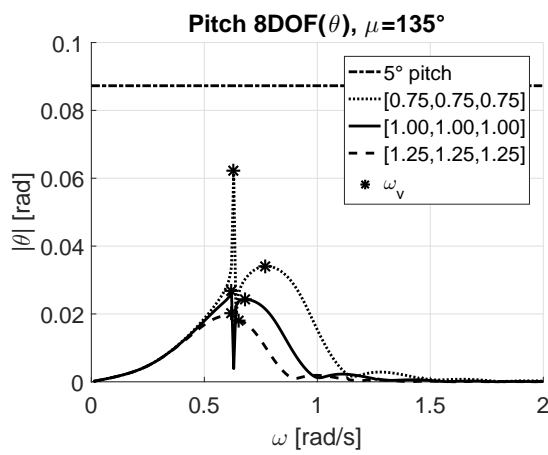
Figure B.1: Frequency response function pitch governed motion, damping < 10 percent critical damping



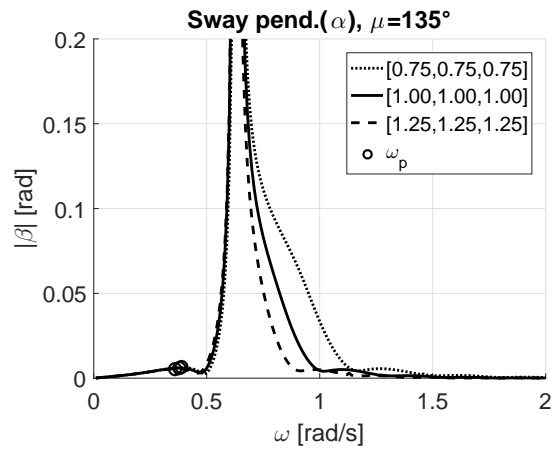
(a) Frequency response pitch 8DOF, 1% critical damping



(b) Frequency response longitudinal sway, 1% critical damping

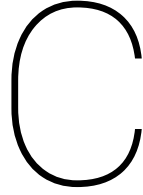


(c) Frequency response pitch 8DOF, 0% critical damping



(d) Frequency response longitudinal sway, 0% critical damping

Figure B.2: Frequency response function pitch governed motion, damping < 10 percent critical damping



Proportional sensitivity analysis 6DOF

This Appendix chapter shows the ineffectiveness of the lump load 6DOF system. The proportional sensitivity analysis implements equal sensitivity multipliers in either X-, Y- and Z- direction.

$$\lambda_X = \lambda_Y = \lambda_Z = \lambda \quad (C.1)$$

$$\underline{\lambda} = \begin{bmatrix} \lambda_X \\ \lambda_Y \\ \lambda_Z \end{bmatrix} = \begin{bmatrix} 0.75 \\ 0.75 \\ 0.75 \end{bmatrix}, \quad \begin{bmatrix} 1.00 \\ 1.00 \\ 1.00 \end{bmatrix}, \quad \begin{bmatrix} 1.25 \\ 1.25 \\ 1.25 \end{bmatrix} \quad (C.2)$$

Seen in figure C.1 both the roll and pitch frequency response, phase shift and damping ratio are on display for the three sensitized vessels. It can be seen that the roll motion frequency response, figure C.1a, is very sharply peaked. At the resonance frequency the amplitude motion becomes increasingly large for ever smaller vessel sizes. This is in consonance with the previously discussed top heaviness as seen in chapter 5. The peak height for smaller vessels increases, this is due to the damping decrease as seen in figure C.4a. The shape of the frequency response differ entirely from the frequency response as seen in chapter 6. Therefore, for increasingly smaller vessel sizes one may say the 6DOF system becomes less and less compatible as means of analysis.

Regarding the pitch analysis, there is no sharp peak like the seen in the roll motion. The frequency response appear to be entirely similar to the frequency response of the 8DOF system as seen in chapter 6.

The effective excitation as seen in table C.1, shows that the 6DOF system especially for the roll motion becomes increasingly different from the 8DOF system for smaller vessel sizes ($\lambda < 1.00$). Regarding the pitch motion, it can be seen that for increasingly smaller vessels the difference between the 6DOF- and 8DOF- becomes greater, similarly the difference becomes less for larger vessels. What this implies is that for increasingly large vessels the pitch motion for the 6DOF system becomes similar to that of the 8DOF system.

Table C.1: Effective excitation (RMS)

$\underline{\lambda}$	RMS roll 6DOF	RMS roll 8DOF	Diff.	RMS pitch 6DOF	RMS pitch 8DOF	Diff.
[0.75;0.75;0.75]	$1.75 \cdot 10^{-2}$ [rad]	$1.89 \cdot 10^{-2}$ [rad]	7.8%	$1.55 \cdot 10^{-2}$ [rad]	$1.49 \cdot 10^{-2}$ [rad]	-3.6%
[1.00;1.00;1.00]	$1.48 \cdot 10^{-2}$ [rad]	$1.40 \cdot 10^{-2}$ [rad]	-5.8%	$1.03 \cdot 10^{-2}$ [rad]	$1.02 \cdot 10^{-2}$ [rad]	-1.1%
[1.25;1.25;1.25]	$1.24 \cdot 10^{-2}$ [rad]	$1.07 \cdot 10^{-2}$ [rad]	-13.4%	$0.77 \cdot 10^{-2}$ [rad]	$0.76 \cdot 10^{-2}$ [rad]	-0.4%

C.0.1. Frequency shift

Seen in figure C.2 the resonance frequency is set out with respect to the sensitivity multiplier λ . It can be seen that both the roll motion as well as the pitch motion are negatively dependent on the sensitivity multiplier λ . I.e., the roll and pitch resonance frequency for smaller vessels will be greater and less for larger vessels. Regarding the roll motion, figure C.2a, it can be seen that there is a nod in the resonance frequency shift at approximately $\lambda = 0.80$. This in effect is due to the instability of the system. This will further be shown in section C.0.2.

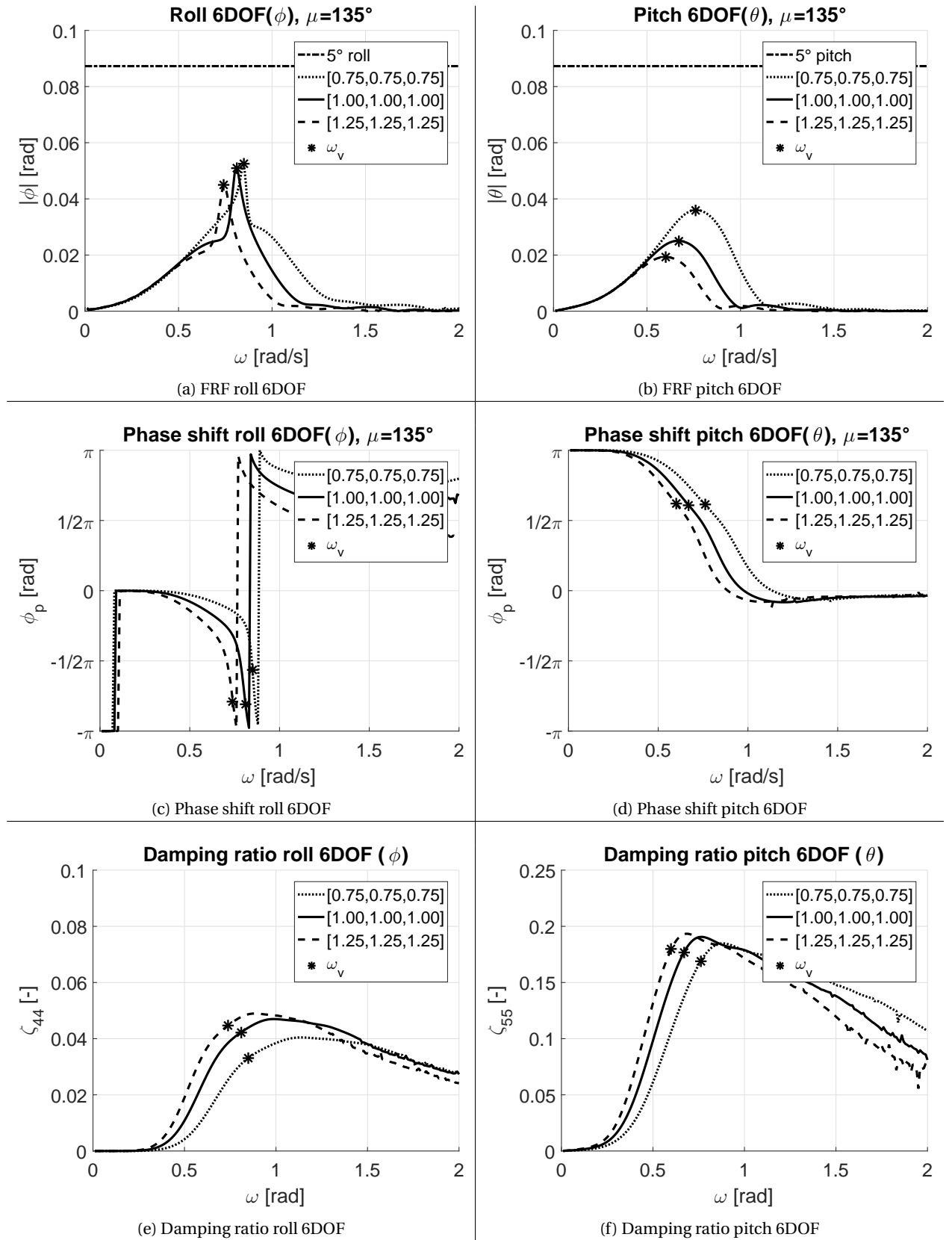


Figure C.1: Frequency response function, phase shift and damping ratio roll governed motion

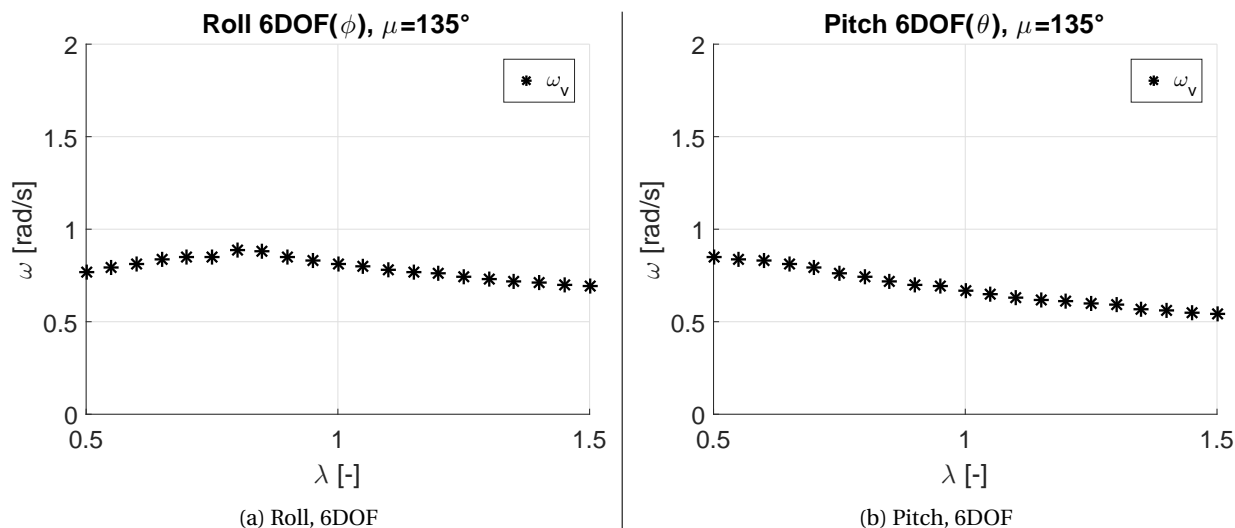


Figure C.2: Frequency shift

C.0.2. Peak shift

Seen in figure C.3a it can be seen that the resonance frequency peak height for vessels smaller than $\lambda < 0.80$ increases significantly and actually appears of the charts ($|\phi| >> 0.1$ [rad]). This implies the vessels will have destructive resonance and in fact tip over. For increasingly smaller vessels one may conclude that the 6DOF system becomes increasingly unreliable.

Regarding the resonance frequency peak height of the pitch motion, it can be seen that the peak height increases more than linearly for increasingly smaller vessels. This shape appears to be largely similar to the 8DOF system.

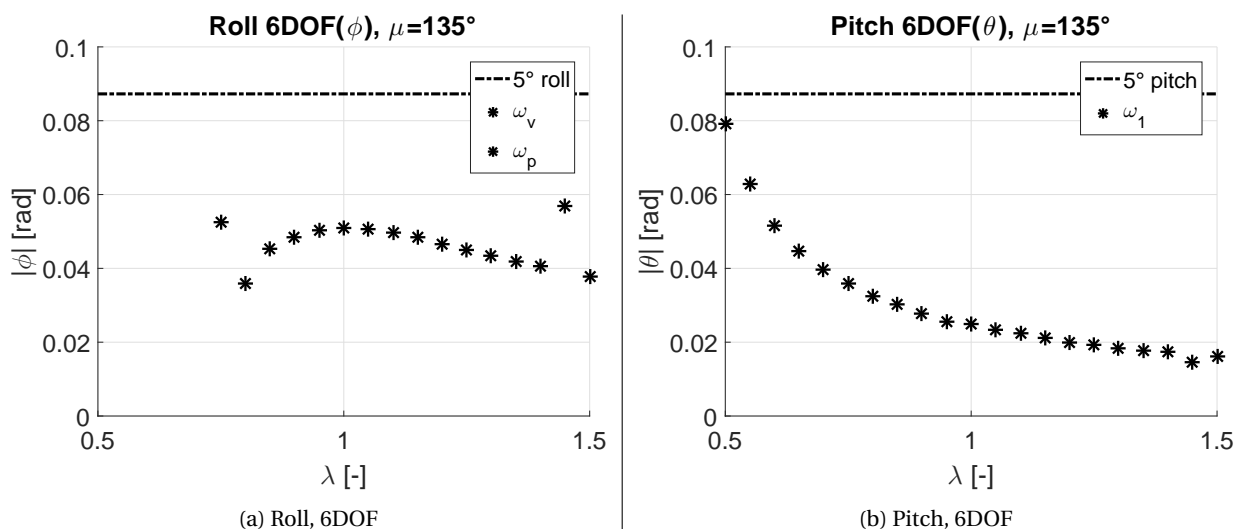


Figure C.3: Peak height shift 6DOF

C.0.3. Damping ratio shift

It can be seen that the damping ratio, figure C.4, decreases for increasingly smaller vessels. Especially regarding the roll case, the damping ratio at the resonance frequency approaches zero. This explains the extreme excitation seen in the peak shift of figure C.3a. The pitch damping ratio, figure C.4b, appears to exert similar behavior, although the decrease of damping is not as significant as with roll motion.

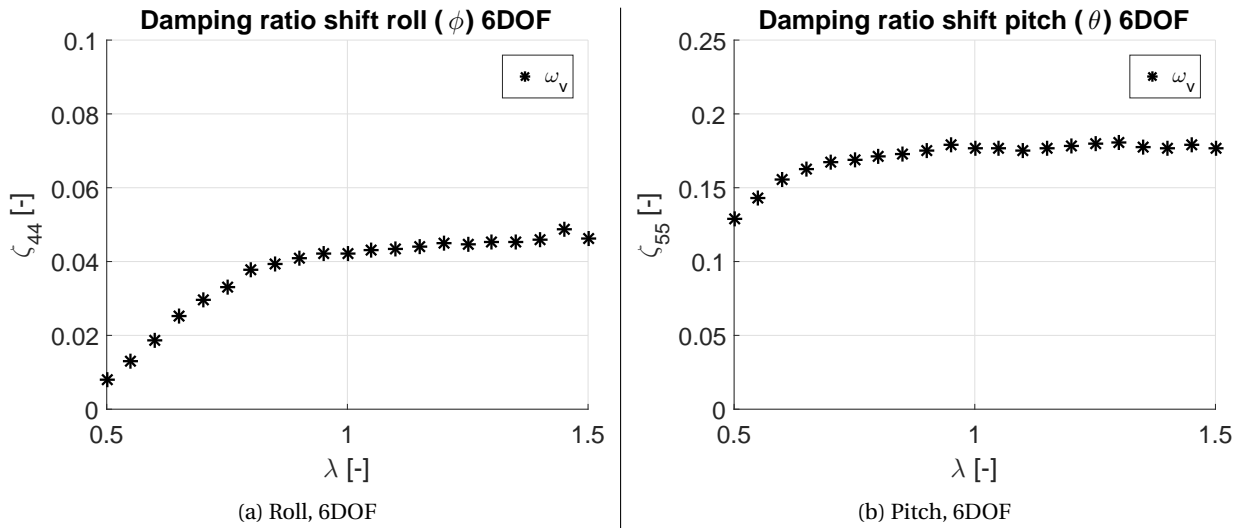


Figure C.4: Damping ratio shift

C.0.4. Effective excitation (RMS)

Looking at the effective excitation motion as seen in figure C.5, it can be seen that the effective excitation increases significantly for increasingly smaller vessels. This is in consonance with the previous asserted top heaviness of the vessel. I.e., due to lump loading of the crane load at the crane tip, the vessel will tip over implying more motion.

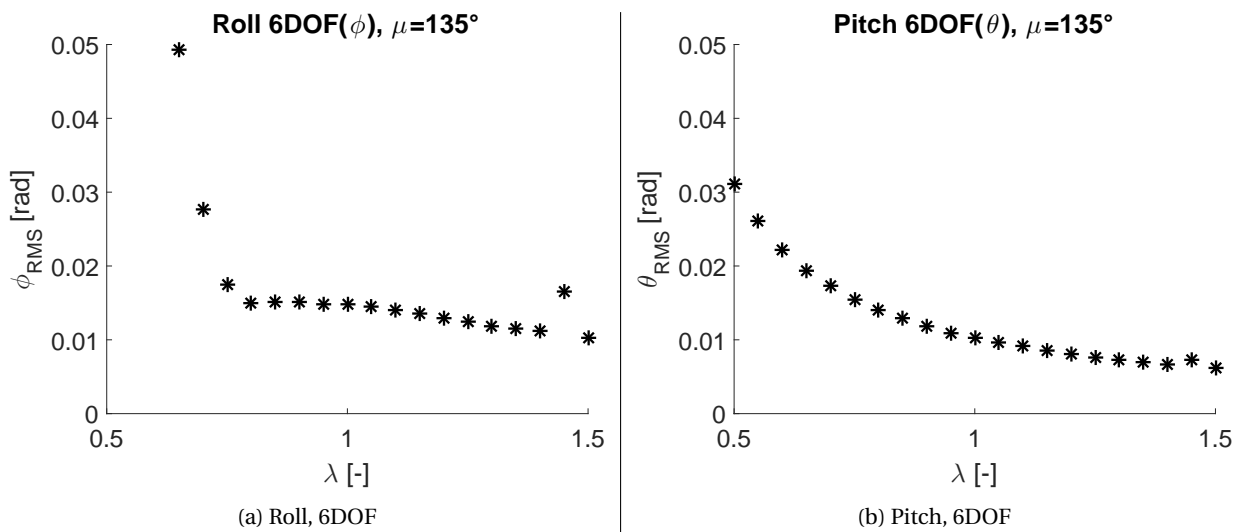


Figure C.5: Total exerted motion 6DOF

C.0.5. Conclusion 6DOF proportional sensitivity analysis

Concluding the 6DOF proportional sensitivity analysis, it may be stated that the 6DOF system is less suitable for increasingly smaller vessels especially with respect to the roll motion.

Table C.2: Summary 6DOF proportional analysis

x	Not present				
✓	Present				
c	Constant				
d	Discontinuous				
↑	Increases				
↑↑	Increases more than linear				
↓	Decreases				
↓↓	Decreases more than linear				
ω_v	Resonance frequency related to the vessel motion				
ω_p	Resonance frequency related to the pendulum motion				
		Roll 6DOF		Pitch 6DOF	
		$\lambda < 1.00$	$\lambda > 1.00$	$\lambda < 1.00$	$\lambda > 1.00$
	Coupled motion	x	x	x	x
	Strong dynamic coupled motion	x	x	x	x
	Effective motion (RMS)	↑↑	↓	↑↑	↓
	Freq. shift	↑	↓	↑	↓
ω_v	Peak height shift	↑↑	↓	↑↑	↓
	Damping ratio	↓↓	c	↓↓	c

Bibliography

- [1] Marketing EMAS AMC. Lewek connector, ultra deepwater multipurpose, flex-lay subsea construction vessel/dp3, 2016. URL http://www.emas.com/images/uploads/articles/Lewek_Connector_Web_062012_Booklet_1.pdf.
- [2] RED Bishop and WG Price. A note on structural damping of ship hulls. *Journal of Sound and vibration*, 56(4):495–499, 1978.
- [3] Većeslav Čorić, Ivan Ćatipović, and Vedran Slapničar. Floating crane response in sea waves. *Brodogradnja*, 65(2):111–1202, 2014.
- [4] WE Cummins. The impulse response function and ship motions. Technical report, DTIC Document, 1962.
- [5] Katrin Ellermann, Edwin Kreuzer, and Marian Markiewicz. Nonlinear dynamics of floating cranes. *Nonlinear Dynamics*, 27(2):107–183, 2002.
- [6] Yoji Himeno. Prediction of ship roll damping-a state of the art. Technical report, University of Michigan, 1981.
- [7] RA Ibrahim and IM Grace. Modeling of ship roll dynamics and its coupling with heave and pitch. *Mathematical Problems in Engineering*, 2010, 2009.
- [8] C Jarquin Laguna, A.; Keijndener, editor. *Lecture notes 'Introduction to Computational Dynamics for Offshore Structures OE4650'*, 2015.
- [9] JMJ Journée and WW Massie. *Offshore hydromechanics*. TU Delft, 2000.
- [10] Kien Vu Khac, Yang Zhang, Xiaofang Deng, and Zhibin Yang. Monohull dynamics during heavy lift. In *ASME 2014 33rd International Conference on Ocean, Offshore and Arctic Engineering*, pages V01AT01A005–V01AT01A005. American Society of Mechanical Engineers, 2014.
- [11] Zhiyun Lin. *Coupled dynamic systems: From structure towards stability and stabilizability*. PhD thesis, University of Toronto, 2006.
- [12] NASA. Center of gravity - cg, 2015. URL <https://www.grc.nasa.gov/www/k-12/airplane/cg.html>.
- [13] Ingela Nystroem, Jayaram K Udupa, George J Grevera, and Bruce E Hirsch. Area of and volume enclosed by digital and triangulated surfaces. In *Medical Imaging 2002*, pages 669–680. International Society for Optics and Photonics, 2002.
- [14] The Engineering Toolbox. Center of gravity - center of buoyancy, 2016. URL http://www.engineeringtoolbox.com/centre-gravity-buoyancy-d_1286.html.
- [15] DNV Wadam. Wave analysis by diffraction and morison theory. *SESAM user manual*. Det Norske Veritas, Høvik, 2010.